TALTECH

DOCTORAL THESIS

Research and Implementation of Electrical Bioimpedance Measurement Solutions

Anar Abdullayev

Research and Implementation of Electrical Bioimpedance Measurement Solutions

ANAR ABDULLAYEV

TAL TECH PRESS

TALLINN UNIVERSITY OF TECHNOLOGY
School of Information Technologies
Thomas Johann Seebeck Department of Electronics

The dissertation was accepted for the defence of the degree of Doctor of Philosophy (Information and communication technology) on 05 September 2025

Supervisor: Senior researcher Dr. Olev Märtens,
Thomas Johann Seebeck Department of Electronics
Tallinn University of Technology
Tallinn, Estonia

Co-supervisor: Senior researcher Dr. Margus Metshein,
Thomas Johann Seebeck Department of Electronics
Tallinn University of Technology
Tallinn, Estonia

Opponents: Prof. Dr.-Ing. Olfa Kanoun,
Faculty of Electrical Engineering and Information Technology
Chemnitz University of Technology
Chemnitz, Germany

Prof., Dr.-Ing., Dr. rer. medic. Daniel Teichmann,
The Maersk Mc-Kinney Moller Institute
University of Southern Denmark
Odense, Denmark

Defence of the thesis: 06 October 2025, Tallinn

Declaration:
Hereby I declare that this doctoral thesis, my original investigation and achievement, submitted for the doctoral degree at Tallinn University of Technology, has not been submitted for any academic degree elsewhere.

Anar Abdullayev   _____

                                                                                            signature

Elektrilise bioimpedantsi mõõtmise lahenduste uurimine ja teostus

ANAR ABDULLAYEV

Contents

List of Publications

The present Ph.D. thesis is based on the following publications that are referred to in the text by Roman numbers.

Publications related to the thesis topic, published

I Olev Martens, Margus Metshein, Anar Abdullayev, Benoit Larras, Antoine Frappe, Antoine Gautier, Maryam Saeed, Deepu John, Barry Cardiff, Andrei Krivošei, Paul Annus, and Marek Rist. Fiducial point estimation solution for impedance cardiography measurements. *2022 IEEE International Instrumentation and Measurement Technology Conference (I2MTC)*, pages 1–6, 2022

II Anar Abdullayev, Olev Martens, Marek Rist, Margus Metshein, Mart Min, and Paul Annus. A DSP-based impedance measurement device. *2022 18th Biennial Baltic Electronics Conference (BEC)*, pages 1–5, 2022

III Olev Martens, Margus Metshein, Gert Tamberg, and Anar Abdullayev. Impedance cardiography signal processing with Savitzky-Golay and frequency sampling kernels. *2022 18th Biennial Baltic Electronics Conference (BEC)*, pages 1–5, 2022

IV Anar Abdullayev, Paul Annus, Andrei Krivošei, Margus Metshein, Olev Märtens, and Marek Rist. Improved PWM-based sinewave generation: Example of the impedance measurement. *Automatic Control and Computer Sciences*, pages 1–13, 2023

V Anar Abdullayev, Marek Rist, Olev Martens, Margus Metshein, Benoit Larras, Antoine Frappe, Antoine Gautier, Mart Min, Deepu John, Barry Cardiff, Andrei Krivosei, and Paul Annus. A DSP-based EBI, ECG and PPG measurement platform. *IEEE Transactions on Instrumentation and Measurement*, pages 1–8, 2023

VI Anar Abdullayev, Olev Martens, Margus Metshein, Marek Rist, Raul Land, and Andrei Krivosei. A DSP-based multichannel EBI measurement device. *2024 IEEE International Instrumentation and Measurement Technology Conference (I2MTC)*, pages 1–6, 2024

VII Anar Abdullayev, Marek Rist, Margus Metshein, and Olev Martens. DSP-based electrical impedance tomography device: Implementation and experiments. *2025 IEEE International Instrumentation and Measurement Technology Conference (I2MTC)*, pages 1–6, 2025

Patent applications

VIII O. Märtens, A. Abdullayev, M. Metshein, A. Gautier, A. Frappe, A. Krivošei, M. Rist; P. Annus, B. Larras, D. John; B. Cardiff. The impedance cardiography device, October 23, 2023. Estonian patent application P202200004, US patent application US2023/0320606 A1

IX O. Märtens, A. Abdullayev, M. Metshein, M. Rist, P. Annus, A. Krivošei. A method and device for synthesizing binary waveforms, December 19, 2024. Estonian patent application P202300017, US Patent application US2024/0421805 A1

Author's other publications

Margus Metshein, Andrei Krivošei, Anar Abdullayev, Paul Annus, and Olev Märtens. Non-standard electrode placement strategies for ECG signal acquisition. *Sensors*, 22(23), 2022

Author's Contributions to the Publications

I In publication I, I contributed to the design and proposed the algorithm for fiducial point detection used in automated testing of the circuit performance. I prepared the simulation, analyzed the results in terms of accuracy, and created the figures illustrating simulation results for the manuscript.

II In publication II, I was the main author and responsible for the complete development of the first version of the impedance measurement device. I designed and implemented the hardware and software, conducted experiments including repeatability tests, capacitive load evaluation, fine-step resistor box sweeps, and dynamic emulation. I analyzed the results, prepared related figures, and wrote the manuscript with input and feedback from co-authors.

III In publication III, I contributed to the development of the initial concept, provided the dataset used as a benchmark for evaluating the results, and prepared supporting simulations in Python. I created the simulation results figures and contributed to the manuscript by writing and explaining the sections related to those results.

IV In publication IV, I was the main author, I contributed to the initial concept development, prepared LTspice simulations, generated and analyzed the results, prepared the corresponding figures, and wrote the proposed solution section of the manuscript.

V In publication V, I was the main author. I implemented the software, conducted the experiments, and evaluated the results. I also prepared the hardware and software diagrams and documented the proposed solution and evaluation results in the manuscript.

VI In publication VI, I was the main author. I implemented the software, conducted the experiments, and evaluated the results. In the manuscript, I contributed the state-of-the-art background in the introduction, prepared the hardware diagram and documented the proposed solution, and provided the evaluation results.

VII In publication VII, I was the main author. I implemented the software, conducted the experiments, and evaluated the results. In the manuscript, I contributed the state-of-the-art background in the introduction, prepared the hardware diagram and documented the proposed solution, and provided the evaluation results.

VIII In publication VIII, I prepared the simulation and analyzed the results. The patent application builds on the work presented in publication I, where I contributed to the initial design and proposed the algorithm for automated testing of circuit performance.

IX In publication IX, I prepared the simulation and analyzed the results. The patent is based on the work in III, where I contributed to the development of the initial concept, provided the benchmark dataset for evaluation, and prepared supporting simulations.

Abbreviations

AC	Alternating Current
ADC	Analog-to-Digital Converter
AFE	Analog Front-End
B,C,X	Fiducial points in ICG waveform
CMRR	Common-Mode Rejection Ratio
CO	Cardiac Output
DAC	Digital-to-Analog Converter
DC	Direct Current
DMA	Direct Memory Access
DFT	Discrete Fourier Transform
DSP	Digital Signal Processor
EBI	Electrical Bioimpedance
ECG (EKG)	Electrocardiography
EIS	Electrical Impedance Spectroscopy
EIT	Electrical Impedance Tomography
EMD	Empirical Mode Decomposition
FFT	Fast Fourier Transform
FR	Frequency Response
FPGA	Field-Programmable Gate Array
IC	Integrated Circuit
ICG	Impedance Cardiography
I2C	Inter-Integrated Circuit
IIR	Infinite Impulse Response
LVET	Left Ventricular Ejection Time
MAC	Multiply-Accumulate
MIT	Magnetic Induction Tomography
PCB	Printed Circuit Board
PGA	Programmable Gain Amplifier
PPG	Photoplethysmography
PWM	Pulse Width Modulation
PEP	Pulse Ejection Period
SG	Savitzky–Golay
SNR	Signal-to-Noise Ratio
SV	Stroke Volume
THD	Total Harmonic Distortion
Wi-Fi	A family of wireless network protocols for local area networking and Internet access

1 Introduction

When a circuit or material is exposed to an alternating current (AC), its resistance to the flow of electrical current is measured as impedance, a term introduced by Oliver Heaviside in 1886 [11]. Impedance is a complex number, typically measured in ohms, consisting of both resistance and reactance components. This property finds extensive applications in the measurement and characterization of diverse systems — from biological tissues and physiological processes (such as hemodynamics estimation) to alloys, composite materials, and industrial structures.

A wide range of instruments is used for impedance measurement, including impedance analyzers [12, 13], network analyzers [14], digital signal processor (DSP)-based devices [15, 16, 17], LCR meters [18], and general data acquisition systems [19]. In the biomedical field, bioimpedance methods have attracted special attention for their non-invasive nature and versatility. Common techniques include bioelectrical impedance analysis (BIA) for body composition assessment, electrical impedance spectroscopy (EIS) for tissue characterization, impedance cardiography (ICG) for cardiac monitoring, and electrical impedance tomography (EIT) for imaging applications [20].

However, open, low-cost bioimpedance instruments with laboratory-grade accuracy are scarce; commercial options are usually closed, costly, and tied to a single modality. This thesis fills that gap by delivering a battery-powered, open platform that combines electrical bioimpedance(EBI)/ICG, electrocardiography(ECG), photoplethysmography(PPG), and 32-electrode EIT on a single TMS320F28379D DSP board. Alongside the hardware, it addresses two outstanding challenges—low-THD binary excitation and reliable fiducial points extraction—thereby covering the full measurement chain from stimulus generation to physiological interpretation.

1.1 Motivation

The motivation for this thesis arises from clinical demand and by technical gaps in current bioimpedance instrumentation.

Clinical demand and market limitations

Globally, populations are aging at an unprecedented pace due to declining birth rates and increasing life expectancy. This demographic transition is projected to nearly double the proportion of people over 60 by 2050 (from 12% to 22%) [21], intensifying pressure on healthcare systems as age-related conditions such as cardiovascular disease, hypertension, and heart failure become increasingly prevalent [22]. This demographic shift underscores the urgent need for personal, non-invasive medical devices that enable early detection, continuous monitoring, and at-home disease management to reduce hospital burden and improve patient outcomes. Fortunately, advances in health technologies are making such solutions increasingly accessible and cost-effective [23, 24].

In particular, non-invasive, wearable biosensors and imaging systems have shown significant improvements in performance and cost-efficiency [25]. Among these, electrical impedance-based systems stand out for their ability to safely and effectively assess key physiological functions and has found use in various healthcare applications [20, 26, 27, 28, 29]. Impedance cardiography, for example, has long been used for non-invasive assessment of stroke volume and cardiac output by measuring thoracic impedance variations during each heartbeat [30]. Similarly, electrical impedance tomography employs small currents to non-invasively visualize conductivity changes within tissues and is already used in clinical applications such as bedside monitoring of lung function in intensive

care units [31].

However, despite their potential, existing commercial impedance devices (for both EIT imaging and ICG monitoring) have limitations that motivate the development of a custom solution. Many commercial systems are expensive, closed-source, or optimized for a narrow set of use-cases, which impedes wide adoption and flexible research use [32]. High cost and proprietary designs mean that researchers and clinicians often cannot easily modify the hardware or access raw data and firmware to implement new algorithms. There is, therefore, a clear need for a fully custom, portable impedance-measurement device that gives researchers complete access to both hardware and firmware. However, impedance measurement is a broad discipline encompassing hardware, software, and signal processing, so shortcomings can emerge at many stages and cannot be resolved by hardware alone. Building a system from the ground up ensures it is tailored to biomedical applications and can be fully instrumented for validating novel techniques.

Need for custom-designed platform

A custom-designed platform also allows integration of advanced signal processing algorithms to enhance performance and broaden the device's diagnostic capabilities. By combining photoplethysmography signals with impedance measurements, it becomes possible to calculate pulse transit time, which is used for cuffless blood pressure estimation [33], and to assess oxygen saturation levels [34]. Additionally, simultaneous recording of electrocardiography and bioimpedance have been explored for various clinical applications. For instance, thoracic impedance can serve as a surrogate respiratory waveform, and its phase coupling with respiratory sinus arrhythmia derived from ECG can be effectively used to detect sleep apnea [35]. Furthermore, ECG recording can serve as a timing reference to segment ICG data per heartbeat, facilitating ensemble averaging for improved signal quality [36]. Also, ECG and bioimpedance can be used to perform lead-off detection and to implement motion artifact reduction [37]. By fusing these modalities, a more complete picture of a patient's cardiovascular and respiratory status can be obtained in real time. This thesis is motivated by the potential of a multi-modal impedance device to simultaneously capture cardiac, vascular, and respiratory dynamics, enabling advanced feature extraction (such as beat-to-beat stroke volume, cardiac output trends, and continuous blood pressure surrogates) that can greatly aid in diagnosis and monitoring. This motivation is reinforced by two Estonian Research Council projects that frame and support the present work. The need for a reconfigurable test-bed —an open, high-resolution impedance platform—arises directly from **MOBERA20** (JEDAI) "Event Driven Artificial Intelligence Hardware for Biomedical Sensors," which investigates near-sensor machine learning on level-crossing analog-to-digital converter (ADC) data and therefore requires ICG datasets for algorithm validation. At the same time, the work aligns with and is supported by the Estonian Research Council project **TEM-TA43** "Novel solutions for clinical monitoring of soft tissues," which targets continuous intra-operative impedance monitoring of the myocardium during cardiac surgery and the wider characterisation of muscle, fat, and connective tissues.

Need for improved excitation signal

Designing such a device demands careful consideration of excitation signal generation strategies and signal conditioning methods to ensure measurement accuracy, linearity, and stability [38]. Optimal excitation signals should exhibit high linearity, cover wide frequency ranges, minimize distortion, and adhere to safety standards [39]. Electrical impedance spectroscopy typically employs excitation signals that can be classified as single-

frequency or multi-frequency. Single-frequency excitation methods measure frequencies sequentially, offering higher sensitivity and SNR at the expense of slower acquisition times. Ideally, a sinewave is preferred for single-tone excitation due to its absence of harmonics. However, there are challenges involved in generating and multiplying the response signal with a sine wave in the analog domain. Similarly, in the digital domain, discrete quantization errors and non-linearity of digital-to-analog converters (DAC) affect the precision of the generated signals. Several studies have focused on addressing these issues [40, 41, 42, 43, 44]. Multi-frequency signals, including multi-sines, linear and exponential chirps, maximum length binary sequences, and discrete interval binary sequences, enable simultaneous multi-frequency measurements, with multi-sines being favored for their balance of accuracy and measurement speed [45]. Parallel to the frequency classification, excitation signals can also be differentiated by waveform type, namely analog versus binary. Binary excitation signals have gained attention due to their simplicity and ease of generation [46, 47, 48]. Despite their advantages, studies focusing on different methods for generating binary excitation signals — particularly with respect to amplitude and SNR performance — remain scarce [49]. This gap highlights the need for further research into alternative binary excitation signals, motivating the exploration presented in this work. The need for higher-resolution, wider-bandwidth, and lower-power excitation aligns with the Estonian Research Council project **PRG1483** "Solutions and Applications of Innovative Impedance Spectroscopy," which investigates new metrological principles and low-cost, low-power EIS components—including advanced excitation schemes and signal processing—for healthcare, biological, and industrial sensing.

Signal-processing challenges

Effective filtering and signal processing methods are crucial for enhancing bioimpedance measurement accuracy and reliability. bioimpedance signals typically contain various artifacts and noise sources, such as respiration, motion artifacts, baseline wander, and powerline interference, which can compromise diagnostic accuracy [50]. Therefore, careful selection and implementation of both analog and digital filtering techniques are essential. Analog filtering methods are employed initially to condition signals prior to digitization, whereas digital filtering techniques provide further noise reduction and artifact suppression, enhancing signal quality for subsequent analyses.

Additionally, advanced signal processing techniques, including analysis of the time derivative of thoracic impedance—which corresponds to the timing of intervals within the cardiac cycle [51] and the extraction of fiducial points is required in deriving meaningful physiological parameters such as cardiac output and stroke volume [50, 52]. Consequently, this thesis aims to investigate different filters and signal processing techniques to enhance the accuracy of vital physiological information extracted from bioimpedance measurements. These low-power, near-sensor processing goals are directly supported by the Estonian Research Council project **MOBERA20** (JEDAI), which supplies both motivation and resources for developing the analog front-end and event-driven algorithms used in this work.

1.2 Research Framework

This section sets out the overall research framework: it begins with the research tasks, then details the methods, tools and resources employed, highlights the work's theoretical and practical novelty, summarises its approbation and dissemination, and closes with a brief outline of the thesis structure.

Research Tasks

Building on the challenges and opportunities outlined in the motivation section, the thesis pursues three research tasks:

1. **Design and implementation of a reconfigurable, multifunctional impedance measurement platform**. The primary objective is to create an open, fully custom hardware–software test-bed that delivers high-accuracy magnitude and phase measurements over a broad frequency range (kHz–hundreds of kHz). The platform must support accurate EBI/ICG acquisition, scalable electrode multiplexing for electrical impedance tomography, and time-aligned ECG/PPG inputs for multimodal studies. Emphasis is placed on ease of use, portability, and functionality so that the platform can serve as a flexible system for future biomedical research.

2. **Investigation of excitation-signal strategies for accurate, low-distortion measurement**. To maximise measurement fidelity, the work focuses on excitation signal generation, with particular attention to binary and PWM-based sources that simplify circuitry while suppressing total harmonic distortion. Experimental comparison of waveform linearity, spectral purity and implementation complexity informs design rules for selecting or synthesising optimal stimuli in portable systems.

3. **Development of efficient signal-processing techniques for physiological feature extraction**. The third task explores analog and digital methods to filter, differentiate and interpret noisy bioimpedance waveforms. This includes front-end filtering to remove motion, baseline and power-line artefacts, robust calculation of the first derivative of thoracic impedance; and automatic detection of key fiducial points (B, C, X) that enable beat-to-beat estimation of pre-ejection period, left-ventricular ejection time, stroke volume and cardiac output. Special attention is given to low-power analog solutions that off-load processing from the microcontroller.

In Table 1, the mapping of the research tasks onto the publications is depicted.

Methods, tools and initial resources

In this thesis, a heuristic workflow was followed: rapid prototypes were built and repeatedly refined, while key choices such as filter parameters, software variables tied to hardware utilization, and timing were optimized numerically. The work drew on several core resources:

- **Heritage work**: The author's MSc thesis, *"DSP-Based Impedance Spectroscopy Device"* [53], together with the research group's earlier *"Quadra-1"* [54] impedance measurement device, supplied essential know-how.

- **Design tools**: Code Composer Studio, Arduino IDE, C/C++, Assembly, Python and R for data analysis; PCB layouts were drawn in EAGLE; different editorial tools are used for diagrams generation, figures formatting and text editing.

- **Instrumentation**: Wayne Kerr 6500B precision impedance analyser, Hewlett-Packard 34401A 6½-digit multimeter, Keysight InfiniiVision MSOX2014A mixed-signal oscilloscope, National Instruments USB-6215 DAQ module, Digilent Analog Discovery 2 USB oscilloscope/logic analyser.

- **Literature review**: IEEE Xplore, PubMed and Google Scholar supplied primary sources on bioimpedance instrumentation, excitation signal generation and signal processing.

Table 1: Research tasks, supporting publications, and specific contributions

Task	Relevant Publications	Contribution Summaries
RT 1: Custom multifunctional impedance measurement device	II, V, VI, VII	Three-generation DSP platform; dual-channel magnitude/phase read-out (1–200 kHz); 32-electrode MUX for EIT; integrated ECG/PPG front-ends; wireless comms; bench & *in-vivo* validation
RT 2: Excitation signal design	IV, IX	Alternative method for low-THD binary PWM excitation generation; microcontroller-friendly implementation
RT 3: Signal processing and feature extraction	I, III, VIII	Savitzky–Golay (SG)/frequency response (FR) derivative filters for low-noise ICG; low-power analog B, C, X detector for real-time beat-to-beat pulse ejection period (PEP) and left ventricular ejection time (LVET) estimation

Novelty and contribution

This research delivers both instrumentation advances and methodological innovations in the field of biomedical impedance measurement.

- **Versatile three-generation DSP platform**. Three prototype devices based on the TMS320F28379D DSP have been developed. The latest iteration combines programmable PWM/DAC excitation, dual-channel magnitude–phase read-out, a 32-electrode EIT multiplexer, and synchronous ECG/PPG capture. With open hardware and firmware, every signal path and algorithm can be reconfigured, making the platform a flexible test-bed for new biomedical-impedance techniques and enabling the first ethics-approved thoracic EIT images recorded with in-house hardware (TAIEK decision 1385).

- **Level-quantised binary excitation signal with low total harmonic distortion (THD)**. A new method is proposed to convert a sine wave used for the excitation signal into a compact binary sequence with minimal harmonic distortion, which can be generated by a standard microcontroller PWM. This innovation is the subject of a patent application (Appendix VIII, [8]).

- **Low-power analogue fiducial points detector**. A low-power analogue circuit is proposed to capture ICG fiducial points in real time, relieving the DSP and extending wearable battery life. This innovation is the subject of a patent application (Appendix IX, [9]).

Approbation and communication

The results have been shared through

- conference presentations at **I2MTC** - International Instrumentation and Measurement Tehnology Conferece (2022, 2024, 2025), **BEC** - Baltic Electronics Conference (2023), **IWoEDI** (2022) - International Workshop on Embedded Digital Intelligence.

- the TalTech **Deep-EST Spin-off 2022** programme (*"Next-Generation Holter"* concept).

- discussions with clinicians at **Tartu University Hospital**.

- a demo booth at the TalTech **Innovation Festival 2025**.

Thesis organization

The remainder of this thesis is organised as follows: Chapter 2 describes the three generation hardware platform alongside the associated publications; Chapter 3 discusses excitation-signal generation, including the proposed PWM scheme; Chapter 4 details the signal-processing solutions, from filtering to fiducial points detection; and Chapter 5 summarises the key findings and outlines future work.

Altogether, **five conference papers**, **two peer-reviewed journal articles**, **two patent applications** and an **ethics-approved human study** attest to the academic and practical impact of the research.

2 Development of Impedance Measurement Solutions

This chapter is based on a series of publications describing the development of three generations of bioimpedance devices: the first-generation system introduced in [2] (Appendix II), the second-generation platform described in [5] (Appendix V), and two conference papers on the third-generation device [6, 7] (Appendices VI and VII).

Various methods exist for measuring and calculating the impedance of an unknown object, including AC bridges, phase-sensitive detectors, direct measurement with an oscilloscope, automated frequency response analysis, and synchronous detector based impedance measurement systems [55].

A typical schematic of a synchronous impedance measurement system—including a signal generator, in-phase (sine) and quadrature (cosine) reference signals, a reference resistor for current conversion, a multiplier (mixer), and low-pass filters—is shown in Fig.1. Excitation signal generation is discussed in Chapter 3 and filters in Chapter 2, while this chapter focuses on system-level design.
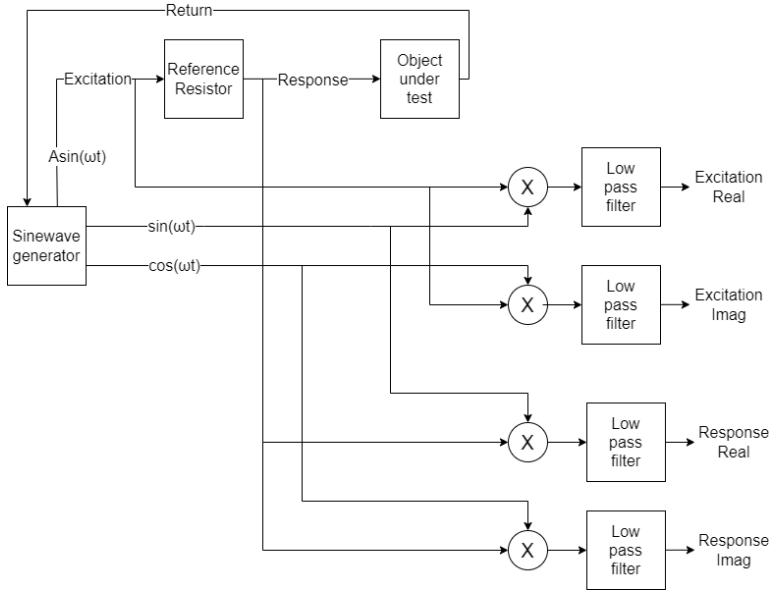

Figure 1: Typical impedance measurement system diagram

The complex impedance value can be represented in either cartesian form, using real (resistive) and imaginary (reactive) components, or in polar form, with magnitude and phase. Quadrature demodulation involves multiplying the measured voltage signal by two orthogonal reference signals, in-phase cosine and quadrature sine, both synchronized with the excitation current. The resulting signals contain both DC and high-frequency components, which require low-pass filtering to remove undesired harmonics. Note that, various parts of such system can be implemented both in analog or digital domains.

Impedance can also be determined by directly measuring the magnitude using a peak detector and extracting the phase delay with phase detectors. Several studies have explored this approach [56]. In polar demodulation technique, reference resistor in series can be used to extract timing information. Polar demodulation is particularly advantageous in frequency sweep applications, as it eliminates the need for generating synchronous reference signals. This is especially advantage over digital demodulation sys-

tems, where storing high-resolution reference waveforms for multiple frequencies would require significant memory resources.

2.1 Existing Devices and Integrated Circuits

Several portable bioimpedance measurement devices have been developed on DSP, micro-controller, or Field-Programmable Gate Array (FPGA) platforms.

Vargas et al.[57] presented a mobile, low-cost, 4-terminal bioimpedance system based on a Red Pitaya FPGA board and a front-end, evaluated across $1\,\Omega$ to $1\,\mathrm{mega}\Omega$ and 10Hz to 1MHz. The system uses a 14-bit, 125MS/s DAC and ADC with 50MHz low-pass filtering, achieving accuracy better than 2%, and standard deviations in magnitude and phase of less than 0.02% and 0.47%, respectively. The software supports both single- and multi-frequency real-time measurements, with single-frequency acquisition taking about 72ms and multi-frequency (five points) taking 200 ms.

Kusche et al. [58] developed a dual-channel bioimpedance spectrometer for muscle contraction detection, using time-multiplexing for dual-channel measurements and mul-tifrequency excitation (8 frequencies in the range of 20–230 kHz) per channel. Arbitrary current excitation waveforms are generated by a microcontroller (ATSAM4S2BA) with an integrated 12-bit, 1 MHz DAC. The system, built around a custom analog front-end (in-cluding ATSAM4S2BA) and a Teensy 4.1 microcontroller, records 25 spectra per second per channel. Phantom tests showed statistical errors below 1% in magnitude and 0.4 degrees in phase.

A notable commercial example is the handheld SFB7 bioimpedance spectroscopy unit [59] from ImpediMed (Australia), which features a tetrapolar, single-channel configuration and rapidly sweeps 256 frequencies from about 3kHz to 1 MHz. It is designed to estimate body composition metrics, including total body water and fluid distribution.

Another commercial example is the DSP-based Quadra [60] by Eliko (Estonia), which employs a binary excitation signal and a 12-bit ADC to enable simultaneous measurements at 15 frequencies with a sampling rate of 1 kHz. This device has validated applications in identifying non-ferrous metal alloys, medical diagnostics in cardiology, and meat quality measurement in food technology.

Integrated Circuits

Several integrated circuits are also designed for impedance measurement applications.

One widely used example is the Analog Devices **AD5933**[14], a high-precision imped-ance converter with a built-in frequency generator and a 12-bit, 1MSPS (million samples per second) analog-to-digital converter (ADC). The AD5933 simplifies impedance mea-surement by integrating key functions such as excitation signal generation, response mea-surement, and digital processing.

Another available integrated circuit (IC) is the Analog Devices **AD5940**[61], a low-power analog front end designed for portable impedance measurement applications, including bioimpedance and electrochemical sensing. The AD5940 offers two high-precision ex-citation loops capable of generating signals from DC to 200 kHz and a 16-bit, 800 kSPS multichannel ADC with programmable gain amplifiers for accurate signal acquisition. It features a programmable switch matrix that allows flexible connections between external pins and internal circuits, such as the high-speed DAC excitation amplifier and the invert-ing input of the transimpedance amplifier, making it flexible for high-accuracy impedance measurements in compact and low-power designs.

The Maxim Integrated **MAX30001** [62] is another commercially available, low-power

analogue front-end that combines biopotential (ECG) and bioimpedance (BioZ) acquisition for wearable applications. It offers a single ECG channel for waveform capture, heart-rate monitoring and pacemaker-edge detection, and a dedicated BioZ channel for respiratory-impedance measurement. Both channels feature IEC-compliant ESD protection, on-chip EMI filtering, lead biasing, DC lead-off detection and calibration voltages for built-in self-test. The BioZ path includes a programmable current source and supports two- or four-electrode configurations, delivering $17\,\mathrm{bit}$ ENOB with $1.1\,\mu V_{\mathrm{P-P}}$ noise while dissipating only $158\,\mu W$. A high input impedance exceeding $1\,\mathrm{G}\Omega$ enables two-electrode measurements.

Fully integrated SoCs that combine several physiological modalities also exist. Song *et al.* [63] present a $55\,\mathrm{nm}$ Bluetooth-enabled device that merges ECG, BioZ and PPG read-outs with an on-chip Cortex-M4F processor and hardware accelerators; the complete platform averages only $769\,\mu W$. In a similar $55\,\mathrm{nm}$ CMOS implementation, Shu *et al.* [64] realise a compact ($\approx 3\,\mathrm{mm}^2$) analog front-end (AFE) supporting PPG, ECG and BioZ. The BioZ path employs direct-digital-synthesis to deliver sine-wave stimulation from $1\,\mathrm{kHz}$ to $128\,\mathrm{kHz}$ and uses active shielding to suppress parasitic capacitance.

Overall, the commercial and research trend is toward ever more capable single-chip solutions that achieve impressive noise and power figures, yet their fixed architectures, lack of synchronization signals, and limited firmware access restrict algorithm-level experimentation and orchestration required for impedance tomography, as well as integration with other biomedical measurement modalities such as ECG and PPG.

2.2 Electrical Impedance Tomography

Electrical impedance tomography is an imaging technique that reconstructs internal conductivity distributions from surface electrode measurements, enabling the observation of physiological processes and detection of tissue contrasts indicative of underlying conditions [65]. For instance, cancerous and ischemic tissues exhibit altered impedance spectra, which can serve as diagnostic markers [66, 67]. Additionally, functional contrasts, such as those caused by the movement of fluids and gases during respiration, blood flow, and digestive activities, further enhance EIT's utility in clinical diagnostics [68, 69].

It is possible to reconstruct conductivity distributions from a single set of measurements using a technique called absolute EIT. However, this method is highly sensitive to modeling inaccuracies [69]. Time-difference EIT, which requires two sets of measurements (a homogeneous baseline and an absolute measurement), is less susceptible to static interference, making it ideal for applications like ventilation monitoring [69]. Alternatively, frequency-difference EIT can be used when it is not possible to obtain homogeneous data. This approach employs multiple excitation frequencies, allowing for the detection of frequency-dependent changes in tissue conductivity [68].

In EIT, data collection is influenced by the choice of current excitation and measurement patterns. Common patterns include adjacent, opposite, and trigonometric configurations, each of which affects reconstruction quality differently [70, 71]. Optimization of electrode placement and current patterns has become an area of interest, with machine learning models offering potential improvements in spatial resolution and image quality [72]. While traditional patterns such as the adjacent method are still widely used, they have been shown to introduce inaccuracies compared to more advanced techniques [73]. Optimizing these patterns, together with advancements in electrode placement strategies, can significantly enhance EIT's overall performance [74].

Numerous EIT systems design have been documented in the literature. For example,[75] proposes an analog modulator using the AD630ADZ with a 50kHz fixed excitation fre-

quency. The system is open source, with an approximate frame rate of 0.5 Hz. A potential issue is the long integration period required by the low-pass filter after analog demodulation. Additionally, only one reference signal is used—there is no quadrature component and therefore no complex impedance value is obtained.

In [76], the authors present a low-cost EIT system using the AFE4300 IC with an ESP32 controller, with a total cost of US $49.17. The setup features four rings of eight electrodes (pseudo-3D), and supports both Bluetooth and USB connections via the ESP32. System evaluation was performed by measuring global impedance (the sum of pixel values in a frame, which should be linear with changes in conductivity). Only the modulus of impedance was used, obtained via full-wave rectification (i.e., not capturing the complex value—no phase or quadrature demodulation). The system does not operate in real time, as measurements were taken and later processed manually in MATLAB.

In [77], the use of active electrodes is proposed. Each electrode includes an instrumentation amplifier that is connected to its neighboring electrodes, and there is only one readout track. With a summing amplifier at the end of the readout track, it is possible to obtain the voltage difference between any two electrodes. Selection of current source and voltage measurement electrodes is managed using five analog switches per electrode. As a result, the design achieves high common-mode rejection ratio (CMRR) and simplifies cabling, albeit at the expense of more complex electronics for each electrode.

Yang et al.[78] describe a DSP-based EIT system that includes components such as a digital signal processor, a direct digital synthesizer for excitation signals, amplifiers, filters, and a multiplexer for electrode switching. The study highlights the limitations of fixed-gain amplifiers in handling varying signal amplitudes across different electrode pairs, which impacts measurement accuracy. To address this, the authors propose dynamically adjusting the gain of programmable amplifiers to enhance the signal-to-noise ratio (SNR) and reduce image error. Their results show a reduction in SNR variation from 26.42dB to 6.33 dB and a decrease in maximum image error from 28.17% to 15.60%, demonstrating the effectiveness of the adaptive approach.

In [79], the authors propose a wideband electrical impedance tomography system. The hardware consists of a direct digital synthesizer for signal generation, a dedicated ADC chip for signal acquisition, an AD8302 gain/phase detector IC to obtain impedance values, and a channel selection unit to multiplex electrodes, all integrated with a microcontroller and PC.

There are also several commercial EIT products, including the scalable Sciospec EIT32 [80] platform for general EIT applications, and specific lung-imaging system LungEIT [81] by ScioSpec (Germany), Lumon EIT [82] by Sentec (Switzerland/USA), and PulmoVista [83] 500 by Draeger (Germany).

To sum up, EIT devices have become increasingly advanced and accessible over the past decade, as evidenced by the growing number of research prototypes and commercial products adopted in research and clinical practice, although open-source designs remain limited [32], restricting flexibility for researchers who require access to hardware, firmware, and raw data for developing and validating new methods.

2.3 Implementation of DSP-Based Devices

Newer, more advanced DSPs offer enhanced peripheral units, including improved resolution (e.g., 16-bit instead of 12-bit high-speed ADC), higher digital clock rates, and dual DSP cores. These advancements present new opportunities for simple and low-cost impedance measurement devices by enabling real-time Discrete Fourier Transform (DFT) calculations for higher frequency content signals.

Rationale for Selecting the *C2000* DSP / LaunchPad Platform

A digital signal processor was chosen instead of a low-power microcontroller to meet the demands for accurate, broadband, and high-speed impedance measurements. Among the available options, the Texas Instruments C2000 series *TMS320F28379D* was selected. Key features of the *TMS320F28379D* are summarized below:

- **Dual 200 MHz 32-bit C28x cores** two parallel MAC engines. At a single tone the impedance algorithm requires four real-time MAC paths (real + imaginary for both excitation and response); one CPU can service a channel while the second CPU handles additional communications with external sensors.

- **On-chip 16-bit ADCs** (4 × 1.1 MSPS, differential inputs) enable simultaneous sampling of drive and sense voltages with direct memory access (DMA) off-loading, eliminating external converters.

- **Rich mixed-signal peripherals** : 24 ePWM channels for binary/PWM excitation and three 12-bit DACs.

- **High-speed DMA and ePIE interrupt controller** guarantee sub-μs latency between ADC triggers and DSP computation.

- **LaunchPad availability and cost** : the *F28379D* LaunchPad combines all silicon options (dual-core, full analogue set) on a \$69 board.

Digital synchronous detection is realised as a discrete Fourier transform: every incoming sample is multiplied by pre-computed $\sin$ and $\cos$ values and the products are accumulated to obtain the in-phase and quadrature terms. Each ADC sample therefore consumes *four* MAC operations (two for the response and two for the simultaneously sampled excitation needed for accurate voltage and current measurement). The TMS320F28379D executes two MACs per 200 MHz clock cycle, i.e. $200\,\text{MHz} \times 2 = 400\,\text{MMAC/s}$. At a 1 MSPS sampling rate a single tone costs $4\,\text{MAC} \times 1\,\text{MSPS} = 4\,\text{MMAC/s}$, so one core could, in principle, demodulate about $400/4 \approx 100$ frequency bins. Practical limits are lower: dual-MAC instructions share the same data path, some overhead is incurred in loop control, and the total excitation amplitude must be kept within biomedical safety margins, which constrains the number of simultaneous tones before signal-to-noise substantially degrades. Nevertheless, the chosen DSP comfortably supports multi-tone demodulation for 1 MHz sampled data.

Figure 2 shows a simplified internal block diagram of the TMS320F28379D DSP system, highlighting the CPU and key peripherals relevant to the impedance measurement device. For clarity, only one of the two CPU cores is shown; however, the actual TMS320F28379D features a dual-core architecture, with the second core (CPU2) having identical RAM and FLASH resources. The depicted peripherals—such as ADC, DAC, DMA, and communication interfaces—can also be assigned to CPU2, which has its own dedicated data buses and DMA controller.

These capabilities—dual-MAC hardware, four simultaneous 16-bit ADCs, abundant PWMs and DACs, and high-speed DMA—directly satisfy the first research objective by delivering the accuracy, parallel throughput, and peripheral versatility needed for a fully reconfigurable, multifunctional impedance-measurement platform within a single open-hardware environment.
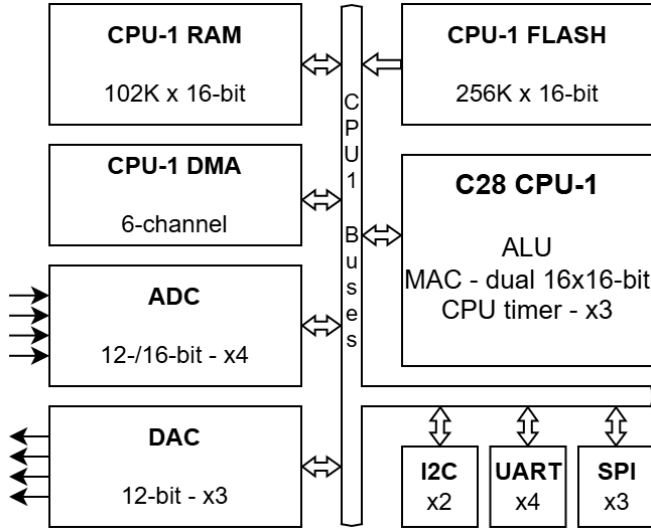
Figure 2: Functional block diagram of TMS320F28379D

The first prototype

A series of impedance measurement devices were developed based on the Texas Instruments TMS320F28379D dual-core DSP, progressing through successive iterations to improve measurement accuracy, expand signal modality support, and enable more advanced applications such as electrical impedance tomography (EIT). The first prototype (Appendix II, [2]), shown in Fig. 3, was created to explore synchronous demodulation techniques for impedance measurement on the chosen DSP platform. It employed a modular analogue front-end mounted directly on the DSP LaunchPad and used screw-terminal for connecting electrical components. The conference paper evaluates the device through several metrological tests.

- **Repeatability.** Three resistors (1, 10, 100 kΩ) were measured repeatedly at 1, 10 and 100 kHz; repeatability results are reported in Table 1 of the paper.

- **Dynamic emulation.** A cardio-respiratory impedance phantom developed in earlier work [84] verified that the device reliable captures respiratory and cardiac modulations.

- **Capacitive load.** To verify complex-impedance value (magnitude and phase) measurement capability, a capacitive load was measured at 10 kHz; the results closely matched those obtained with a reference instrument.

- **Fine-step resistor box.** Six incremental values around 11 kΩ (10.000, 11.000, 11.100, 11.110, 11.111 kΩ) were acquired after a simple distant two-point calibration; Fig. 4 (adapted from Fig. 6 of the paper) shows errors under 1 Ω at 11.111 kΩ, i.e. $< 0.01\,\%$ relative.

Presented at the 2022 18th Biennial Baltic Electronics Conference (BEC), this first prototype achieved measurement errors below 0.01 % within its limited operating range, confirming the feasibility of precise impedance acquisition using a DSP-based system.

Figure 3: Photo of the first-generation DSP-based impedance measurement prototype, developed during this PhD work.
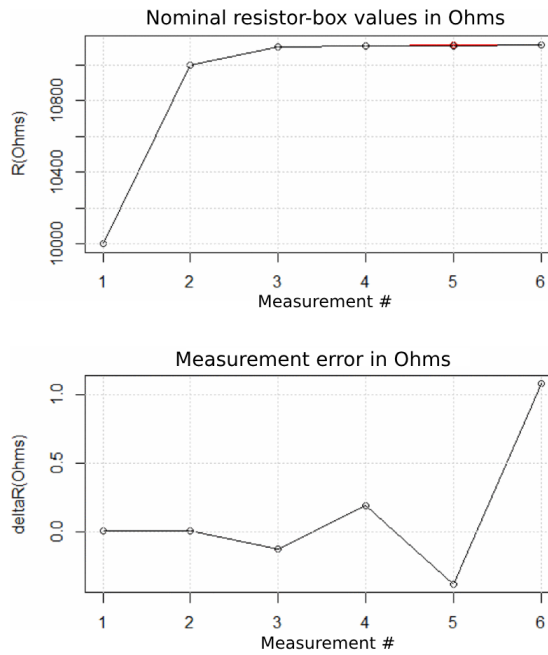

Figure 4: Accuracy assessment of the first prototype with metrological resistor box (adapted from Fig. 6 in [2]). Top: measured resistance steps (10–11.111 kΩ). Bottom: corresponding absolute errors, all below 1 Ω.

The second prototype

The second-generation platform (Appendix V, [5]) extends the concept to multi-modal acquisition. Figure 6 [5] recaps the hardware architecture, Figure 7 [5] the dual-CPU firmware and Figure. 8 [5] the Python GUI used for real-time visualisation. Like the first prototype, its metrological performance was verified by repeatability tests, fine-step resistor-box sweeps, dynamic emulation and a capacitive load tests.The measured magnitude errors remained below 0.002% throughout the operating frequency range. A photo of the device with attached electrodes is shown in Figure 5. Further figures, evaluation procedures, and detailed result tables are provided in the paper. Improvements over the first-generation design are listed below:

- **Four-electrode impedance acquisition** via a 1.5 mm DIN socket that is shared with the ECG leads.

- Integrated 16-bit ADCs stream **EBI/ICG, ECG and PPG** simultaneously at 1 kHz, enabling direct multimodal data fusion.

- **Battery operation** with an isolated USB interface for safe charging and biomedical use.

- **Graphical User Interface** for real-time waveform display, logging and configuration (frequency selection, impedance-calculation mode, filter control).

- **Built-in signal-processing** options: Median filter and a moving-average filter for power-line suppression; the resulting waveforms are illustrated in Figure 8.

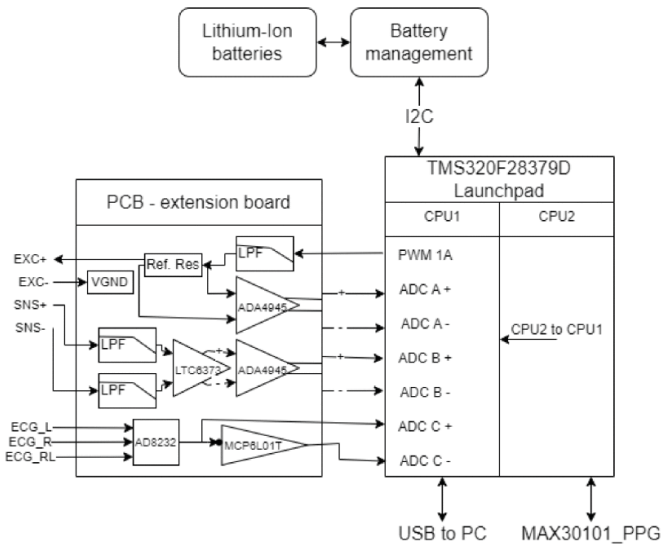*Figure 5: Photo of the second-generation DSP-based EBI, ECG, and PPG device*

Figure 6: System block diagram of the second-generation platform (adapted from Fig. 2 in [5]).
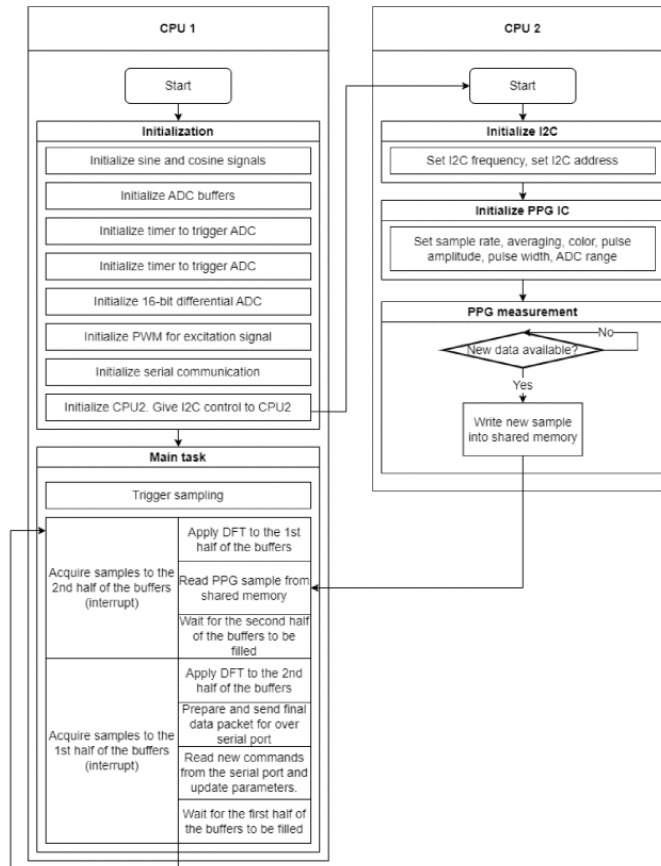

Figure 7: Firmware flowchart of the second-generation platform (adapted from Fig. 4 in [5]).
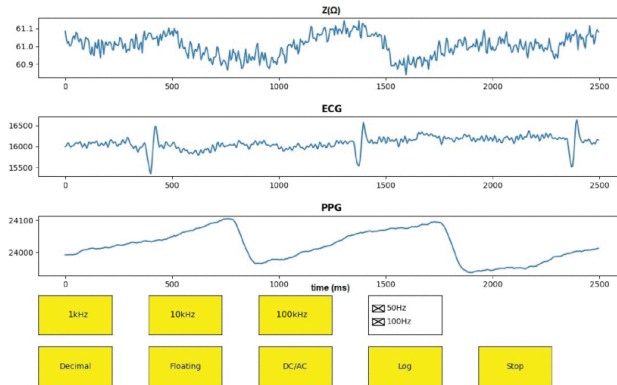
Figure 8: Python GUI of the second prototype used for real-time display and logging of EBI, ECG, and PPG signals (adapted from Fig. 5 in [5]).

In summary, the second-generation platform provides high-precision four-electrode bioimpedance measurement with time-aligned ECG and PPG acquisition in a portable, battery-powered form factor; its design, validation and application examples are detailed in a full journal article published in *IEEE Transactions on Instrumentation and Measurement*, Vol. 72.

The third prototype

The third prototype extends the platform from single-point impedance measurements to EIT while still acquiring ECG and PPG in synchrony. Its hardware has been improved: multiplexers route both excitation and response signals, PGAs widen the dynamic range, and an on-board DAC complements the PWM source with true analogue excitation. To handle the larger quantity of control signals, shift registers are used. The new layout is shown in Fig. 9 [6], and a photo of the assembled unit with its custom electrode belt is shown in Fig.10. Key enhancements over the second-generation device include:

- **32-electrode multiplexing** for tomographic imaging.

- **Dual-channel measurement**—two impedance channels are sampled simultaneously at 1 kHz, enabling pulse transit time measurements.

- **Two measurement modes** (Fig. 11) [6]: simpler *reference-resistor* mode and *transconductance amplifier* mode that enforces IEC-compliant current—preferred for biomedical use

- **Wireless interface**. An on-board ESP32 streams real-time data over wireless fidelity (Wi-Fi) or Bluetooth while the USB port remains galvanically isolated for bench work.

- **Extended frequency span**. 1–200 kHz operation with finer frequency steps.

- **Programmable gain amplifiers** (0.25x–16x) to sustain accuracy over wider measurement range.

The technical evaluation of this latest device as a multifunctional dual-channel impedance measurement system including repeatability tests and capacitive-load tests capacitor test
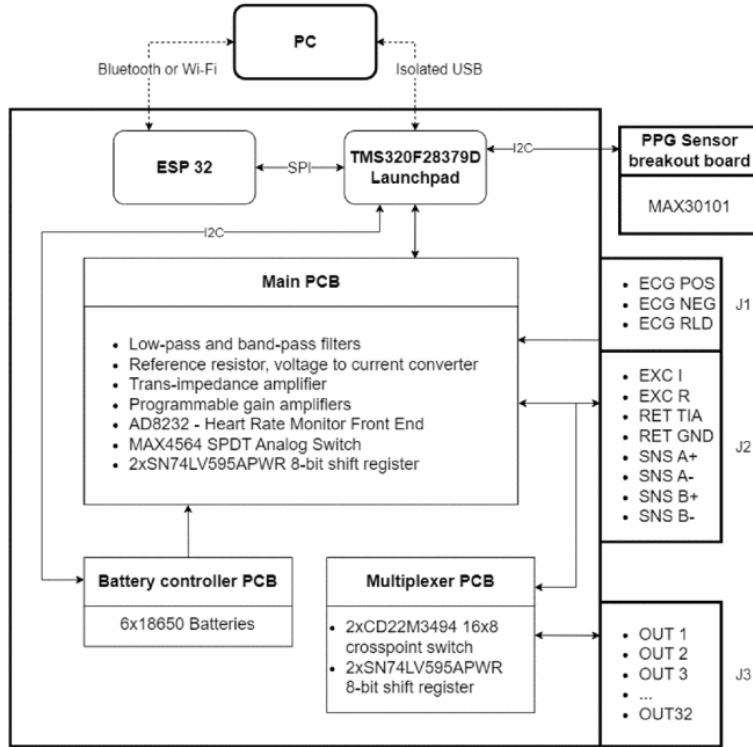
Figure 9: Block diagram of the third generation device (adapted from Fig. 5 in [6]).
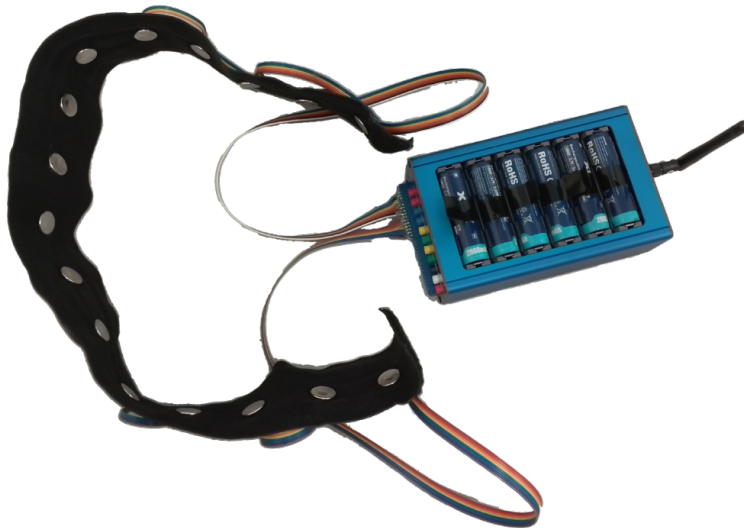

Figure 10: Photo of the third-generation DSP-based EIT device with tomography belt connected to the multiplexer output
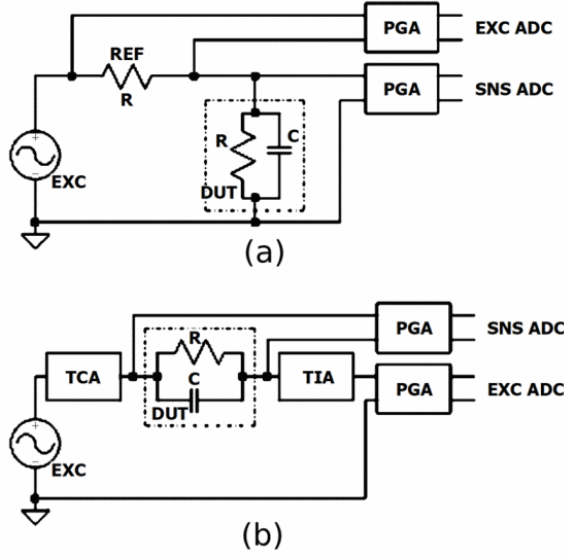
Figure 11: Two impedance-measurement modes implemented on the main PCB (adapted from Fig. 6 in [6]). Top: reference-resistor mode; bottom: current-source mode.

is reported in Appendix VI, [6], presented at the 2024 IEEE International Instrumentation and Measurement Technology Conference (I2MTC).

The follow-up study, included as Appendix VII and presented at the 2025 IEEE International Instrumentation and Measurement Technology Conference (I2MTC) [7], examines the EIT capability of the third-generation platform. The paper describes a EIT measurement routine that injects current through a 16-electrode setup, records differential voltages, and reconstructs conductivity maps at 2 fps. Table 2 (adapted from [7]) compares the device with other recent open-source or low-cost EIT instruments, highlighting its 1–200 kHz frequency span, magnitude–phase read-out, and competitive SNR. Image quality was benchmarked with three standard metrics proposed by Yasin *et al.* [85]—amplitude response, resolution, and detectability—reported in the paper for several target positions. These results provide a quantitative view of spatial fidelity and contrast under controlled conditions. Subsequently, following the approval of the Estonian ethical committee TAIEK (decision number 1385), the device was used for non-invasive lung visualization in human subjects. Figure 12 presents a representative EIT image obtained using the developed device and electrode belt. It depicts the reconstructed conductivity difference between the empty and full lungs, based on both time and frequency difference EIT data. The results indicate similar air filling in both lungs, as expected. One observed limitation was inconsistent electrode contact with the skin. Another factor affecting reconstruction accuracy is the use of a generic thorax shape, which could be improved in the future by detecting patient-specific belt geometry using camera-based methods.

The three DSP-based prototypes progressively addressed the first research task, evolving from a single-channel EBI unit into a portable multimodal platform and ultimately into a 32-electrode EIT system that maintains high-accuracy magnitude and phase measurements across 1–200 kHz.

Table 2: Comparison of EIT devices [7]

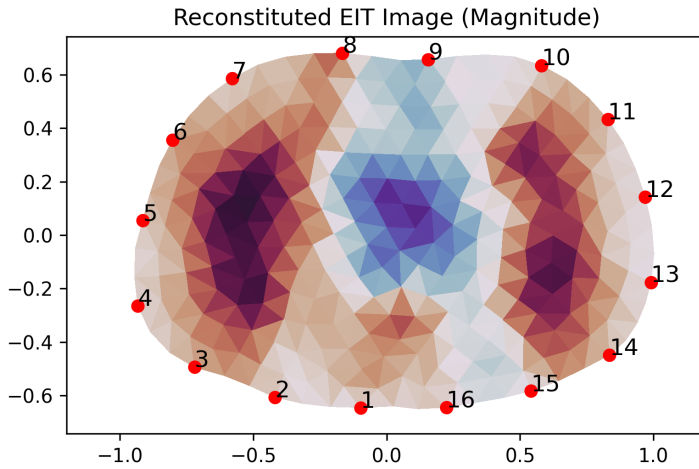| Feature	Analog Modulator System [75]	Wearable EIT System [32]	AFE4300 EIT System [76]	FPGA EIT System [86]	DSP EIT System (This Work)
Controller	AD630ADZ	Teensy	ESP32	Altera Cyclone V SoC	TMS320F28379D
Cost	N/A	$260	$49.17	N/A	$200
Excitation Frequency	50 kHz (fixed)	Configurable	1kHz–50 kHz	2 kHz–500 kHz	1 kHz–200 kHz
Frame Rate	0.5 fps	up to 25 fps	50 fps	0.5 fps	2 fps
SNR	60.6 dB	36 dB to 63 dB	N/A	89 dB	78.4 dB
Connection	Wired	Wired	Bluetooth, Wired	Wired	Bluetooth, Wired
Impedance Measurement	Magnitude only	Magnitude and phase	Magnitude only	Real part only	Magnitude and phase
Application Focus	Biological phantom	Lung monitoring	Body composition	Skin sodium	Biomedical
Demodulation	Analog demodulation	Digital (Microcontroller-based)	AFE4300 IC	Digital (FPGA-based)	Digital (DSP-based)
Electrodes	16	16	32	16	32

Figure 12: Visualization of lung activity using the developed DSP-based EIT device and electrode belt (photo taken during human subject measurements approved by TAIEK, decision no. 1385)

3 Excitation Signal Generation

This chapter is based on prior work describing a novel PWM-based excitation technique for impedance spectroscopy, presented in a journal paper [4] (Appendix IV) and supported by a related patent application [9] (Appendix IX).

An essential component of any electrical impedance spectroscopy and bioimpedance measurements systems is the excitation signal. These devices demand compact, low-power excitation signal generators with high precision and flexible frequency control. Excitaion signal, which can be either a single frequency or multifrequency is applied to the system or material under investigation. The waveform of the excitation signal is chosen based on the specific needs of the measurement and can vary among several types, such as sine waves, square waves, multi-sine waves, or chirp signals.

Different waveforms are employed in diverse scenarios to best match the measurement requirements:

- **Sine wave:** Often used for examining the impedance at a single frequency, providing a focused analysis of the material's characteristics.

- **Square wave:** Preferred for their simplicity in implementation, square waves facilitate clear time-domain analysis through their distinct high and low transitions.

- **Multi-sine wave:** Allows for the simultaneous examination of impedance across multiple frequencies, giving a comprehensive overview of the system's response in a single measurement cycle [87].

- **Chirp signal:** With its frequency varying over time, the chirp signal is advantageous for rapidly spanning a wide frequency range, making it efficient for broad-spectrum analysis.

Fig.13 illustrates these waveforms, demonstrating the specific applications of sine, multi-sine, square, and chirp signals in impedance measurements.

Excitation signals can also be classified as either binary or multi-valued (analog). Binary signals, such as those generated by Sigma-Delta modulation [88], linear feedback shift registers (LFSR) [89], or pulse-width modulation (PWM), offer advantages in terms of simplicity, noise immunity, and power efficiency. These signals require fewer components, making them suitable for applications where power and space are limited, like in multi-electrode arrays. Due to their digital nature, binary signals are also easier to distribute and multiplex between measurement channels. In contrast, multi-valued signals, like analog sine or multi-tone waveforms, provide more precise control over the signal's amplitude and deliver a higher SNR. However, they come with increased complexity, requiring DACs and additional circuitry, which can lead to higher power consumption and larger system size.

3.1 State of the Art

Excitation signals can be generated by DAC or Oscillator.

DAC-based generator

DAC-based waveform generation is a widely used method for EIS excitations and offers excellent frequency control. Modern implementations can cover multiple decades of frequency (from Hz to MHz) with precise tuning, limited mainly by clock stability [39]. However DAC-based systems can suffer from quantization noise and sampling errors. To mit-
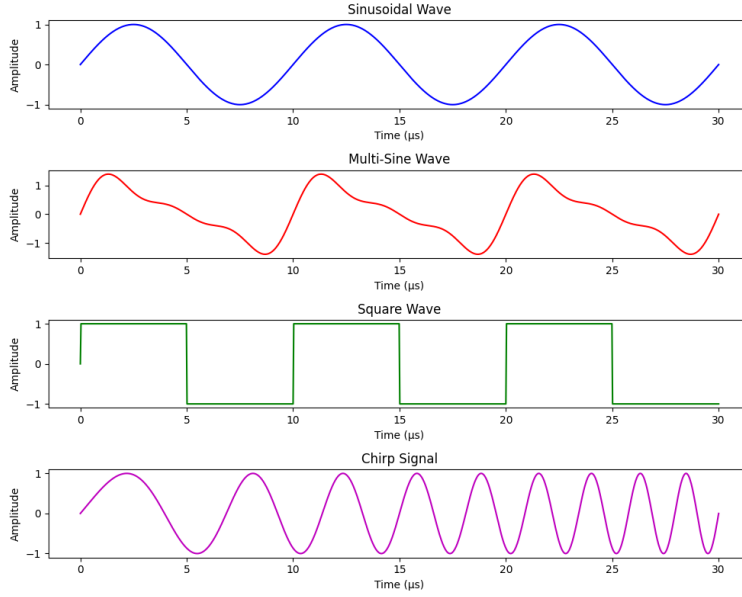
Figure 13: Different excitation signals

igate these, increasing the oversampling ratio (OSR) or the number of DAC bits is necessary, but this requires higher clock speeds or more circuit elements, which can increase power consumption or complexity. Sinusoidally tapped DACs can improve performance by reducing quantization error while maintaining the same number of DAC bits [90].

Alternatively, single-bit excitation can replace a multi-bit DAC with a fast two-level switch, encoding the desired analogue waveform in pulse density or width; square-wave, PWM, and delta–sigma bit-streams are the most common forms. Since the raw binary output carries substantial out-of-band energy, stringent low-pass filtering is essential [91, 92]. Delta–sigma modulation mitigates in-band quantisation error by pushing noise above the signal band, and can approach the spectral purity of multi-bit DACs [93].

It is also possible to use multifrequency binary signals for EIS. For example, [94] investigates the use of two types of multisine binary sequences to shorten measurement time. Sigma–delta modulated multisine sequences (SDMSs) and maximum length binary sequences (MLBSs) were both shown to be suitable for fast measurement and simple hardware integration. More advanced approaches have also been proposed. To reduce aliasing error, a model-based post-correction method was introduced in [48]. Another study [49] proposes multifrequency binary sequences based on evolutionary role-playing game theory for crest factor optimization, showing better performance than those obtained with chirp signals.

Overall, binary excitation is useful for simple, power- and cost-efficient devices, but the trade-off is a high oversampling ratio and, hence, increased clock speed, which limits practical use at higher excitation frequencies.

Oscillator-based generators

Oscillator-based systems do not suffer from quantization and sampling errors, but they often encounter challenges related to linearity and frequency precision due to variations in analog components [39]. Another limitation is that analog oscillators may require power-

hungry amplifiers for high frequencies, which is problematic for power-constrained wearables [39]. These systems are typically used in moderate frequency ranges, where they can balance power consumption and performance without requiring high-precision tuning. Wien-bridge oscillators, for instance, are commonly employed for generating signals up to 200 kHz.

In practice, some wearable impedance analyzers have used oscillators as the excitation source. Song *et al.* [95], proposed a tunable oscillator for a portable bioimpedance system, where a two-step frequency sweep sinusoidal oscillator is used to accurately identify the resonant frequency and minimum impedance within a given range. This method involves an initial coarse frequency sweep with 8 levels (frequency step of 9.4 kHz) over 10–76 kHz, followed by a fine analog frequency sweep over a narrower range of 18.9 kHz.

Similarly, [96] proposes a differential oscillator architecture using two operational transconductance amplifiers (OTAs) and an RC bridge network to suppress the second harmonic. By switching resistors and capacitors in the RC network, this approach generates four discrete frequencies: 10, 50, 100, and 200 kHz.

3.2 Novel PWM Solution

Among the publications underlying this thesis, the conference paper reproduced in Appendix IV [4] introduces an improved pulse-width–modulation scheme that converts a target sinewave into a sequence of binary pulses. Compared with conventional PWM the method lowers THD while remaining much sparser than a delta–sigma bit-stream.
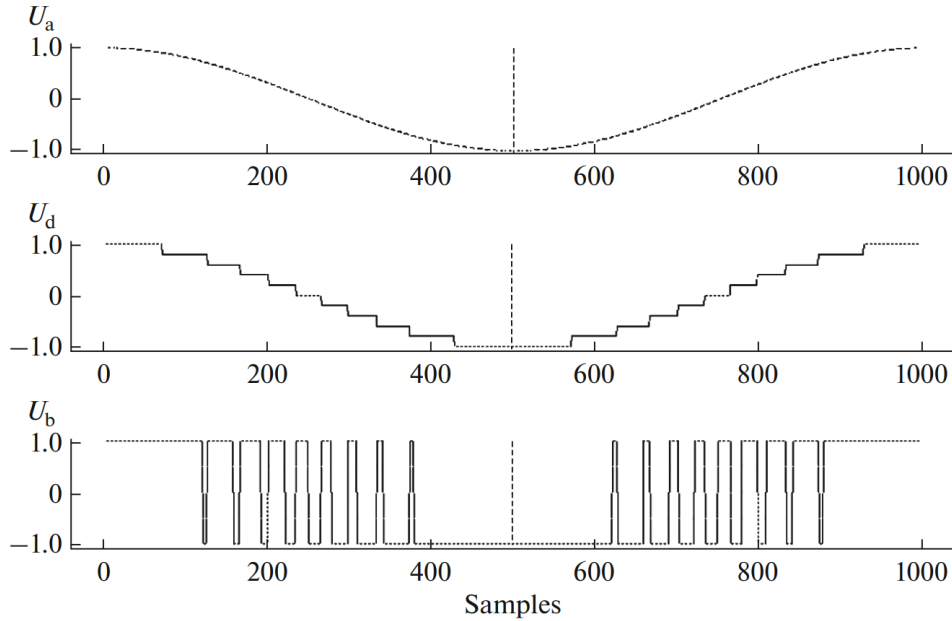

Figure 14: *Working principle of the quantised-level PWM. A sine period is first uniformly quantised; each segment is then rendered as one binary pulse whose duty cycle equals the segment's mean value (adapted from Fig. 4 in [4]).*

The proposed algorithm can be summarized in two steps:

1. **Quantisation:** the analogue template is sampled into M equal amplitude levels.

2. **Duty-cycle encoding:** every quantised segment is mapped to a single binary pulse with matching duty cycle.

The proposed PWM bit-stream can also serve as the lock-in reference in an impedance-measurement front-end. LTspice simulations (paper Figs. 9–10) illustrate a simple analogue demodulator that drives the sensor with the PWM excitation, feeds the same pattern to the multiplier as the reference signal, and thus demonstrates the feasibility of impedance read-out with the proposed method.

For a fair test the free parameter of each technique was swept at an oversampling ratio of 1:1000. The proposed method varies the number of quantisation levels M; classical PWM varies the number of samples per period N_s. Figure 15 (adapted from Fig. 5 in [4]) shows that the new scheme reaches its minimum THD of about 2 % at $M \approx 32$, whereas conventional PWM bottoms out near 4 % at $N_s \approx 75$. This reduction in THD is significant for impedance spectroscopy, as harmonic components fold into the baseband during demodulation, degrading accuracy. Lower THD minimizes such interference and improves measurement accuracy.
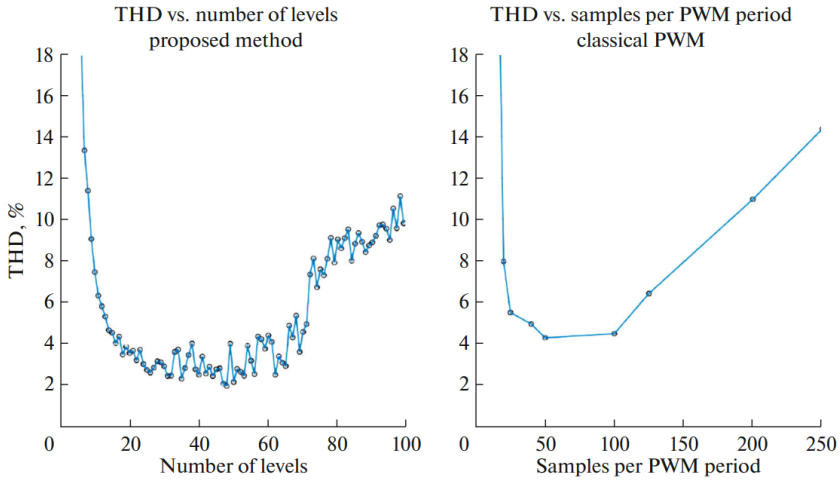

Figure 15: THD versus tuning parameter for (left) the proposed method and (right) classical PWM [4].

Figure 6 of the paper (not reproduced here) gives the corresponding time and frequency domain plots: the new PWM attains lower THD than classical PWM while using far fewer pulse edges than a delta–sigma stream—an advantage when the minimum pulse width of the microcontroller is limited. The paper also derives a formula that links the required number of levels to the shortest attainable pulse duration. Additional results, including harmonic optimisation across several frequency bins (10–70 kHz) and the effect of level count on THD, are provided in [4].

The study shows that the quantised-level PWM produces a sine-like binary signal with lower THD than classical PWM and far fewer switching edges than a delta–sigma bit-stream, hence offering a practical middle ground between the two methods and making it suitable for low-power, portable impedance devices. The same principle can be extended to multi-tone excitation without changing the algorithm and can be used for impedance spectroscopy applications.

4 Signal Conditioning and Feature Extraction for EBI

This chapter is based on prior works in signal processing for impedance cardiography, including a comparative study of two digital differentiator filters [3] (Appendix III), the development of a low-power analogue ICG fiducial points detector [1] (Appendix I), and corresponding patent application [8] (Appendix VIII).

Bioimpedance measurement systems rely on signal processing to extract small physiological signals from noisy measurements. This involves a combination of analog filtering at the front-end and digital filtering after demodulation, as well as techniques for feature extraction

Analog continuous-time filters play a crucial role in conditioning bioimpedance signals before digitization. bioimpedance is typically measured by injecting a small AC current and sensing the resulting voltage. Sometimes binary signals are used for excitation, which require filtering; similarly, for DAC output signals, a low-pass filter is needed to reduce quantization noise [91, 97]. Filtering is also necessary when reading the signal, since the raw signals contain a large carrier component, physiological modulations, and various noise or harmonics, including direct current (DC) electrode offset, stray capacitance in the environment [98], cross-talk [99], and so on. To handle this, the analog front-end usually includes band-pass filtering stages to isolate the desired signal band and reject out-of-band content.

After the analog front-end and demodulation, the bioimpedance signal undergoes digital processing. Digital filtering offers flexibility to further reduce noise, remove residual interference, and extract specific components of the signal. Commonly used digital filters in bioimpedance work include the Savitzky–Golay, median, moving-average, and Butterworth infinite impulse response (IIR) filters [100]. More advanced approaches have also been explored: wavelet-based denoising has shown improved performance [101], and beat-by-beat ensemble averaging can further suppress noise in cardiac recordings [36, 102].

4.1 Signal Filtering in the Proposed Device

In the latest version of the developed device, described in Appendix VI, careful attention was paid to the analog signal chain, particularly in terms of filtering the excitation signal. This is essential to ensure clean and spectrally pure current injection into the biological tissue, especially since DAC-based waveform generation can introduce harmonics and quantization noise.

To suppress high-frequency components and attenuate harmonics generated by the DAC, a two-stage active low-pass filter was implemented, as shown in the schematic in Fig. 16.

The frequency response of the excitation filtering path is shown in Fig. 17. The design ensures approximately flat gain of around 6 dB from 1 kHz to about 40 kHz, after which attenuation begins gradually, reaching around 4.7 dB at 200 kHz. This behavior effectively eliminates unwanted harmonics while maintaining a clean sinusoidal signal over the desired operating bandwidth of 1–200 kHz.

By proportionally reducing the capacitor values, simulations show that the -3 dB corner can be shifted to 1 MHz, enabling the same hardware to support applications that benefit from higher-frequency excitation.
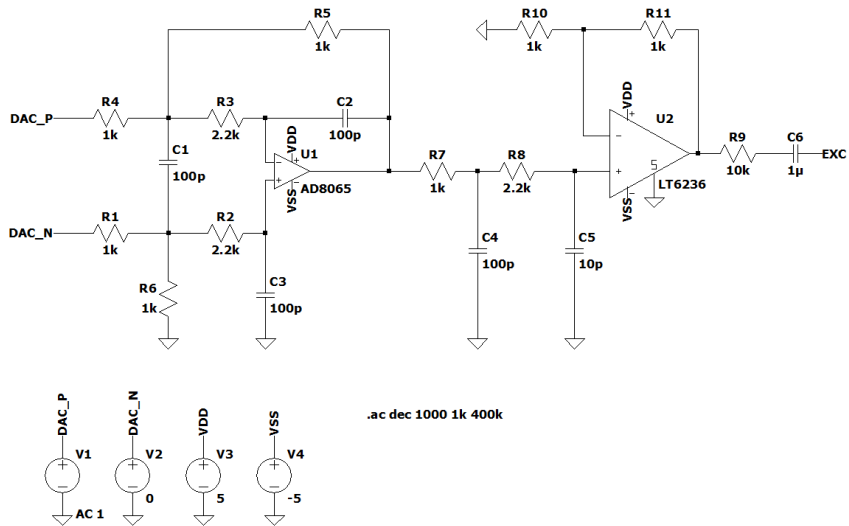
Figure 16: Schematic diagram of the excitation signal filtering stage in the latest impedance measurement device
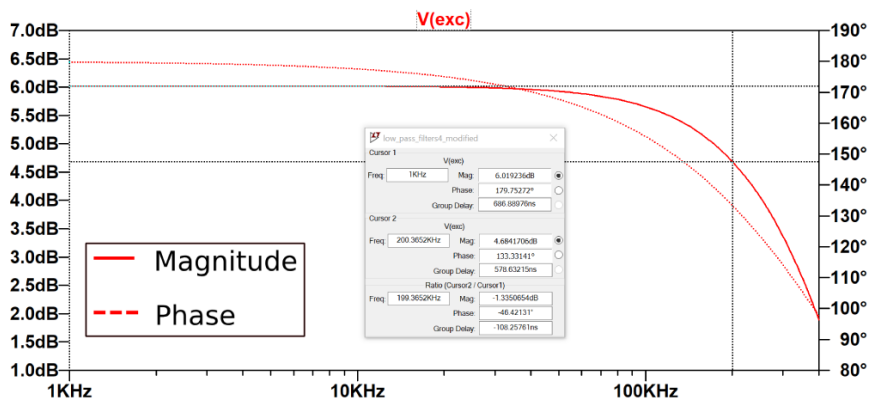

Figure 17: Simulated frequency response of the excitation signal filter showing magnitude and phase characteristics

4.2 ICG — Derivative of EBI

The impedance-cardiography waveform is the first time-derivative of the thoracic bio-impedance signal $Z(t)$ and therefore accentuates high-frequency noise [103]. Reliable estimation of dZ/dt requires a cascade of low- (or band-) pass filtering and numerical differentiation. Within the works supporting this dissertation, a conference article [3] presented in Appendix III, investigates two finite-impulse-response kernels designed to execute both tasks concurrently on uniformly sampled data:

- *Savitzky–Golay* (SG) kernel: local least-squares polynomial fitting is used to produce a smoothed first derivative;

- *Frequency-Sampling* (FS) differentiator: coefficients are obtained by sampling the ideal differentiator response below a chosen cut-off and setting the remaining samples to zero.

A Savitzky–Golay filter was configured with $N = 99$ coefficients, polynomial order $p = 3$, and first-order derivative setting $m = 1$, whereas the FS design, likewise using $N = 99$ taps, retained the ideal differentiator response $K = j\omega$ up to a cut-off frequency of $f_c = 5$ Hz.

ICG waveforms from a variety of electrode placements on the thorax (TEPC-1, TEPC-4) and wrist (AEPC-1 – AEPC-4) were analysed; detailed descriptions of electroce locations are given in [104]. Initial data for this paper were gathered with the DSP-based measurement device developed in this thesis.

Figure 18 reproduces one example (TEPC-1) from this paper [3]. Similar plots for the remaining locations are presented in the paper.
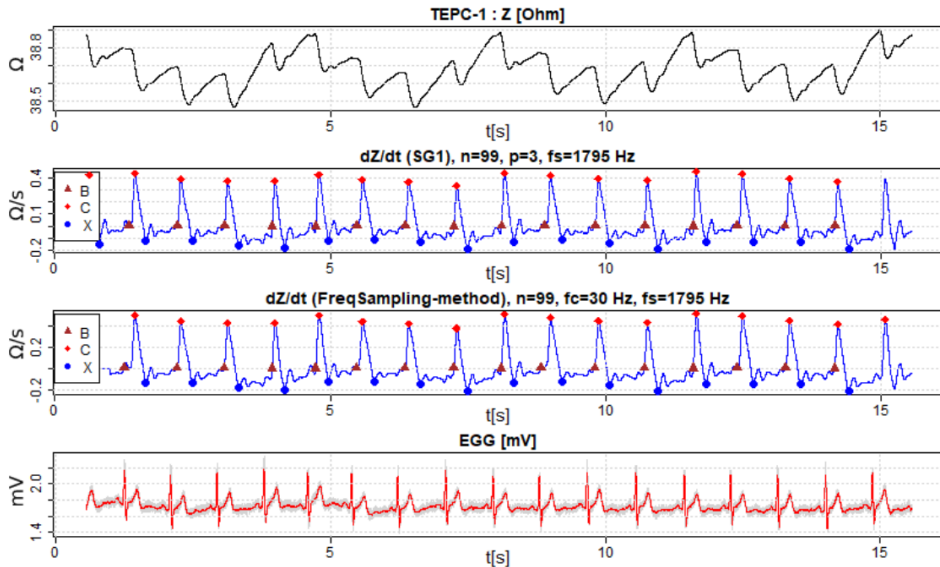
Figure 18: Example thoracic recording (TEPC-1). From top to bottom: raw impedance $Z(t)$; dZ/dt obtained with the SG kernel; dZ/dt obtained with the FS kernel; reference ECG. Fiducial points B, C and X, detected by the automated script, are marked on each derivative trace. [3]

A simple R script automatically detected the B, C and X fiducials in each beat, computed the C–C, C–X and B–C systolic-time intervals, and compared them with reference values

(C−C ≈ 900 ms, B−C ≈ 60 ms, C−X ≈ 200 ms). Table 3 lists the number of interval-detection errors for each recording and both kernels. Each missed interval indicates a beat in which noise or waveform variability masked the target fiducial, so the counts in Table 3 offer an indirect measure of the resilience of each algorithm to the signal degradation.

Table 3: Interval-detection errors for the two derivative kernels

#	Location	Kernel	C–C errors	C–X errors	B–C errors	Total beats
1	TEPC-1	SG	0	0	0	16
		FS	0	0	1	15
2	TEPC-4	SG	7	10	0	22
		FS	7	11	0	22
3	AEPC-1	SG	0	1	0	17
		FS	0	1	1	16
4	AEPC-2	SG	1	6	1	18
		FS	1	4	1	18
5	AEPC-3	SG	2	2	0	18
		FS	1	0	0	16
6	AEPC-4	SG	0	0	1	17
		FS	0	1	0	16

SG = Savitzky–Golay differentiator; FS = frequency-sampling differentiator

The study confirms that both kernels are viable for ICG processing. The SG kernel retains more waveform detail, as seen in TEPC-1 (16 vs. 15 beats) and AEPC-1 (17 vs. 16 beats), where it detects slightly more beats than FS. Meanwhile, the FS kernel shows better noise suppression in noisier cases like AEPC-2, with fewer C-X errors (4 vs. 6). Further optimisation of filter length and cut-off frequency, together with a larger clinical data set, is required before a definitive choice can be made.

4.3 ICG Feature Extraction

Impedance cardiography signals contain several characteristic fiducial points that correspond to specific cardiac events. The primary fiducial points are the B point, C point, and X point, which are crucial for assessing systolic time intervals and calculating hemodynamic parameters like left ventricular ejection time (LVET), stroke volume (SV), and cardiac output (CO) [105]

As shown in Figure 19, the bioimpedance signal (Z), its first derivative (dZ/dt), which corresponds to the (ICG) waveform, are plotted alongside the (ECG). The **C point** corresponds to the peak of the first derivative of thoracic impedance (dZ/dt), representing the moment of *maximum aortic blood flow*. The **B point** appears at the onset of the rapid upslope, marking the aortic valve opening and transition from isovolumic contraction to systolic ejection. The **X point** is the first minimum following the C peak and represents the aortic valve closure, marking the end of the ventricular ejection phase. The time interval between the ECG Q-point and the ICG B point corresponds to the pre-ejection period (PEP), while the interval from B to X defines the left ventricular ejection time (LVET) [105, 106].

Since ICG waveforms have low amplitudes and are easily masked by motion artefacts, respiration, and inter-subject morphological differences, reliable detection of the B, C, and X points remains challenging [105]. Recent studies address this by moving beyond fixed thresholds to adaptive signal-processing and machine-learning approaches. Wavelet and
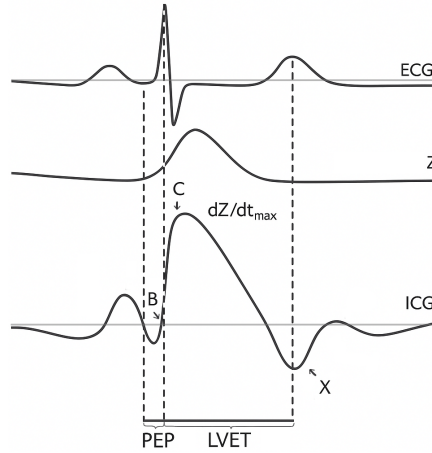
Figure 19: Illustration of bioimpedance signal (Z), its time-derivative ($-dZ/dt$) — ICG signal and the simultaneous ECG signal

empirical mode decomposition (EMD) techniques, for instance, enhance characteristic features before landmark detection; Trybek et al. [107] show that an EMD-based scheme improves automatic identification of all three fiducial points. Pattern-recognition methods—including neural networks—have also been trained to locate fiducials in noisy data [105]. For wearable or ambulatory use, emphasis has shifted to lightweight, beat-to-beat algorithms: Pale et al. [102] introduced "ReBeatICG," which runs on an ultra-low-power microcontroller and detects B, C, X, and O points from ICG alone with accuracies above 90 % for B and C and about 84 % for O, confirming the feasibility of real-time, ECG-independent feature extraction. Complementary open-source efforts, such as the Bio-SP toolbox [108], further promote automated feature extraction across peripheral biosignals.

In light of these developments, a novel low-power analog circuit is proposed for real-time extraction of the B, C, and X fiducial points from the ICG signal. In contrast to digital algorithms running on microcontrollers, this approach implements the detection of B, C, and X in analog hardware for ultra-low power consumption. The design continuously tracks the dZ/dt waveform and latches the relevant peaks and inflection points, eliminating the need for high-rate digitisation and energy-intensive digital processing. Current draw is limited to a few tens of microamperes—over an order of magnitude lower than a typical microcontroller plus fast ADC implementation, which can exceed 0.5 mA during continuous operation. Detailed in publication [1] (Appendix I) and covered by a related patent application [8] (Appendix VIII), the circuit enables estimation of pre-ejection period, left-ventricular ejection time, and other hemodynamic indices with minimal power and calculation overhead.

5 Conclusion

This research focused on developing a versatile and multifunctional impedance measurement platform intended to support a wide range of experimental and biomedical applications. The system emphasizes configurability and flexibility, providing a foundation for future research. In addition to prototyping, parallel research on excitation signal generation and signal processing aspects of bioimpedance measurement was conducted. By innovating across hardware, analog-digital integration, and signal processing, improvements in device functionality and accuracy were achieved.

5.1 Main Results and Contribution

The key outcomes align with the three research tasks and are summarised below.

RT 1 – Multifunctional DSP Platform

The first outcome was the development of an impedance-measurement device (Appendix II, [2]) based on the Texas Instruments TMS320F28379D LaunchPad. Careful analogue design and a built-in 16-bit ADC yielded a measurement error of 0.01 %, surpassing earlier instruments of comparable size and cost [16].

Building on this foundation, a second-generation instrument (Appendix V, [5]) added synchronous ECG and PPG capture on the same DSP platform. A four-electrode measurement and refined front-end circuitry pushed the impedance error below 0.002 %, a tenfold improvement over the first prototype.

A third-generation system (Appendix VI, [6]; EIT evaluation in Appendix VII, [7]) extended the platform to 32-electrode electrical-impedance tomography. Dual-channel magnitude/phase read-out at 1 kHz, on-board multiplexer, and wireless connectivity enabled real-time thoracic imaging and pulse-transit-time studies. The device delivered the first ethics-approved lung EIT images obtained with in-house hardware (TAIEK decision 1385).

These successive DSP designs explored the feasibility and the practical constraint of building a fully multifunctional bioimpedance and EIT instrument around a Texas Instruments DSP that relies on its on-board ADC, DAC and PWM resources. The platforms serve as open test-beds for researchers who wish to investigate biomedical sensor fusion, new electrode configurations, excitation signals or EIT reconstruction algorithms directly on embedded hardware. Their educational value is illustrated by a recently completed bachelor's thesis [109], co-supervised by the present author, which used the third-generation board to implement multi-frequency operation and a memory-efficient reference-signal algorithm.

RT 2 – Excitation-Signal Generation

A level-quantised PWM method was developed to generate binary excitation signals with lower total THD than classical PWM, while requiring significantly fewer switching transitions than delta–sigma bitstreams. The approach involves quantising a sinewave and assigning each level a binary segment of corresponding duty cycle. Simulations demonstrated that the resulting waveform can serve both as a clean excitation source and a reference signal for synchronous demodulation, making it well-suited for low-power impedance systems. The concept can also extend to multi-tone excitation for broadband spectroscopy. This work was presented in a journal paper (Appendix IV, [4]) and is protected by a patent application (Appendix VIII, [9]).

RT 3 – Signal-Processing Techniques

To reduce computational load and extend battery life in wearable devices, a novel low-power analogue circuit was developed to directly latch the B, C, and X fiducial points of the ICG signal in real time. These points are essential for estimating cardiac parameters such as stroke volume and cardiac output. Unlike conventional ADC-based approaches, the proposed analogue solution enables asynchronous capture with lower power consumption and potentially higher accuracy, as the signal is not constrained by ADC sampling grids. This method is described in Appendix I [1], with a corresponding patent detailed in Appendix VIII [8]. Additionally, a comparative study was conducted on two digital differentiator designs, namely Savitzky–Golay filters and frequency sampling kernels, to compute the ICG dZ/dt waveform from noisy bioimpedance recordings. Both methods showed reliable performance across different signal types and sampling rates, with tuning potential for future optimization and extension to non-uniformly sampled data. These contributions are presented in Appendix III [3].

Output Summary

In total, the work produced five peer-reviewed conference papers, two journal articles, and two patent applications, collectively advancing the state of the art in biomedical impedance measurement instrumentation, including excitation signal generation and signal processing.

These results demonstrate that a single Texas Instruments DSP can accommodate high-precision excitation, acquisition, and real-time processing for both point-wise and tomographic bioimpedance measurements. The thesis delivers an open three-generation multifunctional DSP platform, a low-THD binary PWM excitation method, an analogue circuit for ICG feature extraction, and digital filters for noise-tolerant signal differentiation. Together, these advances expand the hardware and algorithmic toolbox for the bioimpedance community, paving the way for DSP-based impedance systems, alternative excitation strategies, low-power analogue front-ends, and robust signal processing, and they open new avenues for embedded biomedical-impedance research.

5.2 Future Work

Building on these results, future directions include:

- **Incorporating camera-based boundary shape detection for EIT belt calibration**: In EIT, incorporating accurate torso boundary information is known to significantly improve image reconstruction quality. Traditionally, a generic boundary model is reused across patients, which may introduce artifacts and reduce diagnostic accuracy [110, 111]. Previous methods for personalized shape tracking have relied on accelerometers or bend sensors embedded into each electrode [111, 77], but this adds considerable design and integration complexity. A promising alternative is to employ a lightweight camera and computer vision algorithms to estimate patient-specific belt geometry. This approach could enable shape adaptation without complicating electrode hardware.

- **Implementing simultaneous multi-frequency bioimpedance measurement:** Multi-frequency bioimpedance measurements enhance physiological insight by capturing frequency-dependent tissue characteristics, while simultaneous excitation and demodulation reduce total sweep time [87]. A preliminary implementation supporting up to eight frequencies on the third prototype was presented in a recent bachelor's

thesis co-supervised by the author [109], providing a foundation for continued development.

- **Developing blood pressure estimation methods:** Noninvasive, cuffless blood pressure monitoring remains an open challenge in wearable health technologies [112]. Recent studies have demonstrated that blood pressure can be estimated using bioimpedance signals, either from a single site [113], dual-site measurements [114, 115], combined with PPG [116, 117], or from PPG alone [117]. The current device's dualchannel impedance measurement and integrated PPG sensor offer the required signals for developing and validating various estimation methods.

- **Translating prototypes into commercial, wearable biomedical devices through collaboration with clinicians and industry partners:** Initial discussions with clinicians at Tartu University Hospital have helped clarify clinical needs and application contexts. Participation in the TalTech Deep EST Spin off 2022 programme introduced commercialization pathways through the "Next Generation Holter" concept, and showcasing the prototypes at the TalTech Innovation Festival 2025 created opportunities to connect with potential collaborators. Future developments will continue to build on these experiences by engaging in similar industry events and maintaining dialogue with healthcare professionals to guide product design and adoption.

These future directions aim to extend the impact of the current work by enhancing technical capabilities, exploring new clinical applications, and supporting the transition from research prototypes to practical healthcare solutions.

List of Figures

List of Tables

References

[1] Olev Martens, Margus Metshein, Anar Abdullayev, Benoit Larras, Antoine Frappe, Antoine Gautier, Maryam Saeed, Deepu John, Barry Cardiff, Andrei Krivošei, Paul Annus, and Marek Rist. Fiducial point estimation solution for impedance cardiography measurements. *2022 IEEE International Instrumentation and Measurement Technology Conference (I2MTC)*, pages 1–6, 2022.

[2] Anar Abdullayev, Olev Martens, Marek Rist, Margus Metshein, Mart Min, and Paul Annus. A DSP-based impedance measurement device. *2022 18th Biennial Baltic Electronics Conference (BEC)*, pages 1–5, 2022.

[3] Olev Martens, Margus Metshein, Gert Tamberg, and Anar Abdullayev. Impedance cardiography signal processing with Savitzky-Golay and frequency sampling kernels. *2022 18th Biennial Baltic Electronics Conference (BEC)*, pages 1–5, 2022.

[4] Anar Abdullayev, Paul Annus, Andrei Krivošei, Margus Metshein, Olev Märtens, and Marek Rist. Improved PWM-based sinewave generation: Example of the impedance measurement. *Automatic Control and Computer Sciences*, pages 1–13, 2023.

[5] Anar Abdullayev, Marek Rist, Olev Martens, Margus Metshein, Benoit Larras, Antoine Frappe, Antoine Gautier, Mart Min, Deepu John, Barry Cardiff, Andrei Krivosei, and Paul Annus. A DSP-based EBI, ECG and PPG measurement platform. *IEEE Transactions on Instrumentation and Measurement*, pages 1–8, 2023.

[6] Anar Abdullayev, Olev Martens, Margus Metshein, Marek Rist, Raul Land, and Andrei Krivosei. A DSP-based multichannel EBI measurement device. *2024 IEEE International Instrumentation and Measurement Technology Conference (I2MTC)*, pages 1–6, 2024.

[7] Anar Abdullayev, Marek Rist, Margus Metshein, and Olev Martens. DSP-based electrical impedance tomography device: Implementation and experiments. *2025 IEEE International Instrumentation and Measurement Technology Conference (I2MTC)*, pages 1–6, 2025.

[8] O. Märtens, A. Abdullayev, M. Metshein, A. Gautier, A. Frappe, A. Krivošei, M. Rist; P. Annus, B. Larras, D. John; B. Cardiff. The impedance cardiography device, October 23, 2023. Estonian patent application P202200004, US patent application US2023/0320606 A1.

[9] O. Märtens, A. Abdullayev, M. Metshein, M. Rist, P. Annus, A. Krivošei. A method and device for synthesizing binary waveforms, December 19, 2024. Estonian patent application P202300017, US Patent application US2024/0421805 A1.

[10] Margus Metshein, Andrei Krivošei, Anar Abdullayev, Paul Annus, and Olev Märtens. Non-standard electrode placement strategies for ECG signal acquisition. *Sensors*, 22(23), 2022.

[11] O. Heaviside. "Electrical papers". Volume: 235; 1970; 560 pp, MSC: Primary 78; 01AMS Chelsea Publishing, 2008.

[12] Wayne Kerr Electronics. Precision Impedance Analyzers Datasheet. Available at: `https://www.waynekerrtest.com/products_detail.php?indexs=4`, 2018. Accessed: 2025-06-30.

[13] Keysight Technologies. E4990A Impedance Analyzer Datasheet. Available at: `https://www.keysight.com/us/en/assets/7018-04256/data-sheets/5991-3890.pdf`, 2021. Accessed: 2025-06-30.

[14] Analog Devices. AD5933 1-MSPS, 12-Bit Impedance Converter, Network Analyzer Datasheet. Available at: `https://www.keysight.com/us/en/assets/7018-04256/data-sheets/5991-3890.pdf`, 2017. Accessed: 2025-06-30.

[15] O. Martens, M. Min, R. Land, and P. Annus. Multi-frequency and multi-channel bio-impedance measurement solution. In *Proceedings of the 7th Nordic Signal Processing Symposium - NORSIG 2006*, pages 178–181, June 2006.

[16] M. Rist, M. Reidla, M. Min, T. Parve, O. Martens, and R. Land. Tms320f28069-based impedance spectroscopy with binary excitation. In *2012 5th European DSP Education and Research Conference (EDERC)*, pages 217–220, Sep. 2012.

[17] M. Reidla, O. Martens, and R. Land. Tms320f28335-based high-accuracy complex network analyzer instrument. In *2012 5th European DSP Education and Research Conference (EDERC)*, pages 44–47, Sep. 2012.

[18] Keysight Technologies. Handheld LCR Meter Datasheet. Available at: `https://www.keysight.com/us/en/assets/7018-02950/data-sheets/5990-7778.pdf`, 2021. Accessed: 2025-06-30.

[19] BIOPAC Systems, Inc. MP160 Starter Systems Product Sheet. Available at: `https://www.biopac.com/wp-content/uploads/MP160-Systems-1.pdf`. Accessed: 2025-06-30.

[20] Gurmeet Singh, Sneh Anand, Brejesh Lall, Anurag Srivastava, and Vaneet Singh. A technical review of various bioelectric impedance methods for health monitoring. In *2018 IEEE Long Island Systems, Applications and Technology Conference (LISAT)*, pages 1–6, 2018.

[21] Hafiz T. A. Khan, Kwaku Mari Addo, and Helen Findlay. Public health challenges and responses to the growing ageing populations. *Public Health Challenges*, 3(3):e213, 2024.

[22] Chunrun Qu, Sheng Liao, Jingdan Zhang, Hui Cao, Hao Zhang, Nan Zhang, Luzhe Yan, Gaoyuan Cui, Peng Luo, Qingwei Zhang, and Quan Cheng. Burden of cardiovascular disease among elderly: based on the global burden of disease study 2019. *European Heart Journal Quality of Care & Clinical Outcomes*, 10(2):143–153, 2023.

[23] Sophie Huhn, Miriam Axt, Hanns-Christian Gunga, Martina Anna Maggioni, Stephen Munga, David Obor, Ali Si'e, Valentin Boudo, Aditi Bunker, Rainer Sauerborn, Till B"arnighausen, and Sandra Barteit. The impact of wearable technologies in health research: Scoping review. *JMIR mHealth and uHealth*, 10(1):e34384, 2022.

[24] Conor Wall, Victoria Hetherington, and Alan Godfrey. Beyond the clinic: the rise of wearables and smartphones in decentralising healthcare. *npj Digital Medicine*, 6:Article 219, 2023.

[25] Jaeeun Jang and Hoi-Jun Yoo. Review of non-invasive, wearable biomedical sensor and imaging ic. In *2024 IEEE Biomedical Circuits and Systems Conference (BioCAS)*, pages 1–4, 2024.

[26] Sanna Halonen, Juho Kari, Petri Ahonen, Kai Kronström, and Jari Hyttinen. Real-time bioimpedance-based biopsy needle can identify tissue type with high spatial accuracy. *Annuals of Biomedical Engineering*, 47(3):836–851, Mar 2019.

[27] Orjan G. Martinsen and Sverre Grimnes. *Bioimpedance and Bioelectricity Basics*. Academic Press, 3 edition, Aug 2014.

[28] Souhir Chabchoub and Sofiene Mansouri. Impedance cardiography: recent applications and developments. *Biomedical Research*, Nov 2018.

[29] Ji-Jer Huang, Kuo-Sheng Cheng, and Cheau-Jane Peng. Temperature-compensated bioimpedance system for estimating body composition. *IEEE Engineering in Medicine and Biology Magazine*, 19(6):66–73, 2000.

[30] A. Sherwood, M. T. Allen, J. Fahrenberg, R. M. Kelsey, W. R. Lovallo, and L. J. van Doornen. Methodological guidelines for impedance cardiography. *Psychophysiology*, 27(1):1–23, 1990.

[31] Fedi Zouari, Pak To Cheung, Adrien Touboul, Wang C. Kwok, Venice Sin, Eddie C. Wong, Iris Y. Zhou, Terence C. C. Tam, and Russell W. Chan. Global and regional lung function assessment using portable electrical impedance tomography (eit) system: clinical study. In *2023 45th Annual International Conference of the IEEE Engineering in Medicine & Biology Society (EMBC)*, pages 1–4, 2023.

[32] Andrew Creegan, Joshua Bradfield, Samuel Richardson, Llewellyn S. Johns, Kelly Burrowes, Haribalan Kumar, Poul M. F. Nielsen, and Merryn H. Tawhai. A Wearable Open-Source Electrical Impedance Tomography Device. *HardwareX*, 18:e00521, 2024.

[33] Xiao-Rong Ding, Yuan-Ting Zhang, Jing Liu, Wen-Xuan Dai, and Hon Ki Tsang. Continuous cuffless blood pressure estimation using pulse transit time and photoplethysmogram intensity ratio. *IEEE Transactions on Biomedical Engineering*, 63(5):964–972, 2016.

[34] D. K. Ming, S. Sangkaew, H. Q. Chanh, P. T. H. Nhat, S. Yacoub, P. Georgiou, and A. H. Holmes. Continuous physiological monitoring using wearable technology to inform individual management of infectious diseases, public health and outbreak responses. *International Journal of Infectious Diseases*, 96:648–654, 2020.

[35] Leila Mirmohamadsadeghi, Sibylle Fallet, Andréa Buttu, Jonas Saugy, Thomas Rupp, Raphaël Heinzer, Jean-Marc Vesin, and Grégoire P. Millet. Sleep apnea detection using features from the respiration and the ecg recorded with smart-shirts. In *2014 IEEE Biomedical Circuits and Systems Conference (BioCAS) Proceedings*, pages 61–64, 2014.

[36] B.E. Hurwitz, L.-Y. Shyu, S.P. Reddy, N. Schneiderman, and J.H. Nagel. Coherent ensemble averaging techniques for impedance cardiography. In *[1990] Proceedings. Third Annual IEEE Symposium on Computer-Based Medical Systems*, pages 228–235, 1990.

[37] Nick Van Helleputte, Mario Konijnenburg, Julia Pettine, Dong-Woo Jee, Hyejung Kim, Alonso Morgado, Roland Van Wegberg, Tom Torfs, Rachit Mohan, Arjan Breeschoten, Harmke de Groot, Chris Van Hoof, and Refet Firat Yazicioglu. A 345

µw multi-sensor biomedical soc with bio-impedance, 3-channel ecg, motion artifact reduction, and integrated dsp. *IEEE Journal of Solid-State Circuits*, 50(1):230–244, 2015.

[38] Mart Min, Jaan Ojarand, Olev Märtens, Toivo Paavle, Raul Land, Paul Annus, Marek Rist, Marko Reidla, and Toomas Parve. Binary signals in impedance spectroscopy. In *2012 Annual International Conference of the IEEE Engineering in Medicine and Biology Society*, pages 134–137, 2012.

[39] Soon-Jae Kweon, Ayesha Kajol Rafi, Song-I Cheon, Minkyu Je, and Sohmyung Ha. On-chip sinusoidal signal generators for electrical impedance spectroscopy: Methodological review. *IEEE Transactions on Biomedical Circuits and Systems*, 16(3):337–360, 2022.

[40] D. Fefer, J. Drnovsek, and A. Jeglic. Comparative analysis of digital sinewave generation methods. In *1993 IEEE Instrumentation and Measurement Technology Conference*, pages 668–669, 1993.

[41] Francisco Colodro, Juana María Martínez-Heredia, José Luis Mora, and Antonio Torralba. Correction of errors and harmonic distortion in pulse-width modulation of digital signals. *AEU - International Journal of Electronics and Communications*, 142:153991, 2021.

[42] Jian Liu, Wenxi Yao, Zhengyu Lu, and Xiaoyi Xu. Design and implementation of dsp based high-frequency spwm generator. In *2016 IEEE 8th International Power Electronics and Motion Control Conference (IPEMC-ECCE Asia)*, pages 597–602, 2016.

[43] Kazuyuki Wakabayashi, Takafumi Yamada, Satoshi Uemori, Osamu Kobayashi, Keisuke Kato, Haruo Kobayashi, Kiichi Niitsu, Hiroyuki Miyashita, Shinya Kishigami, Kunihito Rikino, Yuji Yano, and Tatsuhiro Gake. Low-distortion single-tone and two-tone sinewave generation algorithms using an arbitrary waveform generator. In *2011 IEEE 17th International Mixed-Signals, Sensors and Systems Test Workshop*, pages 33–38, 2011.

[44] Olev Martens. Precise mixed signal synchronous detector with spectrally improved binary switching. In *2009 IEEE International Symposium on Intelligent Signal Processing*, pages 77–80, 2009.

[45] Amin Fischer, Ahmed Yahia Kallel, and Olfa Kanoun. Comparative study of excitation signals for microcontroller-based eis measurement on li-ion batteries. In *2021 International Workshop on Impedance Spectroscopy (IWIS)*, pages 44–47, 2021.

[46] M. Min, M. Lehti-Polojärvi, J. Hyttinen, M. Rist, R. Land, and P. Annus. Bioimpedance spectro-tomography system using binary multifrequency excitation. *International Journal of Bioelectromagnetism*, 209:76–79, 2018.

[47] Alessio de Angelis, Roberta Ramilli, Marco Crescentini, Antonio Moschitta, Paolo Carbone, and Pier Andrea Traverso. In-situ electrochemical impedance spectroscopy of battery cells by means of binary sequences. In *2021 IEEE International Instrumentation and Measurement Technology Conference (I2MTC)*, pages 1–5, 2021.

[48] Olev Martens, Raul Land, Mart Min, Paul Annus, Marek Rist, and Marko Reidla. Improved impedance analyzer with binary excitation signals. In *2015 IEEE 9th International Symposium on Intelligent Signal Processing (WISP) Proceedings*, pages 1–5, 2015.

[49] Ahmed Yahia Kallel, Amin Fischer, and Olfa Kanoun. A study of binary excitation sequences for use in battery impedance spectroscopy. In *2023 IEEE International Instrumentation and Measurement Technology Conference (I2MTC)*, pages 1–6, 2023.

[50] S M M Naidu, Prem C Pandey, and Vinod K Pandey. Automatic detection of characteristic points in impedance cardiogram. In *2011 Computing in Cardiology*, pages 497–500, 2011.

[51] Z. Lababidi, D. A. Ehmke, R. E. Durnin, P. E. Leaverton, and R. M. Lauer. The first derivative thoracic impedance cardiogram. *Circulation*, 41(4):651–658, 1970.

[52] D. G. Newman and R. Callister. The non-invasive assessment of stroke volume and cardiac output by impedance cardiography: a review. *Aviation, Space, and Environmental Medicine*, 70(8):780–789, 1999.

[53] Anar Abdullayev. *DSP-põhine impedantsspektroskoopia seade. DSP Based Impedance Spectroscopy Device*. TalTech, 2021.

[54] M. Rist, M. Reidla, M. Min, T. Parve, O. Martens, and R. Land. Tms320f28069-based impedance spectroscopy with binary excitation. In *2012 5th European DSP Education and Research Conference (EDERC)*, pages 217–220, 2012.

[55] Evgenij Barsoukov and J. Ross Macdonald, editors. *Impedance Spectroscopy*. John Wiley & Sons, Inc., apr 2018.

[56] Song-I Cheon, Soon-Jae Kweon, Youngin Kim, Jimin Koo, Sohmyung Ha, and Minkyu Je. A polar-demodulation-based impedance-measurement ic using frequency-shift technique with low power consumption and wide frequency range. *IEEE Transactions on Biomedical Circuits and Systems*, 15(6):1210–1220, 2021.

[57] A Ruiz-Vargas, J W Arkwright, and Antoni Ivorra. A portable bioimpedance measurement system based on red pitaya for monitoring and detecting abnormalities in the gastrointestinal tract. In *2016 IEEE EMBS Conference on Biomedical Engineering and Sciences (IECBES)*, pages 150–154, 2016.

[58] Roman Kusche, Andra Oltmann, and Philipp Rostalski. A wearable dual-channel bioimpedance spectrometer for real-time muscle contraction detection. *IEEE Sensors Journal*, 24(7):11316–11327, 2024.

[59] ImpediMed. SFB7 BIS Research Device. Available at: `https://www.impedimed.com/products/research-devices/sfb7/`, 2025. Accessed: 2025-06-30.

[60] Eliko. Quadra Impedance Spectroscopy Product Sheet. Available at: `https://www.eliko.ee/wp-content/uploads/2016/01/Quadra-Product-Sheet13.03.2018.pdf`, 2018. Accessed: 2023-05-18.

[61] Analog Devices. AD5940/AD5941: High Precision, Impedance, and Electrochemical Front End Datasheet. Available at: `https://www.analog.com/media/en/technical-documentation/data-sheets/ad5940-5941.pdf`, 2024. Rev. D, Accessed: 2025-06-30.

[62] Maxim Integrated. MAX30001-Ultra-Low-Power, Single-Channel Integrated Biopotential (ECG, R-to-R, and Pace Detection) and Bioimpedance (BioZ) AFE Datasheet. Available at: `https://datasheets.maximintegrated.com/en/ds/MAX30001.pdf`, 2020. Accessed: 2025-06-30.

[63] Shuang Song, Mario Konijnenburg, Roland van Wegberg, Jiawei Xu, Hyunsoo Ha, Wim Sijbers, Stefano Stanzione, Dwaipayan Biswas, Arjan Breeschoten, Peter Vis, Chris van Liempd, Chris van Hoof, and Nick van Helleputte. A 769 uw battery-powered single-chip soc with ble for multi-modal vital sign monitoring health patches. *IEEE Transactions on Biomedical Circuits and Systems*, 13(6):1506–1517, 2019.

[64] Yun-Shiang Shu, Zhi-Xin Chen, Yu-Hong Lin, Su-Hao Wu, Wei-Hsiang Huang, Albert Yen-Chih Chiou, Chang-Yang Huang, Hung-Yi Hsieh, Fan-Wei Liao, Teng-Feng Zou, and Ping Chen. 26.1 a 4.5mm2 multimodal biosensing soc for ppg, ecg, bioz and gsr acquisition in consumer wearable devices. In *2020 IEEE International Solid-State Circuits Conference - (ISSCC)*, pages 400–402, 2020.

[65] Andy Adler and Alistair Boyle. Electrical impedance tomography: Tissue properties to image measures. *IEEE Transactions on Biomedical Engineering*, 64(11):2494–2504, 2017.

[66] A. Adler et al. Impedance imaging of lung ventilation: Do we need to account for chest expansion. In *Proc. IEEE Int. Conf. Biomed. Imag.*, volume 43, pages 414–420, 1996.

[67] A. Boyle et al. Cerebral perfusion imaging using eit. In *Proc. Int Conf. Biomed. Appl. Elect. Impedance Tomography*, page 43. IEEE, 2017.

[68] A. Adler et al. Whither lung eit: Where are we where do we want to go and what do we need to get there. *Physiol. Meas.*, 33:679–694, 2012.

[69] B. H. Brown. Electrical impedance tomography (eit): A review. *J. Med. Eng. Technol.*, 27:97–108, 2003.

[70] B. H. Brown and A. D. Seagar. The sheffield data collection system. *Clin. Phys. Physiol. Meas.*, 8:91, 1987.

[71] N. J. Avis and D. C. Barber. Image reconstruction using non-adjacent drive configurations (electric impedance tomography). *Physiol. Meas.*, 15:A153, 1994.

[72] D. Smyl and D. Liu. Optimizing electrode positions in 2d electrical impedance tomography using deep learning. *IEEE Trans. Instrum. Meas.*, 69:6030–6044, 2020.

[73] A. Adler, P. O. Gaggero, and Y. Maimaitijiang. Adjacent stimulation and measurement patterns considered harmful. *Physiological Measurement*, 32:731–744, 2011.

[74] E. Demidenko, A. Hartov, N. Soni, and K. D. Paulsen. On optimal current patterns for electrical impedance tomography. *IEEE Transactions on Biomedical Engineering*, 52:238–248, 2005.

[75] B. Brazey, Y. Haddab, N. Zemiti, F. Mailly, and P. Nouet. An open-source and easily replicable hardware for electrical impedance tomography. *HardwareX*, 11:e00278, 2022.

[76] Joel Escobar Fernández, Cristian Martínez López, and Víctor Mosquera Leyton. A low-cost, portable 32-channel eit system with four rings based on afe4300 for body composition analysis. *HardwareX*, 16:e00494, 2023.

[77] Yu Wu, Dai Jiang, Andy Bardill, Richard Bayford, and Andreas Demosthenous. A 122 fps, 1 mhz bandwidth multi-frequency wearable eit belt featuring novel active electrode architecture for neonatal thorax vital sign monitoring. *IEEE Transactions on Biomedical Circuits and Systems*, 13(5):927–937, 2019.

[78] Dan Yang, Guangle Huang, Bin Xu, Xu Wang, Zuowei Wang, and Zhulin Wei. A dsp-based eit system with adaptive boundary voltage acquisition. *IEEE Sensors Journal*, 22(6):5743–5754, 2022.

[79] Huaiyin Zhu, Baoliang Wang, Manuchehr Soleimani, Haifeng Ji, and Yandan Jiang. A wideband contactless electrical impedance tomography system. *IEEE Transactions on Instrumentation and Measurement*, 73:1–14, 2024.

[80] Sciospec. EIT32/64/128+ Product Page. Available at: `https://www.sciospec.com/product/eit32-64-128/`, 2025. Accessed: 2025-06-12.

[81] Sciospec. LungEIT Kit Product Page. Available at: `https://www.sciospec.com/product/lungeitkit/`, 2025. Accessed: 2025-06-12.

[82] Sentec. The LuMon System Product Page. Available at: `https://www.sentec.com/electrical-impedance-tomography/`, 2025. Accessed: 2025-06-12.

[83] Draeger. Dräger PulmoVista 500 Datasheet. Available at: `https://www.draeger.com/en_uk/Products/PulmoVista-500`, 2025. Accessed: 2025-06-12.

[84] Marek Rist and Mart Min. Dynamic reference for evaluation of bioimpedance spectroscopy devices. In *2016 15th Biennial Baltic Electronics Conference (BEC)*, pages 107–110, 2016.

[85] Mamatjan Yasin, Stefan Böhm, Pierre Olivier Gaggero, and Andy Adler. Evaluation of eit system performance. *Physiological Measurement*, 32(7):851–865, 2011.

[86] Isnan Nur Rifai, Prima Asmara Sejati, Shinsuke Akita, and Masahiro Takei. Fpga-based planar sensor electrical impedance tomography (fpga-pseit) system characterized by double feedback howland constant- current pump and programmable front-end measurement. *IEEE Transactions on Instrumentation and Measurement*, 73:1–10, 2024.

[87] Yuxiang Yang, Fu Zhang, Kun Tao, Lianhuan Wang, He Wen, and Zhaosheng Teng. Multi-frequency simultaneous measurement of bioimpedance spectroscopy based on a low crest factor multisine excitation. *Physiological measurement*, 36:489–501, 02 2015.

[88] Mahdi Rajabzadeh, Jonathan Ungethuem, Holger Mandry, Carolin Schilpp, Oliver Wittekindt, and Maurits Ortmanns. An evaluation study of various excitation signals for electrical impedance spectroscopy. In *2019 IEEE International Symposium on Circuits and Systems (ISCAS)*, pages 1–5, 2019.

[89] Nikola Ivanisevic, Saul Rodriguez, and Ana Rusu. Impedance spectroscopy systems: Review and an all-digital adaptive iir filtering approach. In *2017 IEEE Biomedical Circuits and Systems Conference (BioCAS)*, pages 1–4, 2017.

[90] Chao Yang and Andrew J. Mason. Fully integrated seven-order frequency-range quadrature sinusoid signal generator. *IEEE Transactions on Instrumentation and Measurement*, 58(10):3481–3489, 2009.

[91] Kwantae Kim, Sangyeob Kim, and Hoi-Jun Yoo. Design of sub-10-uw sub-0.1 *IEEE Journal of Solid-State Circuits*, 57(2):586–595, 2022.

[92] Marco Crescentini, Marco Bennati, and Marco Tartagni. A high resolution interface for kelvin impedance sensing. *IEEE Journal of Solid-State Circuits*, 49(10):2199–2212, 2014.

[93] Mahdi Rajabzadeh, Joachim Becker, and Maurits Ortmanns. Evaluation of single-bit sigma-delta modulator dac for electrical impedance spectroscopy. In *2017 IEEE Biomedical Circuits and Systems Conference (BioCAS)*, pages 1–4, 2017.

[94] Roberta Ramilli, Francesco Santoni, Alessio De Angelis, Marco Crescentini, Paolo Carbone, and Pier Andrea Traverso. Binary sequences for online electrochemical impedance spectroscopy of battery cells. *IEEE Transactions on Instrumentation and Measurement*, 71:1–8, 2022.

[95] Kiseok Song, Unsoo Ha, Seongwook Park, and Hoi-Jun Yoo. An impedance and multi-wavelength near-infrared spectroscopy ic for non-invasive blood glucose estimation. In *2014 Symposium on VLSI Circuits Digest of Technical Papers*, pages 1–2, 2014.

[96] Sunjoo Hong, Jaehyuk Lee, Joonsung Bae, and Hoi-Jun Yoo. A 10.4 mw electrical impedance tomography soc for portable real-time lung ventilation monitoring system. *IEEE Journal of Solid-State Circuits*, 50(11):2501–2512, 2015.

[97] Guangyang Qu, Hanqing Wang, Yimiao Zhao, John O'Donnell, Colin Lyden, Yincai Liu, Junbiao Ding, Dennis Dempsey, Leicheng Chen, Donal Bourke, Shurong Gu, Jun Gao, Lizhu Lu, Li Wang, Xuemin Li, Hongxing Li, Chao Chu, and Ling Yang. A 0.28mohm-sensitivity 105db-dynamic-range electrochemical impedance spectroscopy soc for electrochemical gas detection. In *2018 IEEE International Solid-State Circuits Conference - (ISSCC)*, pages 286–288, 2018.

[98] M. P. Bolton, L. C. Ward, A. Khan, I. Campbell, P. Nightingale, O. Dewit, and M. Elia. Sources of error in bioimpedance spectroscopy. *Physiological Measurement*, 19(2):235–245, 1998.

[99] D. Ayllón, R. Gil-Pita, and F. Seoane. Detection and classification of measurement errors in bioimpedance spectroscopy. *PloS One*, 11(6):e0156522, 2016.

[100] Ihsèn Ben Salah and Kaïs Ouni. Denoising of the impedance cardiographie signal (icg) for a best detection of the characteristic points. 2017.

[101] Oscar Escalona, Niamh Cullen, Ibrahim Weli, Niall McCallan, Ka Yan Ng, and Denis Finlay. Robust arm impedocardiography signal quality enhancement using recursive signal averaging and multi-stage wavelet denoising methods for long-term cardiac contractility monitoring armbands. *Sensors (Basel, Switzerland)*, 23(13):5892, 2023.

[102] Una Pale, Nathan Muller, Adriana Arza Valdés, and David Atienza. ReBeatICG: Real-time low-complexity beat-to-beat impedance cardiogram delineation algorithm. In *Proc. 43rd Annual Int. Conf. IEEE Engineering in Medicine & Biology Society (EMBC)*, pages 3973–3976, 2021.

[103] R. P. Patterson. Fundamentals of impedance cardiography. *IEEE Engineering in Medicine and Biology Magazine*, 8(1):35–38, 1989.

[104] M. Metshein, A. Gautier, B. Larras, A. Frappe, D. John, B. Cardiff, P. Annus, R. Land, and O. Martens. Study of electrode locations for joint acquisition of impedance- and electro-cardiography signals. In *2021 43rd Annual International Conference of the IEEE Engineering in Medicine & Biology Society (EMBC)*, pages 7264–7264. IEEE, 2021. DOI not provided.

[105] I. Karpiel, M. Richter-Laskowska, D. Feige, A. Gacek, and A. Sobotnicki. An effective method of detecting characteristic points of impedance cardiogram verified in the clinical pilot study. *Sensors (Basel, Switzerland)*, 22(24):9872, 2022.

[106] C. Tronstad, J. O. Høgetveit, O. Elvebakk, and H. Kalvøy. Age-related differences in the morphology of the impedance cardiography signal. *Journal of Electrical Bio-impedance*, 10(1):139–145, 2019.

[107] Paulina Trybek, Ewelina Sobotnicka, Agata Wawrzkiewicz-Jałowiecka, Łukasz Machura, Daniel Feige, Aleksander Sobotnicki, and Monika Richter-Laskowska. A new method of identifying characteristic points in the impedance cardiography signal based on empirical mode decomposition. *Sensors*, 23(2):675, 2023.

[108] Mohsen Nabian, Yu Yin, Jolie Wormwood, Karen S. Quigley, Lisa F. Barrett, and Sarah Ostadabbas. An open-source feature extraction tool for the analysis of peripheral physiological data. *IEEE Journal of Translational Engineering in Health and Medicine*, 6:1–11, 2018.

[109] Mihkel Aaremae. *DSP-põhine kompaktne impedantsi mõõtja ja meetodid*. TalTech, 2025.

[110] S. de Gelidi, N. Seifnaraghi, A. Bardill, A. Tizzard, Y. Wu, E. Sorantin, S. Nordebo, A. Demosthenous, and R. Bayford. Torso shape detection to improve lung monitoring. *Physiological Measurement*, 39(7):074001, 2018.

[111] Bartłomiej Grychtol, William R. B. Lionheart, Marc Bodenstein, Gerhard K. Wolf, and Andy Adler. Impact of model shape mismatch on reconstruction quality in electrical impedance tomography. *IEEE Transactions on Medical Imaging*, 31(9):1754–1760, 2012.

[112] Ting-Wei Wang, Wen-Xiang Chen, Hsiao-Wei Chu, and Shien-Fong Lin. Single-channel bioimpedance measurement for wearable continuous blood pressure monitoring. *IEEE Transactions on Instrumentation and Measurement*, 70:1–9, 2021.

[113] Deen Osman, Matija Jankovic, Kaan Sel, Roderic I. Pettigrew, and Roozbeh Jafari. Blood pressure estimation using a single channel bio-impedance ring sensor. In *2022 44th Annual International Conference of the IEEE Engineering in Medicine and Biology Society (EMBC)*, pages 4286–4290, 2022.

[114] Fen Miao, Zeng-Ding Liu, Ji-Kui Liu, Bo Wen, Qing-Yun He, and Ye Li. Multi-sensor fusion approach for cuff-less blood pressure measurement. *IEEE Journal of Biomedical and Health Informatics*, 24(1):79–91, 2020.

[115] Kaan Sel, Amirmohammad Mohammadi, Roderic I. Pettigrew, and Roozbeh Jafari. Physics-informed neural networks for modeling physiological time series for cuffless blood pressure estimation. *npj Digital Medicine*, 6(1), jun 2023.

[116] Wan-Hua Lin, Hui Wang, Oluwarotimi Williams Samuel, and Guanglin Li. Using a new ppg indicator to increase the accuracy of ptt-based continuous cuffless blood pressure estimation. In *2017 39th Annual International Conference of the IEEE Engineering in Medicine and Biology Society (EMBC)*, pages 738–741, 2017.

[117] Duc Huy Nguyen, Paul C.-P. Chao, Hiu Fai Yan, Tse-Yi Tu, Chin-Hung Cheng, and Tan-Phat Phan. Predicting blood pressures for pregnant women by ppg and personalized deep learning. *IEEE Journal of Biomedical and Health Informatics*, 29(1):5–16, 2025.

Acknowledgements

Abstract
Research and Implementation of Electrical Bioimpedance Measurement Solutions

Electrical impedance has evolved into a powerful tool for the characterization of both engineered structures and biological tissues. Within biomedicine, bioimpedance techniques enable non-invasive monitoring of tissue composition, blood flow and cardiorespiratory dynamics, making them attractive for emerging wearable and point-of-care devices. Commercial bioimpedance instruments are often costly, proprietary, and tailored to narrowly defined clinical workflows, leaving researchers without low-level access to hardware or firmware. This work centres on the implementation of an open, fully customisable bioimpedance platform that can be configured, from excitation generation to final signal processing. Developing custom hardware and firmware from the scratch grants researchers full control over low-level operation and offers a flexible test-bench for new algorithm development. Three successive prototypes were produced, each based on a Texas Instruments TMS320F28379D dual-core DSP with an integrated 16-bit, 1 MS/s ADC. The final device performs dual-channel magnitude and phase measurements from 1 kHz to 200 kHz; a 32-way electrode multiplexer enables low-cost electrical impedance tomography at 2 fps. Software defined synchronous demodulators, programmable-gain amplifiers, and synchronous ECG/PPG signals support multimodal cardiovascular monitoring, while an onboard ESP32 module provides Bluetooth and Wi-Fi connectivity. Bench tests show magnitude errors below 0.002%, and in-vivo trials confirm possible lung and peripheral hemodynamic measurements. Because measurement accuracy is limited by the quality of the excitation signal, special attention is paid to the the excitation signal. In addition to the complete DSP platform, the thesis contributes to a novel PWM-based excitation method that produces a low-distortion binary approximation of a sine wave, using a minimal logic which is well suited to compact, low-power instruments. The proposed scheme achieves a minimum THD of approximately 2%, compared to 4% for conventional PWM, offering an effective compromise between signal quality and switching rate. Accurate feature extraction from impedance cardiography remains a bottleneck in continuous hemodynamic monitoring. The thesis therefore introduces an ultra-low-power analog circuit that detects the B, C, and X fiducial points of the ICG waveform in real time, delivering beat-to-beat pre-ejection period and LVET without high-rate digitisation or heavy digital filtering. Compared to traditional ADC-based solutions, the proposed approach can reduce power consumption by at least an order of magnitude if implemented in low-power CMOS. All proposed methods were validated experimentally and disseminated through five peer-reviewed conference papers, two journal articles and two patent applications, reproduced in the appendices. Collectively, the work advances the state of the art in portable bioimpedance instrumentation by delivering a flexible DSP-centric platform, a low-distortion binary excitation strategy and an energy-efficient analog feature-extraction method. Taken together, the open measurement platform, low-distortion excitation technique, and power-efficient fiducial extractor form a versatile resource that researchers can readily adapt for bioimpedance experimentation, algorithm development, and more precise non-invasive evaluation of cardiovascular and respiratory dynamics across laboratory and applied settings.

Kokkuvõte
Elektrilise bioimpedantsi mõõtmise lahenduste uurimine ja teostus

Elektrilise impedantsi mõõtmistest on saanud võimas tööriist nii konstrueeritud struktuuride kui ka bioloogiliste kudede iseloomustamiseks. Elektrilise bioimpedantsi tehnika võimaldab mitte-invasiivset koe koostise, verevoolu ja kardiorespiratoorse dünaamika jälgimist, muutes selle atraktiivseks nii kehal kantavate kui meditsiiniliseseadmete jaoks. Kommertslikud bioimpedantsi instrumendid on kallid, patenteeritud ja kohandatud kitsalt määratletud kliinilisteks protseduurideks, jättes teadlastele piiratud juurdepääsu riist- või püsivarale. Käesolev töö keskendub avatud, täielikult kohandatava bioimpedantsi platvormi rakendamisele, mida saab konfigureerida alates ergutuse genereerimisest kuni signaali lõpliku töötlemiseni. Kohandatud riist- ja püsivara arendamine nullist annab teadlastele täieliku kontrolli madala taseme operatsioonide üle ja pakub paindliku katsestendi uute algoritmide väljatöötamiseks. Valmistati kolm järjestikust prototüüpi, mis põhinesid Texas Instrumentsi TMS320F28379D kahetuumalisel DSP-l koos integreeritud 16-bitise, 1 MS/s ADC-ga. Lõplik seade teostab kahekanalilisi magnituudi ja faasi mõõtmisi sagedustel 1 kHz kuni 200 kHz; 32-kanaliline elektroodide multiplekser võimaldab odavat elektrilise impedantsi tomograafiat kiirusega 2 kaadrit sekundis. Tarkvaraliselt määratletud sünkroonsed demodulaatorid, programmeeritava võimendusega võimendid ja sünkroonsed EKG/PPG signaalid toetavad multimodaalset kardiovaskulaarset jälgimist, samas kui sisseehitatud ESP32 moodul pakub Bluetoothi ja Wi-Fi-ühendust. Standtestid näitavad magnituudiviga alla 0,002% ja in vivo katsed kinnitavad võimalikke kopsu- ja perifeerse hemodünaamika mõõtmisi. Kuna mõõtmistäpsust piirab ergutussignaali kvaliteet, pööratakse sellele erilist tähelepanu. Lisaks täielikule DSP-platvormile panustab väitekiri uudsesse PWM-põhisesse ergutusmeetodisse, mis tekitab minimaalse arvutusliku vajaduse juures siinuslaine madala moonutusega binaarse lähenduse ja sobib hästi kompaktsetele ning väikese energiatarbega instrumentidele. Kavandatud skeem saavutab 2% THD, mis on parem kui tavapärane PWM (4%), vältides samal ajal sigma-delta modulatsiooni suurt lülituskiirust. Täpne tunnuste eraldamine impedantskardiogrammilt on pideva hemodünaamika jälgimise kitsaskohaks. Seetõttu tutvustab väitekiri üliväikese energiatarbega analoogahelat, mis tuvastab IKG lainekuju B-, C- ja X-tunnuspunkte reaalajas, pakkudes pingumisperioodi ja vasaku vatsakese väljutusperioodi määramist ilma kiire digitaliseerimise või ulatusliku digitaalse filtreerimiseta. Võrreldes traditsiooniliste ADC-põhiste lahendustega, võib pakutud lähenemisviis energiatarbimist vähendada vähemalt suurusjärgu võrra, kui seda rakendatakse väikese energiatarbega CMOS-is. Kõik pakutud meetodid valideeriti eksperimentaalselt ja tutvustati viie eelretsenseeritud konverentsiettekande, kahe ajakirjaartikli ja kahe patenditaotluse kaudu, mis on esitatud lisades. Kokkuvõttes edendab töö kaasaskantavate bioimpedantsinstrumentide taset, pakkudes paindlikku DSP-kesket platvormi, väikese moonutusega binaarset ergastusstrateegiat ja energiatõhusat analoogsete tunnuste eraldamise meetodit. Kokkuvõttes moodustavad avatud mõõtmisplatvorm, väikese moonutusega ergastustehnika ja energiatõhus hemodünaamiliste tunnuspunktide määramise meetod mitmekülgse ressursi, mida teadlased saavad hõlpsasti kohandada bioimpedantsi katsetamiseks, algoritmide väljatöötamiseks ja kardiovaskulaarse ning hingamisdünaamika täpsemaks mitte-invasiivseks hindamiseks nii labori- kui ka rakenduskeskkonnas.

Appendix 1 — Fiducial Point Estimation Solution for Impedance Cardiography Measurements

I

Olev Martens, Margus Metshein, Anar Abdullayev, Benoit Larras, Antoine Frappe, Antoine Gautier, Maryam Saeed, Deepu John, Barry Cardiff, Andrei Krivošei, Paul Annus, and Marek Rist. Fiducial point estimation solution for impedance cardiography measurements. *2022 IEEE International Instrumentation and Measurement Technology Conference (I2MTC)*, pages 1–6, 2022

Fiducial Point Estimation Solution for Impedance Cardiography Measurements

Olev Martens
Tallinn Univers. of Technol., Estonia
olev.martens@taltech.ee

Margus Metshein
Tallinn Univers. of Technol., Estonia
margus.metshein@taltech.ee

Anar Abdullayev
Tallinn Univers. of Technol., Estonia
anar.abdullayev@taltech.ee

Benoit Larras
Univ. Lille, CNRS, Lille, France
benoit.larras@junia.com

Antoine Frappe
Univ. Lille, CNRS, Lille, France
antoine.frappe@junia.com

Antoine Gautier
Univ. Lille, CNRS, Lille, France
antoine.gautier@junia.com

Maryam Saeed
University College Dublin, Ireland
maryam.saeed@ucdconnect.ie

Deepu John
University College Dublin, Ireland
deepu.john@ucd.ie

Barry Cardiff
University College Dublin, Ireland
barry.cardiff@ucd.ie

Andrei Krivošei
Tallinn Univers. of Technol., Estonia
andrei.krivosei@taltech.ee

Paul Annus
Tallinn Univers. of Technol., Estonia
paul.annus@taltech.ee

Marek Rist
Tallinn Univers. of Technol., Estonia
marek.rist@taltech.ee

Abstract—ICG (impedance cardiography) is in parallel to ECG (electrocardiography) an important indicator of the functioning of the heart and of the overall cardiovascular system. Adding the ICG to ECG measurement functionality into the wearable devices improves the quality of health monitoring, as the ICG reflects relevant hemodynamic parameters (informative time intervals, but also the stroke volume and cardiac output and their variability). The most challenging task of the ICG signal processing is to extract the key points B, C, X of the cardiac period – start, peak-location, and value at this point and the end of the LVET (left ventricular ejection time) sub-period in the cardiac cycle. A novel block diagram and analog implementation of it has been proposed, analyzed, and discussed, with discussion of the benefits of the proposed solution. The proposed solution enables developing of relatively simple very power-efficient solutions, monitoring the ICG values of the person with smart and efficient data acquisition and processing.

Index Terms—impedance cardiography (ICG), electrical bio-impedance (EBI)

I. INTRODUCTION

ECG (electrocardiography) and ICG (impedance cardiography) are both important means to monitor the cardiac activity and heart condition [1]. While ECG (indicating the electrical signals of the heart) has a long history from the end of the 1800-s, then ICG (showing physical work of the heart and reflecting hemodynamical parameters) has been used from the 1960-s [2]. With help of ICG, it is possible to estimate additionally to heart rate (HR) and its variation (HRV), the efficiency of blood pumping -cardiac output (CO) and stroke volume (SV), but also various timings, e.g. left ventricular ejection time (LVET) and pre-ejection period (PEP) [3].

Portable solutions have been developed to monitor these and other parameters [4]. Example waveforms of the ICG signals (with ECG signal in parallel) are shown in Fig. 1 [4]. On the plots, the ECG signal is shown for reference, together with the impedance (Z) signal and the first derivative *(dZ/dt)*, as the actual *"ICG signal"* [2]. While the ECG signal is characterized by the QRS complex (Fig. 1), for ICG the following key points and time intervals are typically used to characterize the cardiac periods [2], [4]:

- B - Opening of the aortic valve;
- C - Maximum systolic flow;
- X - Closing of the aortic valve;
- Y - Closing of the pulmonary valve;
- O - Opening of the mitral valve;
- PEP - Pre-ejection period;
- LVET - Left ventricular ejection time.

For ICG most relevant points are B, C, X -allowing to estimate the LVET, CO, and SV [3].

Historically ICG impedance waveforms have been measured involving the whole thorax [2] (including the heart and the lungs) into the measurement signal path. So, a simple wearable belt can be used for measurement setup, to acquire ECG and ICG signal simultaneously [5]. Alternatively, the cardiac waveforms can be obtained from other places, e.g. by measuring from the wrist [6]–[8], being probably the preferred variant for wearable devices (to implement the devices in the form of smart watches).
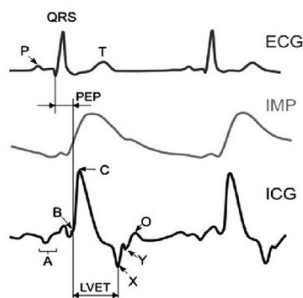
Fig. 1: Typical patterns of the ECG and ICG waveforms [4]

Current paper focuses on the estimation of hemodynamic feature points by using the signal of ICG, gained e.g. from the wrist. A novel solution, directed by the "edge computing" principles, is proposed, analyzed and compared to the closest solution described in designated literature. The presented work is expected to guide closer to the "on-site" estimation and analyze of bio-signals and throughout, innovative solutions in wearable technologies.

II. POSSIBLE ALGORITHMS TO EXTRACT THE KEY POINTS OF ICG

The key- (fiducial) points B, X, C are typically (e.g. in [3]) defined as following - the C is the most positive peak (maximum) value in the ICG signal *(dZ/dt)* and can be found as a global extremum in some reasonable (corresponding e.g. to an expected pulse period) sliding time window. Additionally a threshold can be applied- only the positive extremums over e.g. 50% of the overall signal maximum level are taken into account. For determining the B-point various approaches have been proposed. Most typically the first zero-crossing of the ICG to the left from the C-point is used [3], [4], [9], [10]. The same approach is used in the proposed solution. As for algorithm, the determining of the B-point strategy can be rephrased as "fixing the last zero crossing of the ICG signal before the C-point". Alternatively the B-point has been suggested to take as some local minimum [2] further left from the zero-crossing ("below the zero"), so giving little bit increased value for LVET interval (and related CO and SV values). As another alternative, it has been proposed to move the B-point by applying instead of zero-crossing the crossing at the 15% level between the base-line (close to zero, in practice) and peak value [11].

For determining the X-point most often the global minimum (negative extremum) of the ICG signal, between every C-to-(next) C interval is considered [4], [9], [10]. For the current solution this approach is used, up to further reconsideration.

A. Problem statement

Wearable solutions exist for monitoring of the ICG and ECG (or solely ICG) signals ([4], [12], [13]). In known solutions the wearable part of electronics performs typically only the signal

acquisition and first preliminary signal conditioning - detecting of AC carrier of the impedance signal, filtering and digitizing (e.g. with 12-16 bits and at 200 Hz rate). Detecting of AC carrier of the bio-impedance signal is preferably performed by synchronous detection (known also as *lock-in technique* [14]) giving better performance in the presence of noise, disturbances and artifacts. Also bandpass (combination of highpass and lowpass) filtering is required before further signal processing. The highpass filtering is needed to remove the base component of the bioimpedance Z_0 to process only relatively tiny variations ΔZ of the total impedance $Z = Z_0 + \Delta Z$. Lowpass filtering is needed for several reasons- to fulfill the Nyquist criteria before digitizing, to suppress various noise of acquired signals and sensitive front-end electronics, but also to smooth the output signal of the (e.g. *lock-in*) detector.

Further the digitized data stream with the waveform(s) is transmitted by wireless (e.g. Bluetooth) connection to the computer, tablet, smartphone or some other device for feature extraction (starting from determining the characteristic points of ICG) and further analysis, determination of various (hemo-dynamic) parameters for presentation (and optionally logging) of the waveforms and displaying of the determined values.

Such solutions, with high-rate high-resolution signal sampling analog-to-digital conversion with sophisticated mathematical operations take much energy and involve sophisticated circuitry, not allowing to offer low-cost low-power simple wearable monitor devices.

Much more reasonable alternative, proposed in the current paper, is to use the *"edge computing"* principles, extracting the main information just near the sensor, *"at first possibility"*, still in the analog signal domain. For possible implementation of the cardiac activity (or cardiorespiratory, as ICG is reflecting also the lung activity [15]) monitoring device into the smart chip, with local artificial intelligence (AI) is clearly beneficial. The chip has to be low-power with simple and robust enough algorithms. One approach is to make much of the signal processing in the analog and mixed electronics part, acquiring the sparse filtered samples of the bioimpedance only at the characteristic points, starting with B, C, X-points. The time intervals for these points can be measured simply by digital counters and values sampled at these time instances to be digitized, by relatively slow (e.g. by simple integrating type) ADC, based again on counting of some digital clock ticks.

In addition, as background comment, solutions for generic low power systems with non-uniform sampling, event-driven [16] and combined peak and level-crossing sampling schemes [17] have been proposed by various researchers.

B. About known solutions

While there are several papers describing the locations (and their finding strategies) of these fiducial points, only one example (MatLab) software toolbox has been found for determining of these points ("A Biosignal-Specific Processing Tool", described by the authors of this tool in [3]). Furthermore, no practical implementations such as an analog or digital hardware or even embeddable (e.g. C-code) solutions have
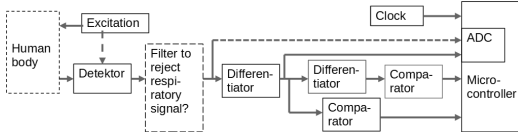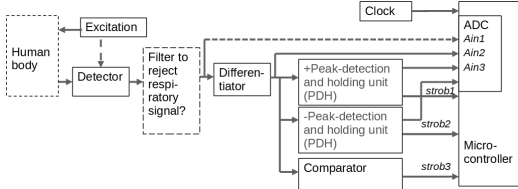
Fig. 2: Solution by B. Sramek [18]
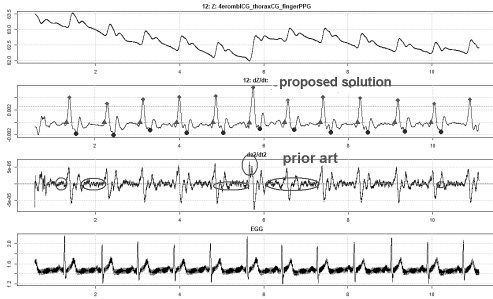

Fig. 3: Proposed solution

Fig. 4: Block diagram level simulation, prior solution vs proposed

been found by authors of this paper for estimating the key points of ICG.

Still, an US patent of B. Sramek [18] is disclosing partly similar approach (on the block diagram level) to the solution, proposed in the current paper. If to compare the solution of Sramek (Fig. 2) and the proposed solution (Fig. 3), the second differentiator and the second comparator are changed to peak-detectors, being less sensitive to the noise, as shown below. As expected, the simulation example with real ICG signal gives for the prior solution [18] much more false signals, compared with the proposed solution, in detecting the key points of ICG signal, as shown in the Fig. 4.

III. PROPOSED SOLUTION

A. Block diagram of the proposed solution

The more specific block diagram of the proposed solution is shown in the Fig. 5. The solution includes the excitation source (typically 10-100 kHz sinewave signal is used) and pickup of the response signal, which is converted by a signal (typically synchronous) detector (SD) to the bio-impedance Z signal. Typically module or real part of the complex Z is used. Also asynchronous detector can be considered [4] by simplicity reason.
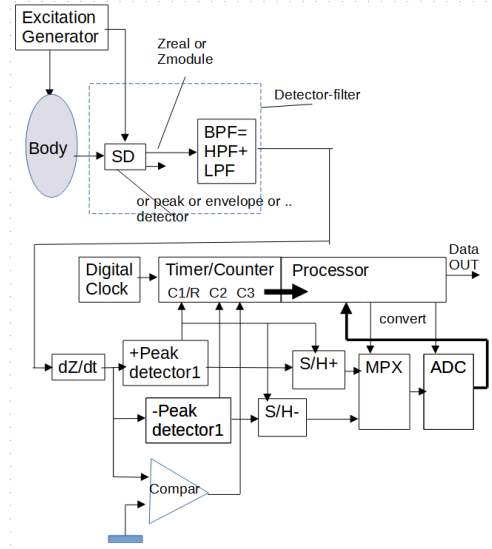

Fig. 5: Block diagram of the proposed solution

This part of the AC excitation and AC detector solution is not shown and analyzed in the solution, as standard solutions, offered also by the authors previously, can be used [14].

Further the high and low-pass filtering and taking of the first derivative *(dZ/dt)* are applied to extract the ICG signal. The ICG signal is then applied to "+peak" detector and "-peak detector" to follow the positive and negative peaks (extremums) and the comparator ("Compar") zero-crossings of the ICG signal. Peak detectors are designed in the way, that at the "event" time instance ("+peak", "-peak" or comparator "zero-crossing") the events are triggered and strobe signals are generated for digital counter (timer) and to control the sample-and-hold (S/H) units to fix the analog values at key points for further analog-to-digital (AD) conversion. The C-point timer ("+peak") is fixed at the C1 ($C1/R$) input of the timer/counter, the X-point count at the C2 input and B-point and C3. Also the "C-point" ("+peak" event), after copying the counts for C1, C2, C3 inputs, resets the timer (by R-input of the C1/R). Also the strobe pulses are generated by peak detectors to control the sample-and-hold units (S/H+ for C- and S/H- for B-point amplitudes). As there will be one (for C-point) or two values (for C- and X-points) to be sampled and AD-converted per cardiac period, the ADC can be reasonably simple, e.g. of counter (timer) based single-slope integrating type.

B. An implementation example of the proposed solution

The schematics of the proposed solution is shown in the Fig. 6. The schematics (made in TINA simulation environment of Texas Instruments (Dallas, TX, US)) include the input signal (generator) V_{ain1}, where the actually (from the wrist) acquired bio-impedance signal is used (as converted to WAV-
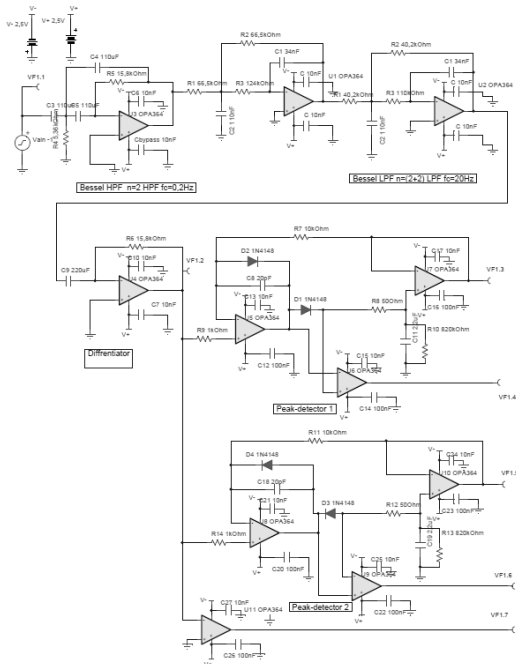
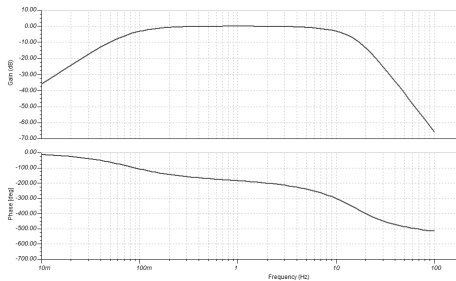Fig. 6: An implementation example of the proposed solution

Fig. 7: Frequency response of the filter part

Fig. 8: An example implementation of the peak detector
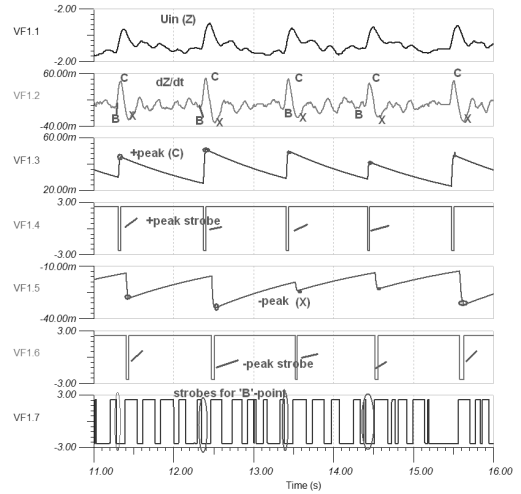
Fig. 9: Waveforms of the proposed solution

file). The op-amps U1-U3 from first the 2-nd order highpass filter (fc=0.1Hz) and two 2-nd order lowpass filter-stages (fc=10Hz), all of Bessel type.

The plot of the overall filter frequency response (magnitude and phase) is given in the Fig. 7. After the differentiator (U4) there are "+peak" and "-peak" detectors to "catch" the C- and X-points. The difference in the implementation of the "+peak" and "-peak" is only in reversing the diodes. The simplified "+peak"-detector is depicted in the Fig. 8. The idea of the peak detector implementation can be a simple "diode-and-capacitor" based circuit, put into the negative feedback path of the op-amp. Also, the voltage drop on the diode can (e.g. through the comparator) generate the strobe pulse, the closing
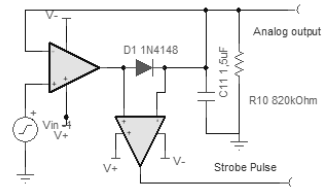
of the diode edge shows, that the peak has been acquired and can be "latched" for further processing, as well as in time domain, as well as by it's amplitude value. The comparator U11 generates from zero-crossings of the *dZ/dt* signal the strobe pulses for B-point location. The additional logic is needed, to use the last pulse before the C-point see the VF1.7 curve int the Fig. 9.

For actual CMOS implementation of the peak detectors various solutions have been proposed [19]–[21].

Some waveform curves of the example implementation from LT-Spice simulations are given in the Fig. 9:

- VF1.1 - acquired impedance signal *Z*(real-life signal acquired from the wrist);
- VF1.2 - signal after filtering and differentiator *(dZ/dt)*;
- VF1.3 - "+peak" signal (for the C-point);
- VF1.4 - strobe signal for the "+peak" signal;
- VF1.5 - "-peak" signal (for the X-point);
- VF1.6 - strobe signal for the "-peak" signal;
- VF1.7 - strobe signals for the B-point (zero crossing of *dZ/dt*) - the last strobe used at the "+peak" (C-point) event;

C. Comparison with previous solutions

In the papers [22], [23] some estimations of the correctly found fiducial points have been given, being on the level of the 90% or even less. Still, the number of correctly found points depend much on the quality and strength of the signals and how sophisticated signal processing is used, compared to the proposed simple mostly analog (and potentially low-power) signal processing.
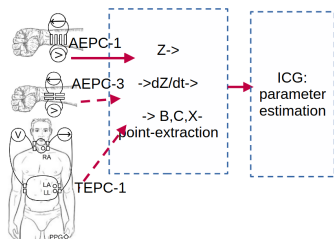

Fig. 10: Measurement setup

The proposed solution is suitable also for weak signals, acquired from the wrist (compared with much stronger signal amplitude from the chest) – see the measurement setup in the Fig. 10. The measurement setups TEPC-1, AEPC-1 and AEPC-3 have been discussed in the paper [24].

Estimation of the correctly found X-X, B-B and C-C time intervals have been carried out in simulations (with real-life signals) for the proposed solution vs the previous solution [18]. The simulation plots are shown in the Fig. 11 (from up to down – original impedance signal Z, first derivative *dZ/dt* (with fiducial points found by the proposed approach), the second derivative *dZ2/dt2* (with fiducial points found by the previous method), and finally the ECG waveform.

The results of the falsely detected fiducial points (time intervals) has been given in the Table I for the proposed and in the Table II for the previous solution, showing just for weak (wrist) signals significantly improved fiducial point determination.

TABLE I: Number of falsely detected fiducial points for the proposed solution

No	Conf	Total periods	B-B errors	C-C errors	X-X errors	Total errors
1	TEPC-1	33	0	0	0	0
1	AEPC-1	20	0	0	1	1
1	AEPC-3	20	0	0	0	0

TABLE II: Number of falsely detected fiducial points for the previous solution

No	Conf	Total periods	B-B errors	C-C errors	X-X errors	Total errors
1	TEPC-1	33	0	0	0	0
1	AEPC-1	20	16	16	15	47
1	AEPC-3	20	20	20	20	60
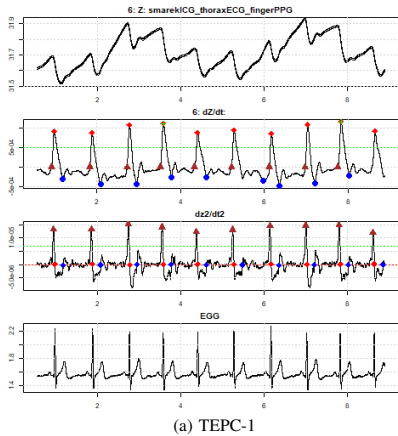
(a) TEPC-1
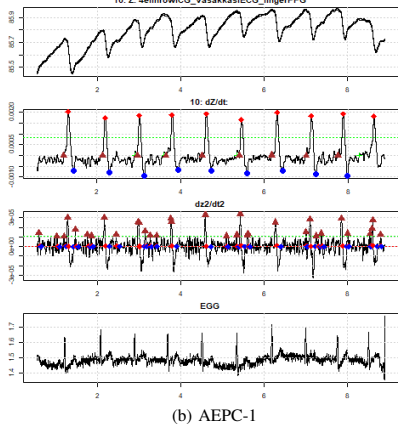
(b) AEPC-1
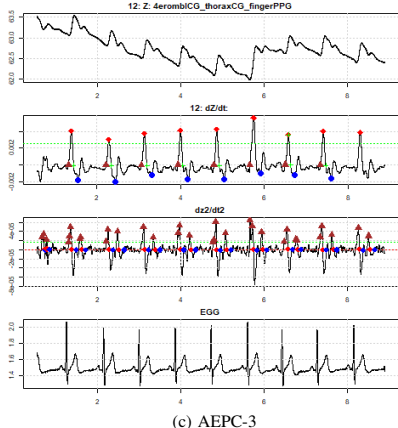
(c) AEPC-3

Fig. 11: Waveforms for setups TEPC-1, AEPC1 and AEPC-3

IV. CONCLUSION, DISCUSSION AND FUTURE WORK

The novel solution for extracting the ICG fiducial points to calculate the cardiac efficiency (CO and SV) -as well as on the block diagram level and as an implementation example in schematics- has been proposed, discussed and analyzed. This work shows, that it is possible and reasonable to embed the solution of the ICG-parameter estimation into the wearable device and also into the dedicated chip. Of course, more signals are needed for testing this solution, to improve their validation.

If compared to classical solutions, with ADC and digital processor analyzing the waveforms, the power consumption of the solution, if implemented in low-power CMOS ASIC, will be by an order less. For example the very low-power microcontroller MSP430 is consuming in active mode at least 400 μA and a 16-bit low power ADC ADS-1118 at least 100 μA, so totally more than 0.5 mA, then commercial low-power op-amps can work at few μA-s (e.g. LTC6258 takes 20 μA at 1 MHz bandwidth) and custom-design ones work even at lower consumption. Also digital CMOS counters, having a fractional complexity of microcontrollers and microprocessors can be easily implemented with extremely small power consumption.

From the accuracy viewpoint of the measurement electronics - the proposed solution can have the same accuracy, as digital implementation with high resolution (16-bit or more) ADC with relatively high sample-rate (in the context of the very low-power electronics, e.g. of 1 kHz) with sophisticated digital signal processing, replaced now by processing of few samples per second, latched precisely in analog domain. Also, as analog values of the fiducial points (especially critical is the C-point amplitude value, defining very much the estimation of the cardiac SV and CO values) are latched asynchronously, not sampled on the grid of the ADC sample-rate, the measurement accuracy will be significantly improved.

As a discussion, an important aspect is the chosen concept for the acquisition of interesting bio-signal - the choice of suitable location for placement of electrodes to the measurement accuracy of the ICG parameters, starting from the fiducial points, their locations in time and amplitudes.

REFERENCES

[1] O. G. Martinsen and S. Grimnes, *Bioimpedance and Bioelectricity Basics*, 3rd ed. Academic Press, Aug 2014.

[2] R. P. Patterson, "Fundamentals of impedance cardiography," *IEEE Engineering in Medicine and Biology Magazine*, vol. 8, no. 1, pp. 35–38, 1989.

[3] M. Nabian, Y. Yin, J. Wormwood, K. S. Quigley, L. F. Barrett, and S. Ostadabbas, "An open-source feature extraction tool for the analysis of peripheral physiological data," *IEEE Journal of Translational Engineering in Health and Medicine*, vol. 6, pp. 1–11, 2018.

[4] H. Yazdanian, A. Mahnam, M. Edrisi, and M. Esfahani, "Design and implementation of a portable impedance cardiography system for noninvasive stroke volume monitoring," *Journal of Medical Signals and Sensors*, vol. 6, pp. 47–56, Jan 2016.

[5] E. Piuzzi, S. Pisa, E. Pittella, L. Podestà, and S. Sangiovanni, "Wearable belt with built-in textile electrodes for cardio—respiratory monitoring," *Sensors*, vol. 20, no. 16, 2020.

[6] J. Xu, X. Gao, A. Lee, S. Yamada, E. Yavari, V. Lubecke, and O. Boric-Lubecke, "Wrist-worn heartbeat monitoring system based on bio-impedance analysis," *2016 38th Annual International Conference of the IEEE Engineering in Medicine and Biology Society (EMBC)*, pp. 6294–6297, 2016.

[7] M. Metshein, P. Annus, R. Land, M. Min, and A. Aabloo, "Availability and variations of cardiac activity in the case of measuring the bioimpedance of wrist," in *2018 IEEE International Instrumentation and Measurement Technology Conference (I2MTC)*, 2018, pp. 1–5.

[8] K. Pesti, M. Metshein, P. Annus, H. Kõiv, and M. Min, "Electrode placement strategies for the measurement of radial artery bioimpedance: Simulations and experiments," *IEEE Transactions on Instrumentation and Measurement*, vol. 70, pp. 1–10, 2021.

[9] J. C. Miller and S. M. Horvath, "Impedance cardiography," *Psychophysiology*, vol. 15, no. 1, pp. 80–91, 1978.

[10] J. Bour and J. Kellett, "Impedance cardiography - a rapid and cost-effective screening tool for cardiac disease," *European journal of internal medicine*, vol. 19, pp. 399–405, Nov 2008.

[11] S. M. M. Naidu, U. R. Bagal, P. C. Pandey, S. Hardas, and N. D. Khambete, "Detection of characteristic points of impedance cardiogram and validation using doppler echocardiography," in *2014 Annual IEEE India Conference (INDICON)*, 2014, pp. 1–6.

[12] K. Dheman, P. Mayer, M. Magno, and S. Schuerle, "Wireless, artefact aware impedance sensor node for continuous bio-impedance monitoring," *IEEE Transactions on Biomedical Circuits and Systems*, vol. 14, no. 5, pp. 1122–1134, 2020.

[13] S. Weyer, T. Menden, L. Leicht, S. Leonhardt, and T. Wartzek, "Development of a wearable multi-frequency impedance cardiography device," *Journal of Medical Engineering & Technology*, vol. 39, pp. 1–7, Jan 2015.

[14] M. Min, O. Martens, and T. Parve, "Lock-in measurement of bio-impedance variations," *Measurement*, vol. 27, pp. 21–28, Jan 2000.

[15] M. Metshein, T. Parve, P. Annus, M. Rist, and M. Min, "Realization and evaluation of the device for measuring the impedance of human body for detecting the respiratory and heart rate," *Elektronika ir Elektrotechnika*, vol. 23, pp. 36–42, June 2017.

[16] G. Roa, T. Le Pelleter, A. Bonvilain, A. Chagoya, and L. Fesquet, "Designing ultra-low power systems with non-uniform sampling and event-driven logic," in *2014 27th Symposium on Integrated Circuits and Systems Design (SBCCI)*, 2014, pp. 1–6.

[17] M. Greitans, R. Shavelis, L. Fesquet, and T. Beyrouthy, "Combined peak and level-crossing sampling scheme," in *9th International Conference on Sampling Theory and Applications (SampTA'11)*, Singapore, Singapore, May 2011, pp. Fr2S12.1 – P0158.

[18] B. Sramek, "Noninvasive continuous cardiac output monitor," U.S. Patent 4 450 527, May 22, 1984.

[19] S. Mandal and S. Dasgupta, "Modified cmos peak detector and sample hold circuit for biomedical applications," in *2018 Conference on Emerging Devices and Smart Systems (ICEDSS)*, 2018, pp. 113–116.

[20] K. Achtenberg, J. Mikołajczyk, D. Szabra, A. Prokopiuk, and Z. Bielecki, "Review of peak signal detection methods in nanosecond pulses monitoring," *Metrology and Measurement Systems*, vol. 27, no. 2, pp. 203–218, 2020.

[21] W. Reklewski, K. Heryan, M. Miśkowicz, and P. Augustyniak, "Real time ecg r-peak detection by extremum sampling," in *2020 6th International Conference on Event-Based Control, Communication, and Signal Processing (EBCCSP)*, 2020, pp. 1–7.

[22] S. Benouar, A. Hafid, M. Attari, M. Kedir-Talha, and F. Seoane, "Systematic variability in icg recordings results in icg complex subtypes - steps towards the enhancement of icg characterization," *Journal of electrical bioimpedance*, vol. 9, no. 1, p. 72—82, January 2018. [Online]. Available: https://europepmc.org/articles/PMC7852018

[23] S. M. M. Naidu, P. C. Pandey, and V. K. Pandey, "Automatic detection of characteristic points in impedance cardiogram," in *2011 Computing in Cardiology*, 2011, pp. 497–500.

[24] M. Metshein, A. Gautier, B. Larras, A. Frappe, D. John, B. Cardiff, P. Annus, R. Land, and O. Martens, "Study of electrode locations for joint acquisition of impedance- and electro-cardiography signals," in *2021 43rd Annual International Conference of the IEEE Engineering in Medicine Biology Society (EMBC)*, 2021, pp. 7264–7267.

Appendix 2 — A Dsp-Based Impedance Measurement Device

II

Anar Abdullayev, Olev Martens, Marek Rist, Margus Metshein, Mart Min, and Paul Annus. A DSP-based impedance measurement device. *2022 18th Biennial Baltic Electronics Conference (BEC)*, pages 1–5, 2022

A DSP-based Impedance Measurement Device

Anar Abdullayev
T. J. Seebeck Department of Electronics
Tallinn University of Technology
Tallinn, Estonia
anar.abdullayev@taltech.ee

Olev Martens
T. J. Seebeck Department of Electronics
Tallinn University of Technology
Tallinn, Estonia
olev.martens@taltech.ee

Marek Rist
T. J. Seebeck Department of Electronics
Tallinn University of Technology
Tallinn, Estonia
marek.rist@taltech.ee

Margus Metshein
T. J. Seebeck Department of Electronics
Tallinn University of Technology
Tallinn, Estonia
margus.metshein@taltech.ee

Mart Min
T. J. Seebeck Department of Electronics
Tallinn University of Technology
Tallinn, Estonia
mart.min@taltech.ee

Paul Annus
T. J. Seebeck Department of Electronics
Tallinn University of Technology
Tallinn, Estonia
paul.annus@taltech.ee

Abstract—A preliminary version of the novel digital signal processor (DSP) based electrical impedance measurement device has been developed and evaluated. Used DSP is TMS320F28379D (of Texas Instruments), being a dual core 16/32 bit DSP/DSC (digital signal processor / digital signal controller) with 4 on-chip 16-bit ADC-s, PWM units, lot of flash and SRAM memory etc. For excitation signal the on-chip PWM is used and for acquiring of the response (and excitation) signal waveforms the internal 16-bit ADC-s. By first evaluation the device can work at least in the frequency range from 1 kHz to 100 kHz with resolution and measurement uncertainty (and so also the potential accuracy) of 0,01% or better. Further work include implementation of the simultaneous multifrequency measurement for impedance spectroscopy and evaluation of the applicability of the proposed device for several impedance applications.

Index Terms—dsp, electrical impedance, impedance measurement, impedance spectroscopy

I. INTRODUCTION

Electrical impedance is usually defined as an expression of opposition of a circuit to alternating current. The term impedance was brought to the literature by Oliver Heaviside in 1886 [1]. Impedance is a complex quantity whereas the resistance forms the real part and reactance makes the imaginary part [2]. Electrical impedance can be used to characterize tissues, materials and structures [3] and electrochemical solutions (like batteries) [2].

Important are bio-impedance applications, e.g identification of human tissues, [4], impedance cardiography (and monitoring of the respiratory function) of humans [5]–[7].

Impedance spectroscopy is measurement and analysis of impedance related variables and plotting of these variables in a complex plane [1]. There are different methods to measure

and calculate impedance of an unknown object, such as AC bridges, phase-sensitive detectors, direct measurement with oscilloscope, automated frequency response analysis and using of the digital signal processing and DSP to transform the calculations into the digital domain [2]. Of course, also in this case still the analog front-end (AFE) is needed, with analog-to-digital and digital-to-analog data converters between the DSP and the object-under-measurement.

In general, the impedance measurement devices usually consist of signal (excitation) generator, response signal sensing part, ADC (analog to digital converter) and DSP engine to process the response signal (most typically by DFT -discrete Fourier transform).

There are available high-accuracy impedance measurement instruments, like Wayne-Kerr 6500B with basic accuracy of 0.05 % and frequency range up to 120 MHz. This and other similar desktop instruments are bulky and costly.

Or there are devices to measure impedance like "lock-in-amplifier" type, such as Zurich Instruments MF-IA, including phase sensitive detector implemented in the DSP. Although having superior precision and wide frequency range, with the development of digital signal processors in parallel with lower power consumption opens new possibility to develop more adaptable, mobile, cheaper and thanks to 16-bit builtin differential ADC-s of the utilized DSP more accurate impedance spectroscopy devices. Impedance spectroscopy can now more-and-more be used for more than just laboratory purposes thanks to these new capabilities.

There are available dedicated impedance measurement chips [8] - like AD5933, which have limited (by internal 12-bit ADC) resolution, bandwidth (up to 100 kHz) and only a single measurement frequency at a time.

By authors of this paper several DSP-based impedance measurement devices with external (to DSP) ADC and DACs have been developed [9], [10]. Still, these solutions cannot be easily micro-miniaturized and are using relatively costly precise data-converters.

More interesting are "almost single-chip (DSP-based)"

Fig. 1. Photo of the developed device

impedance measurement devices, proposed by the same research group [11].

Still, newer more advanced DSP-s with improved peripheral units, with e.g. improved resolution (e.g 16-bit instead of-12 bit at high speed successive approximation principle - ADC), but also with higher digital clock rate and with dual DSP-cores gives new opportunities such as performing DFT calculations for higher frequency content signal in real time for significantly improved simple low-cost impedance measurement devices.

The current research describes and assesses a new DSP-based impedance measurement method that has achieved measurement accuracy that is considerably higher.

II. PROPOSED SOLUTION -HARDWARE

A. DSP-Board Description

In the current first prototype the low-cost processor board LAUNCHXL-F28379D (lower red board in the Fig. 1) of Texas Instruments (TI) is used. The board has USB connected isolated XDS100v2 JTAG debug probe for real-time debug and flash programming, 4x 20-pin headers/connectors (used to plug to there the impedance measurement analog-front end -AFE)- designed specially for the proposed solution.

The TMS320F28379D processor includes 200 MHz dual C28xCPUs, 1 MB Flash, 16-bit ADCs, comparators, 12-bit DACs, delta-sigma sinc filters, high resolution PWM-s (HR-PWM) and more.

The board is supported by Code Composer Studio software development environment and C2000Ware library files, all freely available from TI.

B. Impedance Shield -Hardware

Shield PCB (upper green board in the Fig. 1, block diagram depicted in the Fig. 2) has several functionalities. It consists of low-pass filters, virtual ground section, inverting amplifiers, buffers, voltage regulator and connector to connect reference resistor and the object to be tested. Low-pass filter cut-of frequency is tuned to 250 kHz and its aim is to remove high-frequency harmonics of the PWM based excitation signal as well as external noise. A virtual ground circuit is included on the PCB to remove the DC portion of the input signal and to act as a reference for inverting amplifiers to prepare the signal for differential ADC. Furthermore, when operating within the limits of op-amps (operational amplifier), the PCB can scale signals to optimize ADC dynamic range. This PCB was created using EAGLE software. Its dimensions are 86.4 mm x 58.4 mm, and it was created to fit on a DSP unit.

The developed hardware enables to send the HR-PWM output voltage of the DSP though dedicated analog buffer and low-pass-filters through the external "ref resistor" (upper right screw terminal in the Fig. 1) to the measured object (device under test- DuT- e.g. resistor Rx, (upper left screw terminal in the Fig. 1)). The excitation current, coming from the excitation output through this ref. resistor to Rx generates the voltage drop on DuT.

In the response path one of the four available on-the-DSP-chip 16-bit ADC-s is measuring the total excitation voltage and another 16-bit ADC the voltage drop on DuT.

C. DSP Software

The software for the DSP was developed in TI Code Composer Studio [12] in C language and has the following functionalities:

- Initialization part 1 - setting up of the reference look-up sine- and cosine tables for later DFT fast and real-time calculation;
- Initialization part 2 - setting up one of the PWM channels to generate the ADC sampling interrupts in 2 microsecond period (so the simultaneous sampling frequency in both ADC channels is fs = 500 kHz);
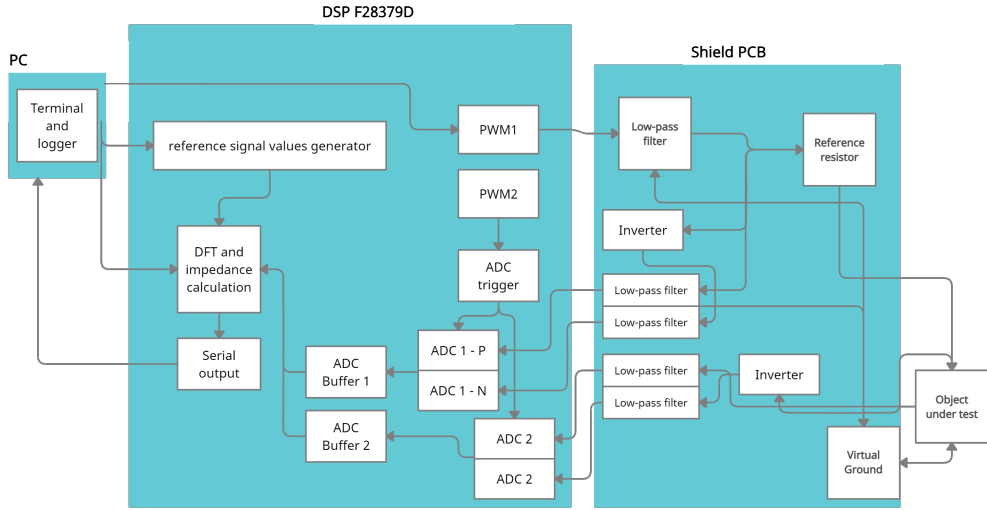
Fig. 2. Block diagram of the proposed solution

- Initialization part 3 - setting up another PWM channel to generate the excitation signal in the simple "chopper mode". In the current first tries the fixed frequencies of 1 kHz, 10 kHz and 100 kHz were used; more sophisticated excitation signal waveforms and patterns will be developed in next stages of the research;
- Inside of the mentioned ADC sampling interrupts the buffers of 500 samples are filled (in every 1 ms the update can be calculated), for both excitation and response channels in parallel; if the buffer is full, the data acquisition will switch over to another set of buffers (so the data acquisition is swapped between A- and B-buffers); and onto the both excitation and response filled ("ready") buffers the DFT will be applied, that means the acquired waveforms are "multiplied and accumulated" with the reference sine- and cosine waves with the same expected (and generated in the excitation) frequency. Then the DFT (actually MAC-computation results) are used as complex values and the complex ratio of the response voltage to the excitation voltage is calculated. This ratio is actually the transfer coefficient of the voltage divider R0 /Zx and as R0 is known (accurately measured by a reference multi-meter), the complex value of Zx can be computed.
- The determined complex ratio or finally estimated Zx value is transmitted by virtual UART (USB) to PC to be displayed and logged;

III. EVALUATION OF THE DEVICE PERFORMANCE

For the evaluation of the hardware a special preliminary (provisional) software was developed as described above. For first simple tests DSP can initiate single excitation frequency

at a time, currently 1, 10 or 100 kHz. The amplitude value of the signal is in the range of the 1 V. The "reference" (actually range-) fixed resistor had value of 10 kΩ (also 1 or 100 kΩ can be used). On PC side a simple Python script was written to receive from UART the result values to display on the computer screen and also to save in log files for further analysis.

By first impression the measurement result (after additional additive and multiplicative calibration corrections at two measurement points- Rx = 0 and Rx = 10 kΩ) was precise, accurate and stable at least on the 0.01 % level, after some (e.g over 20 measurements or in other words over 20 ms time, as the measurement results are updated every 1 ms).

A. The Repeatability Test

To test the repeatability of the device, fixed (constant) resistances were measured 1000 times in 3 different frequencies (1, 10 and 100 kHz) and the span in the outcome evaluated. Span is calculated according to the Equation (I), where span x:

$$x = \frac{Max - Min}{Average \cdot 2} \cdot 100\% \qquad (1)$$

Results are given in the Table I below.

As expected, the smallest uncertainty is seen at the mid-value of the resistor (10 kΩ) and mid-frequency (10 kHz). More detailed analysis of the actual raw-data logs shows that most of the "measurement span" was related to the 50 Hz (so being probably power-) noise, what can be suppressed by better shielding and grounding of the developed measurement device or alternatively by efficient software filters in the DSP, rejecting the power-harmonics.

R (kΩ)	f (kHz)	Max	Min	Average	Span($\pm$%)
1	1	996.4477	995.1446	995.7945	0.0654
1	10	995.8280	995.0020	995.3954	0.0415
1	100	997.1498	995.5846	996.3969	0.0785
10	1	9994.9791	9989.9665	9992.4349	0.0251
10	10	9992.6823	9989.4885	9990.9079	0.0160
10	100	9944.6065	9929.0075	9933.6970	0.0785
100	1	96207.2276	96037.4620	96120.4501	0.0883
100	10	94955.3652	94840.845	94901.2242	0.0603
100	100	94955.4102	94840.845	94901.8316	0.0604

B. The Test With the Emulated Cardio-Respiratory Bio-Impedance Signal

A special test-box to emulate the dynamic electrical bio-impedance modulations has been developed earlier in the research group [13]. In the test box (Fig. 3) two electrical drives are mechanically modifying the position of the axes of the potentiometers, one having the period of the breathing period and another of the cardiac activity. An example of one measurement series with the proposed measurement device is shown in the Fig. 4.

The respiratory component maximum impedances are seen at t = 3, 7, 11, 15 s and smaller cardiac peaks at higher repetition rate.

This experiment shows the possibility to use the proposed solution for bioimpedance (e.g. impedance cardiography) measurements [5], [6]. Of course, appropriate AFE is needed to be developed for such purpose.

C. The Test With the Resistor-Box

Metrological resistor boxes exist, where precise resistors can be switched into series in a decade steps in large dynamical range. Experiments were made to estimate the accuracy and resolution of the proposed measurement device with a such box (Fig. 5) and promising results were achieved.

Fig. 4. Impedance plot with cardio-respiratory emulation

As an example- one of the measurement series included the values of Rx = 10.0000 - 11.0000- 11.1000 - 11.1100 - 11.1110 - 11.1110 kΩ, shown as steps 1 to 6 in the Fig. 6. The upper plot shows the resistance measured (about 10...11 kΩ) and the lower graph the measurement error in Ohms for every measurement point. So it can be seen the measurement error is below 1 Ω at around 11 kΩ, giving the relative error below 0.01 % , what is better number than previous instruments of the same (portable, low-cost, real-time) have had. Note that, simple calibration was applied to the measurements by using two distant load values to cancel out bias error.

D. The Test With the Capacitive Load

A 100 nF nominal capacitor was used as a load at 10 kHz excitation frequency to test the capacitance measurement capability. The measured average impedance magnitude over 1000 samples is 168.34 Ω, with the calculated standard deviation of

Fig. 3. Emulator of the cardio-respiratory dynamic impedance [13]
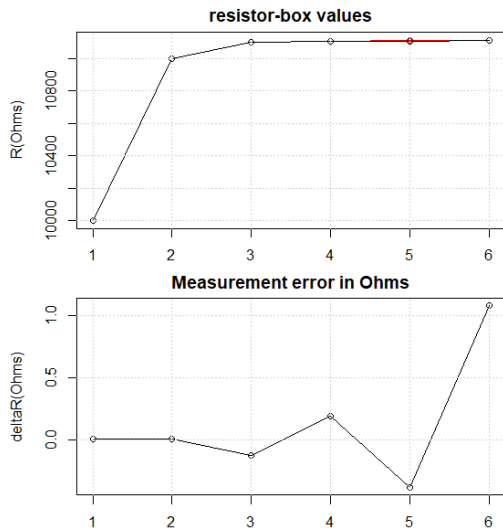

Fig. 5. Metrological resistor box

Fig. 6. Impedance evaluation with resistor box

0.007 Ω. Using the equation

$$|Z| = \frac{1}{2 \cdot \pi \cdot C \cdot f} \qquad (2)$$

where $|Z|$ is magnitude of measured impedance and f is excitation frequency, capacitance (C) is calculated as 94.542 nF and measured phase value is -89.687 deg. These uncalibrated results are comparable with the measurements (94.231 nF and -89.568 deg) of reference device - Agilent Technologies, E4990A impedance analyzer [14].

IV. Conclusion, discussion and future work

The significantly improved DSP-based impedance measurement solution has been proposed, developed and evaluated. The created solution includes hardware in the form of an add-on circuit, as well as software for the DSP and PC to measure, compute, view, and record impedance waveforms. Despite still being in the early and limited stages, significant advancements in the metrological parameters have been made.

The resolution and repeatability at the demonstrable 0.01 % level seems to be fulfilled and achieved, what is by an order better if to be compared to previous solutions with the same price, size etc categories.

Future work could be looking in the measurement accuracy in the extended frequency range (e.g. up to 300 or 500 kHz), adding measurement at several frequencies simultaneously, adding auto ranging feature etc.

Acknowledgment

and discussed relevant matters of the metrological characterization of the proposed device.

References

[1] Heaviside, *Electrical papers*. Providence: AMS Chelsea Publishing, 2008.

[2] E. Barsoukov and J. R. Macdonald, Eds., *Impedance Spectroscopy*. John Wiley & Sons, Inc., apr 2018.

[3] J. García-Martín, J. Gómez-Gil, and E. Vázquez-Sánchez, "Non-destructive techniques based on eddy current testing," *Sensors*, vol. 11, no. 3, pp. 2525–2565, 2011.

[4] S. Halonen, J. Kari, P. Ahonen, K. Kronström, and J. Hyttinen, "Real-time bioimpedance-based biopsy needle can identify tissue type with high spatial accuracy," *Annals of Biomedical Engineering*, vol. 47, no. 3, pp. 836–851, Mar 2019. [Online]. Available: https://doi.org/10.1007/s10439-018-02187-9

[5] O. G. Martinsen and S. Grimnes, *Bioimpedance and Bioelectricity Basics*, 3rd ed. Academic Press, Aug 2014.

[6] W. G. Kubicek, J. N. Karnegis, R. P. Patterson, D. A. Witsoe, and R. H. Mattson, "Development and evaluation of an impedance cardiac output system," *Aerosp Med.*, vol. 37, no. 12, pp. 1208–12, 1966.

[7] M. Metshein, P. Annus, R. Land, M. Min, and A. Aabloo, "Availability and variations of cardiac activity in the case of measuring the bioimpedance of wrist," in *2018 IEEE International Instrumentation and Measurement Technology Conference (I2MTC)*, 2018, pp. 1–5.

[8] *AD5933 1-MSPS, 12-Bit Impedance Converter, Network Analyzer: Datasheet*, Analog Devices, 2017, rev. F.

[9] O. Martens, M. Min, R. Land, and P. Annus, "Multi-frequency and multi-channel bio-impedance measurement solution," in *Proceedings of the 7th Nordic Signal Processing Symposium - NORSIG 2006*, June 2006, pp. 178–181.

[10] M. Reidla, O. Martens, and R. Land, "Tms320f28335-based high-accuracy complex network analyzer instrument," in *2012 5th European DSP Education and Research Conference (EDERC)*, Sep. 2012, pp. 44–47.

[11] M. Rist, M. Reidla, M. Min, T. Parve, O. Martens, and R. Land, "Tms320f28069-based impedance spectroscopy with binary excitation," in *2012 5th European DSP Education and Research Conference (EDERC)*, Sep. 2012, pp. 217–220.

[12] *"Code Composer Studio™ integrated development environment (IDE)"*. [Online]. Available: https://www.ti.com/tool/CCSTUDIO

[13] M. Rist and M. Min, "Dynamic reference for evaluation of bioimpedance spectroscopy devices," in *2016 15th Biennial Baltic Electronics Conference (BEC)*, 2016, pp. 107–110.

[14] *E4990A Impedance Analyzer*, Keysight, 2021. [Online]. Available: https://www.keysight.com/us/en/assets/7018-04256/data-sheets/5991-3890.pdf

Appendix 3 — Impedance Cardiography Signal Processing with Savitzky-Golay and Frequency Sampling Kernels

III

Olev Martens, Margus Metshein, Gert Tamberg, and Anar Abdullayev. Impedance cardiography signal processing with Savitzky-Golay and frequency sampling kernels. *2022 18th Biennial Baltic Electronics Conference (BEC)*, pages 1–5, 2022

Impedance Cardiography Signal Processing with Savitzky-Golay and Frequency Sampling Kernels

Olev Martens
T. J. Seebeck Department of Electronics
Tallinn University of Technology
Tallinn, Estonia
olev.martens@taltech.ee

Margus Metshein
T. J. Seebeck Department of Electronics
Tallinn University of Technology
Tallinn, Estonia
margus.metshein@taltech.ee

Gert Tamberg
Department of Cybernetics
Tallinn University of Technology
Tallinn, Estonia
gert.tamberg@taltech.ee

Anar Abdullayev
T. J. Seebeck Department of Electronics
Tallinn University of Technology
Tallinn, Estonia
anar.abdullayev@taltech.ee

Abstract—**ICG (impedance cardiography) is in addition to ECG (electrocardiography) an important indicator of the functioning of the overall cardiovascular system, including the cardiac (heart) activity. Usage of the ICG, especially in the wearables, improves the health monitoring, as the ICG shows various important hemodynamic parameters (relevant time intervals, also the stroke volume and cardiac output and their variability). ICG waveform is the time-domain derivative of the electrical bio-impedance signal. Two possible sampled data differentiation algorithms are discussed in the paper and demonstrated on the real-life signals, one exploiting the Savitzky–Golay 1-st order differentiation numerical scheme and another the frequency sampling method based FIR-filter design. Both approaches are shown to be promising. Tuning and final evaluation of the superiority of one or another method needs more experimental data and research.**

Index Terms—**impedance cardiography (ICG), electrical bio-impedance (EBI), derivative, *dZ/dt*, cardiac output, stroke volume, Savitzky–Golay filter, frequency sampling filter design**

I. INTRODUCTION

Electrocardiography (ECG) and impedance cardiography (ICG) are relevant methods for monitoring the cardiac activity, heart condition and hemodynamic parameters [1].

ECG is known already more than two centuries, measuring the electrical activity of the heart [1]. ICG, in use from the 1960-s [2], showing the mechanical activity of the heart, reflects the plethysmographic information i.e. volume changes in thoracic region. From ICG waveform one can estimate the heart rate (HR) and its variation (HRV), the efficiency of blood pumping – cardiac output (CO) and stroke volume (SV), but also relevant time intervals, e.g. left ventricular ejection time (LVET) and pre-ejection period (PEP) [3].
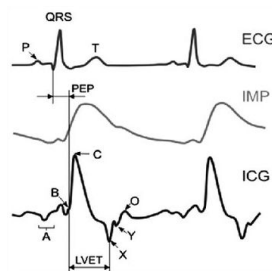
Fig. 1. Typical patterns of the ECG, impedance (IMP) and its resulting ICG waveforms (from top to bottom) [4]

The impedance cardiogram is classically acquired by stationary medical device, however, the development of portable solutions has emerged to a relevant topic [4].

Example waveforms of impedance (IMP) (denoted as Z in the following text) and the resulting (first derivative *(dZ/dt)* of the signal Z) ICG signal (with ECG signal in parallel) are shown in Fig. 1 [4]. On the plots of current research, the ECG signal is shown for reference, together with the impedance (Z) signal and the first derivative *(dZ/dt)*, as the actual "ICG signal" [2].

When considering the signal of ICG, the estimation of cardiac time interval LVET, volumetric flow rate CO and volume of blood SV presumes the determination of the most important hemodynamic fiducial points: B (opening of the aortic valve), C (maximum systolic flow) and X (closing of the aortic valve) (Fig. 1) [3]. The challenge in the ICG signal processing is to determine these points in the cardiac period – start, peak-location, and ICG signal amplitudes.

The method for acquiring the ICG impedance waveforms involves classically the monitoring setup over the whole thorax [2] (including the heart and the lungs). In such case, a kind of wearable belt can be placed around the thorax to acquire

ECG and ICG signals simultaneously, like in [5]. However, the cardiac waveforms can be obtained basically from every artery, e.g. by measuring from the wrist (radial artery) [6], from the neck (carotid artery) [7] etc. Such peripheral locations are preferred in the implementation of wearable devices.

The ICG waveform calculation, containing mostly the mathematical implementation or approximation of the time-domain derivative of the impedance $Z - dZ/dt$ function. However, also lowpass (or bandpass) filtering is needed, as the acquired impedance signals are quite weak and noisy and the differentiation amplifies the high-frequency noise significantly. So the signal processing solution needs combining of the filtering and differentiation.

Example of the possible analog and mixed implementation of the ICG-solution has been given in [8].

While in portable (typically microprocessor-based solutions) and computer-systems the ICG is calculated numerically, so on the sampled data, the computational implementation scheme of these solutions is typically not disclosed.

For more general applications, e.g for taking time-domain derivative (with filtering and smoothing of the time series) of the initially chemical experimental data (later used also for physiological signals) the polynomial approximation of the measured data has been proposed in 1964 and popularized by Abraham Savitzky and Marcel J. E. Golay [9]. While original Savitzky–Golay smoothing and differentiation filters were implemented for odd number of FIR-filter coefficients, there is also solution for even number data [10].

In the paper of 2022 [11] the ideas are developed to improve the frequency domain stopband attenuation of the Savitzky–Golay filter by replacing the original design by the alternative one.

Also to mention, a sliding mode differentiator combined with sliding mode filter for estimating the first and second-order derivatives of noisy signals has been proposed in 2020 [12].

In the frames of current work initial experimental bio-impedance signal acquisition has been performed (described in the following section) and existing measurement data reused (the full acquisition process is described in [13]).

Further, by using the acquired electrical bio-impedance signals from selected locations of the body (variety of electrode placement strategies, formed on the surfaces of thorax and wrist), the two derivative algorithms (Savitzky-Golay and frequency sampling method [14]) have been evaluated with real data. As shown, both methods give very reasonable results.

II. Signal Acquisition and the Results of Experimental Application of Developed Derivative Algorithms

Data from two different experimental ICG measurement datasets were included to this study - firstly an instantly acquired moderately sampled (at 200 Hz) data and secondly by an order more densely sampled data from previous experiment. The proposed derivative algorithms were tested with Z waveforms of both experimental data sets.
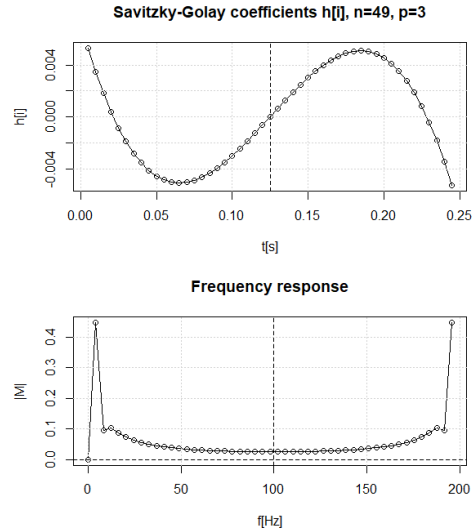

Fig. 2. Savitzky-Golay 1-st order differentiator: coefficients (in time and frequency domains)

The experiments that involve human body, described in the current paper, in all aspects follow the principles outlined in the Helsinki Declaration of 1975, as revised in 2000.

### A. Filter Design for Both Methods

As example Savitzky-Golay FIR filter with coefficient number $N = 49$ (and polynomial order $p = 3$) have been designed, with 1st order derivative function ($m = 1$). The (time-domain) filter coefficients are shown in the upper subplot of the Fig. 2 and frequency-domain representation (as inverse Fourier transform of the coefficient vector (the same samples)) is shown in the lower subplot there.

Let's note – here the suppression of the higher frequencies is quite poor, (including at 50 and 100 Hz), in the order of only 10 – 30 times or 20 – 30 dB, what can cause problems in some environments.

As alternative, the frequency sampling FIR-filter design method have been proposed and later applied. In one example the sampled data filter with $f_s = 200$ Hz with again $N = 49$ coefficients (in both time and frequency domain) (Fig. 3) was designed. The cut-off frequency have been selected as $f_c = 5$ Hz. Below this frequency a linear imaginary frequency response is selected ($K = j\dot\omega$) (shifted to imaginary (capacitive) part) and above f_c the frequency response values are chosen as zeroes. The frequency and time domain representation of the filter coefficients is given in the Fig. 3.

These filters have been applied to the first (moderately sampled) data set. For the second dataset similar filters have been designed and applied, with larger number of coefficients ($N = 99$).
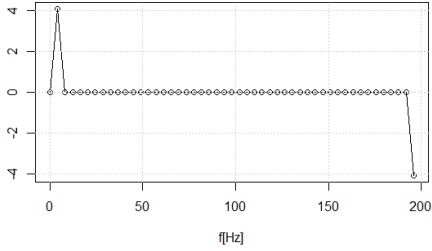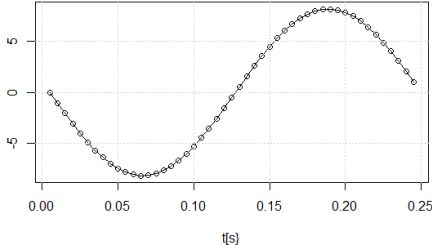
Fig. 3. Filter coefficients of the frequency sampling method, in the time and frequency domains ($N = 49$, $f_{cut} = 5$ Hz)
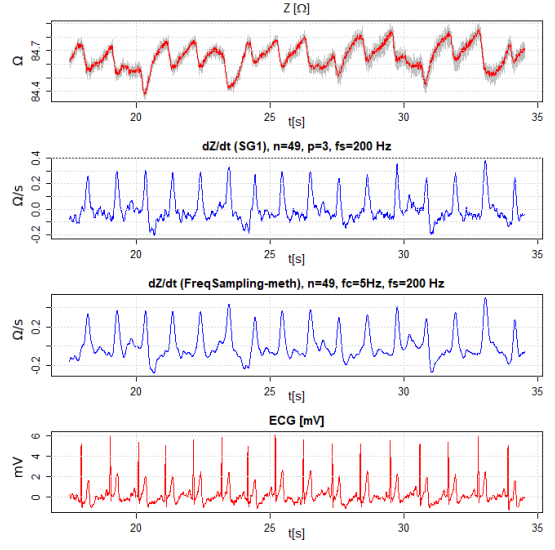

Fig. 4. Impedance Z experimental signal at $f_s = 200$ Hz with estimated (first by Savitzky-Golay and then by frequency sampling method) ICG (dZ/dt) waveform (plus simultaneously acquired ECG)

All the selected numbers of coefficients and properties (cut-off frequencies, orders etc.) of filters applied here have been experimentally determined as the best ones during the tests. However, the research needs extension to fine-tune the most suitable and precise parameters.

B. Experiment With Initial Thoracic Area Acquired Moderately Sampled ECG and ICG Dataset

For initial experiment, data has been collected from the thorax of a single male person (with classical spot-electrode arrangement [15] at the carrier frequency 50 kHz) by using of the DSP-based 16-bit solution (the developed data acquisition solution is not published yet). The sampling frequency was set to 200 Hz – with the aim of reducing the amount of gained data, directed to the possible developments in wearable solutions. The acquired Z (the upper subplot) and ECG (the lowest subplot) waveforms are shown in the Fig. 4 together with the applied derivative (dZ/dt) analysis result for both mentioned methods (second subplot for applied Savitzky-Golay kernel and third subplot for applied frequency sampling method kernel).

C. Experiment With Advanced Variety of Electrode Placement Strategies Containing Densely Sampled ECG and ICG Dataset

For advanced experiment, previously gathered ECG and ICG datasets from variety of locations on the body surface (full description available in [13]) have been utilized. The data was picked up with commercial on-desk impedance spectroscope with the sampling frequency about 1666 Hz (period T: 0.0006 s). ICG waveforms from variety of electrode placements on thorax (TEPC-1 and TEPC-4) and wrist (AEPC-1-4) were
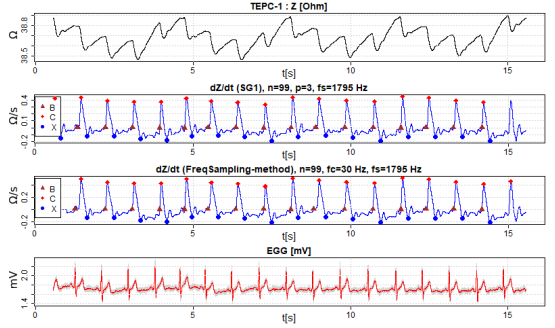

Fig. 5. Signal waveforms in the case of TEPC-1 (from the top: original signal of Z (1); ICG with applied Savitzky-Golay derivative algorithm (2); ICG with applied frequency sampling derivative algorithm (3), signal of ECG (4)

considered (detailed data concerning the electrode placement strategies can be accessed in [13]). Whereby TEPC and AEPC are abbreviations of thoracic electrode placement configuration and arm electrode placement configuration respectively. The numbers following the abbreviation denote certain electrode placement configuration on skin surface - demonstrated in detail in [13] The comparison and qualitative evaluation of both methods can be made based on each selected electrode placement strategy individually: Fig. 5 (TEPC-1), Fig. 6 (TEPC-4), Fig. 7 (AEPC-1), Fig. 8 (AEPC-2), Fig. 9 (AEPC-3) and Fig. 10 (AEPC-4).
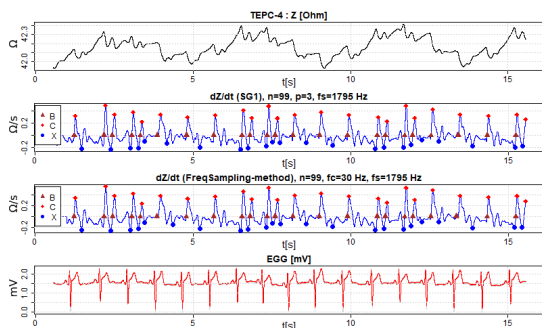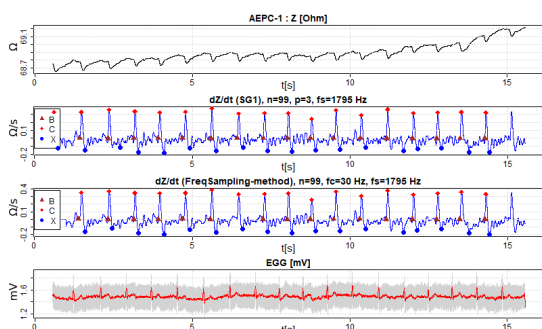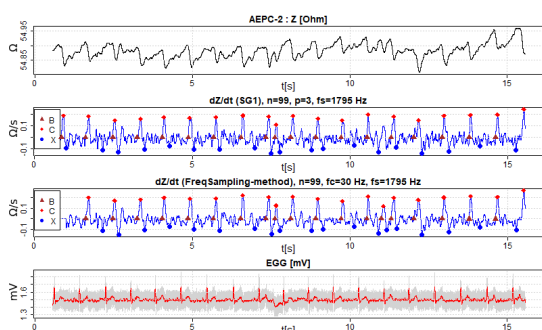
Fig. 6. Signal waveforms in the case of TEPC-4 (from the top: original signal of Z (1); ICG with applied Savitzky-Golay derivative algorithm (2); ICG with applied frequency sampling derivative algorithm (3), signal of ECG (4)

Fig. 9. Signal waveforms in the case of AEPC-3 (from the top: original signal of Z (1); ICG with applied Savitzky-Golay derivative algorithm (2); ICG with applied frequency sampling derivative algorithm (3), signal of ECG (4)

Fig. 7. Signal waveforms in the case of AEPC-1 (from the top: original signal of Z (1); ICG with applied Savitzky-Golay derivative algorithm (2); ICG with applied frequency sampling derivative algorithm (3), signal of ECG (4)
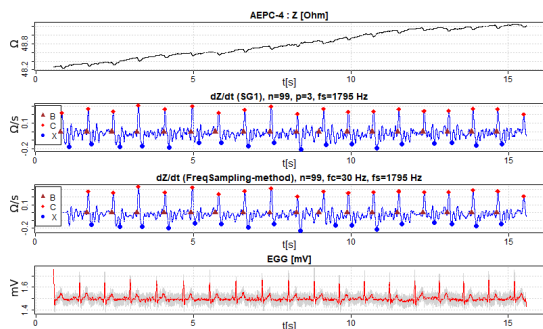
Fig. 10. Signal waveforms in the case of AEPC-4 (from the top: original signal of Z (1); ICG with applied Savitzky-Golay derivative algorithm (2); ICG with applied frequency sampling algorithm (3), signal of ECG (4)

Fig. 8. Signal waveforms in the case of AEPC-2 (from the top: original signal of Z (1); ICG with applied Savitzky-Golay derivative algorithm (2); ICG with applied frequency sampling derivative algorithm (3), signal of ECG (4)

D. Quality Estimation and Evaluation of the Proposed Solutions

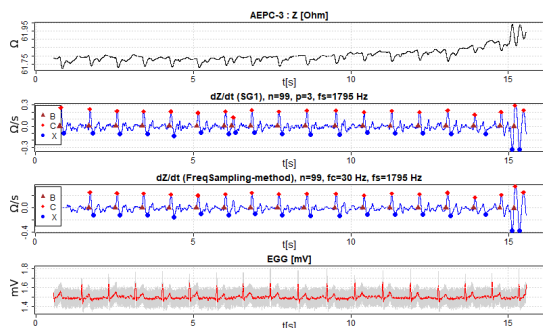Firstly, processed by both filtering methods the differentiated ICG waveforms were evaluated visually, according to the gained plots (Fig. 4 - 10). Visual evaluation, described subsequently, was performed separately for moderately and densely sampled ICG waveforms - so the results are comparable in its frames. In the case of moderately sampled initial ICG dataset, the frequency sampling method tends to visually provide more distinct waveform. However, in all other cases the proposed methods work reasonably well and it is hard to prefer one methods to another. While the Savitzky-Golay approach preserves the waveform in more details, then the key points and characteristics of the ICG waveforms seem to be seen with the same resolution and accuracy. Of course, the frequency sampling method gives better suppression of the noise and disturbances, including the 50 / 100 Hz one.

Secondly, a small software (R-language script) was written for the extraction of the fiducial points B, C and X. The time intervals for all three points were calculated and compared with expected values (900 ms for the interval C-C, 60 ms for the interval B-C and 200 ms for the interval C-X). The intervals were calculated from the point C to next C, from C to X and from B to C in the current cardiac cycle. As a result, the errors in determination of the defined intervals were

TABLE I
EVALUATION OF THE ALGORITHMS

No	Conf	C-C errors	C-X errors	B-C errors	Total cardiac periods
1 (SG*)	TEPC-1	0	0	0	16
1 (FS**)	TEPC-1	0	0	1	15
2 (SG*)	TEPC-4	7	10	0	22
2 (FS**)	TEPC-4	7	11	0	22
3 (SG*)	AEPC-1	0	1	0	17
3 (FS**)	AEPC-1	0	1	1	16
4 (SG*)	AEPC-2	1	6	1	18
4 (FS**)	AEPC-2	1	4	1	18
5 (SG*)	AEPC-3	2	2	0	18
5 (FS**)	AEPC-3	1	0	0	16
6 (SG*)	AEPC-4	0	0	1	17
6 (FS**)	AEPC-4	0	1	0	16

(SG*) - with Savitzky-Golay filter
(FS**) - with frequency sampling filter

counted – visible in the Table I. The direct reason for inability to determine the time interval is the quality of the signal - and the goodness of the method is shown by the ability to find the intervals. However, it is hard to prefer from these results one method from another, as both methods are performing reasonably well.

III. DISCUSSION, CONCLUSION AND FUTURE WORK

As it can be seen from the plots and results, both methods (Savitzky-Golay and frequency sampling kernels) perform reasonably well over various ICG signals (of different sampling frequency and variety of electrode locations). Results demonstrate the capableness of the presented derivative algorithms of calculation to determine the ICG-waveforms and specific cardiac-cycle points on the graph.

The tuning of parameters for both methods is expected to provide further improvement, enabling to output, which method finally outperforms for various conditions and signals. The introduction of tailor-made approach for performance metrics will be part of the extension of this research.

It must be noted that the current study may be limited in some aspects. The number of samples is relatively small i.e., only the data logs of two subjects have been used in verifying the algorithms. Secondly, a single evaluation method (by finding the errors in determining the time intervals for selected fiducial points B, C and X) for comparing the proposed algorithms is applied. In the potential extended study, the sample size is expected to increase and additional evaluation approaches applied.

Also, to mention, both suggested and evaluated methods are limited to uniformly (in both time and frequency domains) sampled filter coefficients (and kernels). At the same time, more advanced (and efficient) data acquisition methods exist for the physiological signals, using e.g. the level-crossing ADC-s (like [16]), generating the non-uniformly sampled data. Hence, additional research and innovations could be beneficial in this field.

REFERENCES

[1] O. G. Martinsen and S. Grimnes, *Bioimpedance and Bioelectricity Basics*, 3rd ed. Academic Press, Aug 2014.

[2] R. P. Patterson, "Fundamentals of impedance cardiography," *IEEE Engineering in Medicine and Biology Magazine*, vol. 8, no. 1, pp. 35–38, 1989.

[3] M. Nabian, Y. Yin, J. Wormwood, K. S. Quigley, L. F. Barrett, and S. Ostadabbas, "An open-source feature extraction tool for the analysis of peripheral physiological data," *IEEE Journal of Translational Engineering in Health and Medicine*, vol. 6, pp. 1–11, 2018.

[4] H. Yazdanian, A. Mahnam, M. Edrisi, and M. Esfahani, "Design and implementation of a portable impedance cardiography system for noninvasive stroke volume monitoring," *Journal of Medical Signals and Sensors*, vol. 6, pp. 47–56, Jan 2016.

[5] E. Piuzzi, S. Pisa, E. Pittella, L. Podestà, and S. Sangiovanni, "Wearable belt with built-in textile electrodes for cardio—respiratory monitoring," *Sensors*, vol. 20, no. 16, 2020.

[6] M. Metshein, P. Annus, R. Land, M. Min, and A. Aabloo, "Availability and variations of cardiac activity in the case of measuring the bioimpedance of wrist," in *2018 IEEE International Instrumentation and Measurement Technology Conference (I2MTC)*, 2018, pp. 1–5.

[7] T.-W. Wang, H.-W. Chu, L. Chou, Y.-L. Sung, Y.-T. Shih, P.-C. Hsu, H.-M. Cheng, and S.-F. Lin, "Bio-impedance measurement optimization for high-resolution carotid pulse sensing," *Sensors*, vol. 21, no. 5, 2021. [Online]. Available: https://www.mdpi.com/1424-8220/21/5/1600

[8] O. Martens, M. Metshein, A. Abdullayev, B. Larras, A. Frappe, A. Gautier, M. Saeed, D. John, B. Cardiff, A. Krivošei, P. Annus, and M. Rist, "Fiducial point estimation solution for impedance cardiography measurements," in *2022 IEEE International Instrumentation and Measurement Technology Conference (I2MTC)*, 2022, pp. 1–6.

[9] A. Savitzky and M. J. E. Golay, "Smoothing and differentiation of data by simplified least squares procedures." *Analytical Chemistry*, vol. 36, no. 8, pp. 1627–1639, 1964. [Online]. Available: https://doi.org/10.1021/ac60214a047

[10] J. Luo, K. Ying, and L. Bai, "Savitzky–golay smoothing and differentiation filter for even number data," *Signal Processing*, vol. 85, pp. 1429–1434, 07 2005.

[11] M. Schmid, D. Rath, and U. Diebold, "Why and how savitzky–golay filters should be replaced," *ACS Measurement Science Au*, vol. 2, no. 2, pp. 185–196, 2022. [Online]. Available: https://doi.org/10.1021/acsmeasuresciau.1c00054

[12] G. Byun and R. Kikuuwe, "An improved sliding mode differentiator combined with sliding mode filter for estimating first and second-order derivatives of noisy signals," *International Journal of Control, Automation and Systems*, vol. 18, 06 2020.

[13] M. Metshein, A. Gautier, B. Larras, A. Frappe, D. John, B. Cardiff, P. Annus, R. Land, and O. Martens, "Study of electrode locations for joint acquisition of impedance- and electro-cardiography signals," in *2021 43rd Annual International Conference of the IEEE Engineering in Medicine & Biology Society (EMBC)*, 2021, pp. 7264–7264.

[14] K. Pushpavathi and B. Kanmani, "Frequency sampling method of fir filter design: A comparative study," in *2018 International Conference on Electrical, Electronics, Communication, Computer, and Optimization Techniques (ICEECCOT)*, 2018, pp. 588–595.

[15] B. Sramek, "Status report on bomed's electrical bioimpedance," in *Proceedings of the Annual International Conference of the IEEE Engineering in Medicine and Biology Society*, 1988, pp. 51 vol.1–.

[16] A. Gautier, B. Larras, O. Martens, D. John, and A. Frappé, "Embedded icg-based stroke volume measurement system: Comparison of discrete-time and continuous-time architectures," in *2021 IEEE 34th International System-on-Chip Conference (SOCC)*, 2021, pp. 46–51.

Appendix 4 — Improved PWM-based Sinewave Generation: Example of the Impedance Measurement

IV

Anar Abdullayev, Paul Annus, Andrei Krivošei, Margus Metshein, Olev Märtens, and Marek Rist. Improved PWM-based sinewave generation: Example of the impedance measurement. *Automatic Control and Computer Sciences*, pages 1–13, 2023

Improved PWM-based Sinewave Generation:
Example of the Impedance Measurement

Anar Abdullayev[a, *], Paul Annus [a], Andrei Krivošei [a], Margus Metshein [a],
Olev Märtens [a], and Marek Rist [a]

[a]*Tallinn University of Technology, Thomas Johann Seebeck Depertment of Electronics,
Tallinn, Estonia*
*e-mail: anar.abdullayev@taltech.ee

Abstract—Using the pulse-width modulation (PWM) is a very convenient and efficient way to generate the approximation of the AC, in the simplest case sinewaves in the embedded test & measurement solutions. Partly, because the on-chip PWM modulator is available in most of the microcontroller and DSP chips. In the current paper improved (compared with conventional PWM) implementation of the binary waveforms is proposed. The idea is based first on the conversion of the desired AC (e.g., sinewave) to quantized in the amplitude domain waveform, to be further converted to the binary pulses with a duty cycle, corresponding to each quantization level. Such an approach is described and analyzed, with several examples of the implementation and application for impedance measurement solutions. The results show the significant improvements of the approximated binary signals both in the frequency and time domain, by optional simple low- or bandpass filtering of the binary signal, over classical PWM, while still preserving simplicity (e.g., number of needed binary signal segments) of the generated waveforms (e.g., compared with delta-sigma bitstreams). The beneficial usage of the proposed approach for the impedance measurement applications is described, as well as to generate excitation waveforms, as well as to be used as reference waveforms for synchronous demodulation of the response signal. It is shown, that for the frequency range of 10 to 70 kHz total harmonic distortion below 2.5 % can be achieved by the proposed improved PWM solution.

Keywords: pulse-width modulation, sine wave, impedance measurement, binary representation, waveform

1. INTRODUCTION

In the field of electronics generation of sinewaves is important, as well as e.g., in the AC power sources, as well as to generate measurement signals (e.g., in the function generators), but also to generate the carriers for excitation from one side and demodulate (preferably by synchronous detectors) the modulation of these carriers. The latter is also often known as "lock-in technology", having many applications, including the measurement of the impedance and specifically of the bio-impedance [1], [2].

The preferable and most natural waveforms for AC could be the continuous (so analog) and ideal (distortion-free) sinewaves, with accurate amplitude and phase – for the excitation signal itself, but also to be used as a reference signal in the synchronous ("lock-in") detectors or

mixers to down- or upconvert the signals in the frequency domain. Especially for the instrumentation solutions the measurement accuracy is highly dependent on the quality of the excitation signal (but also of the reference waveform) used in the measurement.

Still, as the generation and usage of pure analog sinewaves are sophisticated, so digital approaches are used, as being more simple, more precise, power efficient, etc. An overview of digital sinewave generation methods is given in [3].

There are known solutions, using digitally generated sinewave(s), converted by a precise digital-to-analog converter (DAC) to the analog waveform, used also in the instrumentation [4]. However, limitations of the DACs such as the speed, complexity, and resolution make this technique impractical in many applications, particularly at higher frequencies and for low-cost and low-power solutions.

About PWM generally

In the embedded solutions it is very convenient and reasonable to generate the sinewaves by existing on-chip hardware for the pulse-width modulation (PWM) of microcontrollers and digital signal processors (DSP-s).

PWM is a modulation technique, that generates pulses with variable width representing the amplitude (current value) of an input (analog or digital) signal to be coded (Fig. 1). The conventional PWM includes the dividing of the (single or multiple) period(s) of the signal to be generated into an integer number of the segments of equal time duration (length in the time domain, so also in the digital, e.g., processor ticks). And for each segment, a binary pulse is generated with a duty cycle (width) carrying/representing the value (e.g., average/mean value) of the current segment.
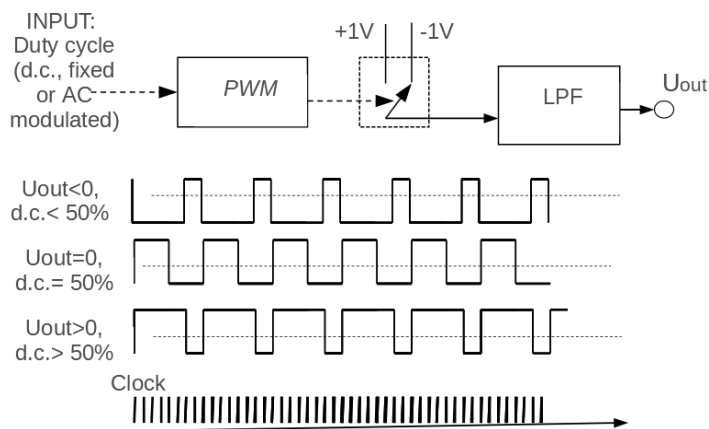

Fig. 1. Idea of the PWM - modulation of the duty cycle (d.c.) of the binary waveform by input signal

Examples of usage of the PWM for the generation of AC, approximating the single sinewaves or more complex analog signals could be:

(1) PWM is used in motor control, for example, to regulate the speed of electric motors by altering the duty cycle of the signal transmitted to the motor or even to generate an approximation of the sinewaves of the controllable frequency and amplitude [5];

(2) in the power conversion electronics PWM can be used to manage voltage or current to a load by switching the power supply on and off at high frequency, also for approximation of the sinewave(s) [6];

(3) PWM is also used in audio processing to produce analog signals, nowadays more likely from digital signals for audio amplifiers or speakers [7], [8].

Application of the electrical impedance measurement

From the measurement and instrumentation field, one important class of applications is the measurement of electrical impedance. But of course, there are many similar impedance measurement applications, where measurements are carried out also by the usage of the AC carrier, and the measurement information is got after (preferably synchronous) detection of the carrier (excitation) and variation of it. As only one example of many, electromagnetic flowmeters are working similarly, using excitation and synchronous detectors to get the measurement results [9].

Electrical impedance, being the complex resistance to AC, is widely used to measure and characterize various tissues, alloys, structures, and physiological processes through the estimation of hemodynamics, etc.

Electrical bio-impedance (EBI) can be used to identify and assess the condition of the tissues [10], monitor the hemodynamics and the impedance cardiography (ICG) of humans, and is used in other healthcare applications [11], [12]. Also, the electrical impedance and spectra of it can characterize materials and structures by direct impedance measurement or through inductive coupling [13].

By definition, the ratio of the applied AC voltage to the resulting current is the impedance of the material or tissue at the given (preferably characterizing in the best way the object under test) frequency.

Therefore, an excitation signal of predefined frequency, so preferably of sinusoidal waveform is necessary to initiate a response from the material or tissue to be measured to obtain an accurate measurement of its impedance.

The typical impedance measurement solution (Fig. 2) includes the generator to generate the excitation signal (typically sinewave) and also in-phase ("I") and quadrature ("Q") reference signals. The excitation signal is applied to the object under test (OuT) and the response signal (optionally pre-amplified and filtered by low-pass filter) is demodulated by two parallel channels of synchronous detectors (SD1I and SD1Q) to get in-phase ("I") and quadrature ("Q") outputs of the demodulated signal.
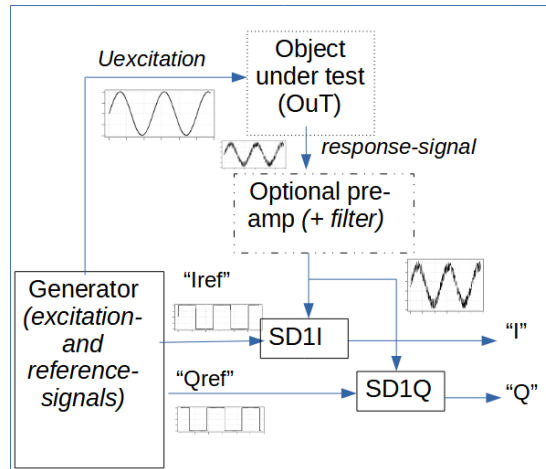
Fig. 2. Block diagram of the typical impedance measurement solution

The typical synchronous detector solution (Fig. 3) includes the multiplier, multiplying the input signal (to be demodulated) and the reference signal (waveform). Further, the multiplication product is needed to be low-pass filtered (averaged) to get rid of the ripple, as in the multiplication process of two sinewaves (input and reference signals) in additionally to the DC component, depending on the amplitudes and phase-shift between them, also ripple with the double frequency of the measurement carrier occurs. Also, to mention, the excitations and reference signals share the same frequency, so the information detected is in the amplitude and phase of the input signal. If either excitation (measurement) signal or reference waveform is not sinusoidal, more sophisticated spectra will occur in the synchronous detection process.
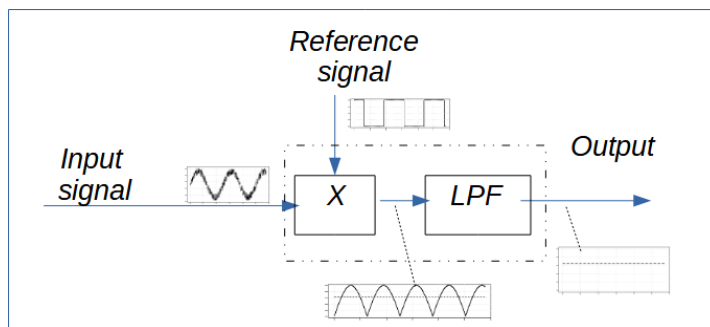
Fig. 3. Block diagram of the typical impedance synchronous detector

In the case of analog implementation of the synchronous detectors typically rectangular reference waveforms are used, as binary switching with transfer value of "+1" and "-1" (or even "+1" and "0") can be easily implemented in the analog hardware. In the digital implementation of the synchronous detectors, accurate multiplication by e.g., 16-bit sinewave can be easily implemented.

While also for the impedance measurement applications the most preferable is to use real sinewaves as the excitation signal, still usage of the PWM or some other binary waveforms have been proposed for excitation [14] – [16].

But it is less known, that the PWM or other binary approximations of the sinewaves can be used as a reference signal for synchronous demodulator, as proposed e.g., in [17].

2. PROPOSED SOLUTION OF THE IMPROVED PWM

Description of the design of the improved PWM-waveforms

As PWM is an easily implementable approximation of the sinewaves, it is reasonable to investigate its possible usage of it and possible improvements. The goal is to reduce the number of unwanted harmonics and to have a better analog waveform of sinewaves after simple low-pass filtering while preserving the simplicity of the generated waveforms and the possibility to use the on-chip PWM-modules of microcontrollers or DSP-s.

In the proposed solution:

(1) the initial sinewave to be approximated, e.g., a single period of the sinewave in the frame, as shown in Fig. 4, upper plot;

(2) is first quantized with some number of uniformly distributed levels, e.g., M= 5 positive and also M=5 negative levels, so with 0 (zero)-level total of 11 quantized levels are used in this example, as shown in Fig. 4, middle plot;

(3) Further the quantized levels (segments) are converted to binary pulses, one pulse per each segment and with duty cycle carrying the mean value of the sinewave during this segment duration, as shown in Fig. 4, lower plot;

(4) It is reasonable, that the binary pulse for the given segment is starting with a positive value during the falling part of the original waveform (left side in Fig. 4) and vice versa (the pulse starting with a negative value during the rising part of the original waveform).
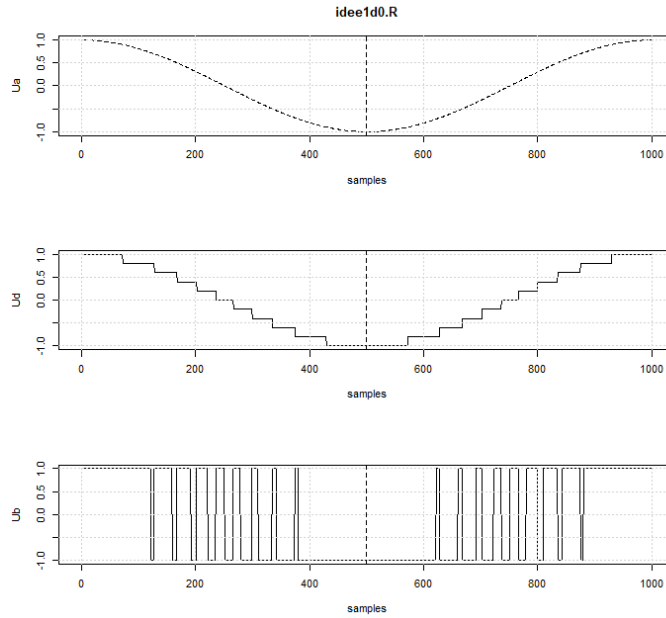
Fig. 4. Idea of the proposed solution to generate quantized waveform-based PWM, converting first the sinewave to quantized waveform

The difference between the classical PWM and the proposed solution is the fact, that in the conventional case, the pulses (with some duty cycle) are generated with fixed time step, then in the proposed solution, the pulses are generated with shorter time steps in the regions, where the signal is changing more rapidly (and vice versa). The selection of the quantization levels (mid plot of Fig. 4) is currently chosen empirically.

Example: optimizing the 10 first harmonics

To compare the proposed solution and the conventional PWM, a simulation was performed, where from the 10 first harmonics total harmonic distortion (THD) is calculated as the function of the quantization levels (left plot) for the proposed novel solution and on the right plot THD as the function for the conventional PWM (uniformly in time) generated pulsed samples (Fig. 5). While the values on the x-axis on left and right plots are not comparable we can notice, that by using of the proposed solution lower level of THD could be achieved.
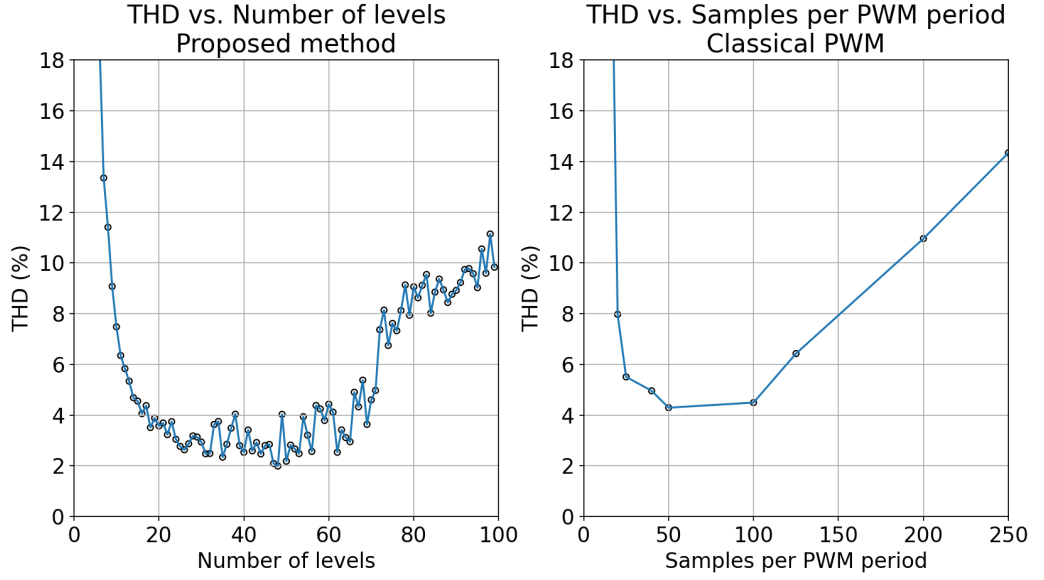
Fig. 5. THD as a function from the number of used quantization levels for the proposed solution (left plot); THD as a function from the number of uniformly sampled PWM-pulses for the conventional PWM (right plot)

The formula for calculation of such THD is:

$$THD_{10} = \frac{\sqrt{\sum_{i=2}^{10} V_i^2}}{V_1} \quad , \quad (1)$$

where THD_{10} = Total harmonic distortion up to 10th harmonic
V_i = RMS voltage of the i-th harmonic.

From this plot, we can see, with the number of levels around 25 THD about 2.5 % is achieved. For conventional PWM the minimum level is higher, about 4 % and even higher level.

Further, for found reasonable parameters various binary modulations are compared (Fig. 6).
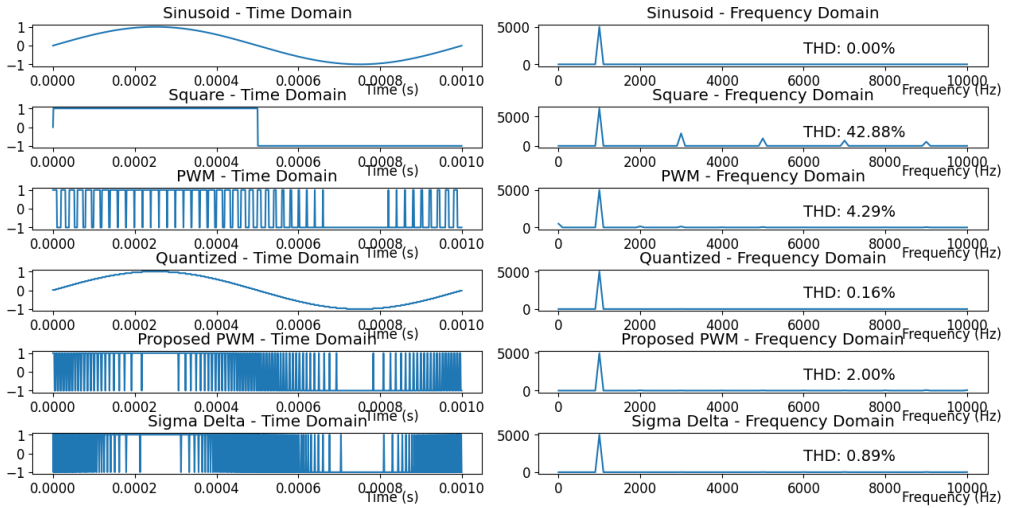
Fig. 6. Comparison of generation of a single period of the sinewave by (from up to down) conventional PWM, the proposed improved PWM, and delta-sigma modulated wave

As we see, the proposed quantized PWM has improved THD, compared to conventional PWM. Also, it is interesting to mention, while delta-sigma modulated bitstreams have even better harmonic content, compared to PWM, this comes on account of the denser binary signal, with a much larger number of edges and binary segments (binary samples) in the binary waveform (up to 10 thousand edges). Also, in some places of the waveform, the pulse durations are so small that real embedded hardware can have problems generating so short pulses. On the other hand, it is possible to limit the minimum pulse (on and off time added) duration in the proposed solution by controlling the number of quantization levels. Assume that signal S = sin(ωt) is to be quantized with the N quantization levels. Since quantization uniformly divides amplitude, each level corresponds to 1/N. On the other hand, the duration of the pulse for each level is different and the shortest duration corresponds to the level where the rate of change is maximum. The maximum rate of change of amplitude is shown in Equation (2) below.

$$\max\left(\frac{d}{dt}\sin(\omega t)\right) = \max(\omega\,cos(\omega t)) = \omega \qquad (2).$$

The minimum pulse duration for this level can be obtained by dividing the level amplitude to ω as shown in Equation 3.

$$T_{min} = \frac{1}{\omega N} \qquad (3).$$

From the simulation, we have obtained that N = 48 leads to the minimum THD for a 1 kHz sinusoidal signal obtained by a 1 MHz binary grid with the proposed method. Using Equation 3, we obtain $T_{min} \approx 20$ μs for the proposed method which is notably longer than the delta-sigma method which utilizes maximum binary grid and leads to minimum pulse length $T_{min} = 2$ μs (1 μs for on and 1 μs for off-time). While these results are got empirically by simulations, more systematic mathematical optimization methods could be tried, as future work.

Example: Generating of sinewewave from 10 to 70 kHz

In the bio-impedance measurements typically a single frequency signal with frequency in the range of 10 to 100 kHz is used. It is beneficial to generate a signal with user-defined frequency in this range and just the proposed solution is very suitable for this. For example, for the periodic signal generation (and later analysis) a reasonable time window for the impedance generation and acquisition and analysis can be 1 ms. So, any integer number of sinewave periods can be fitted into this window and so any integer value of kHz-s is generated. The digital clock to generate binary PWM can be in practice for typical DPS-s and microcontrollers in the range of 10 to 100 MHz. In the current example, a 20 MHz clock is considered. Various modulation schemes are compared:

a) conventional PWM with 1000 pulsed samples (segments), by the way - overall signal periods;

b) proposed novel PWM, with 11 levels (5 on both positive and negative polarity and zero level);

c) delta-sigma modulation for the background.

In all simulations also the 3-rd order fixed Butterworth low-pass filter has been considered at the output of the binary signal, and the THD overall frequency grid in the Nyquist band, so up to 10 MHz, has been calculated.

The 3-rd order Butterworth low-pass filter has the transfer function H(s):

$$H(s) = \frac{1}{(s + 1)(s^2 + s + 1)} \qquad . \ (4)$$

Here $s = j \times \omega_n = j \times 2 \times \pi \times f_n$, where f_n is the normalized frequency of the signal.

The results are given in Fig. 7. We see the overall THD below 2.5 % in the whole range from 10 to 70 kHz for the proposed solution, which is very reasonable, and such distortion of the sine wave is not noticed for example on the oscilloscope screen. Still, the range of possible frequencies generated is limited by about one decade, e.g., we see the increase of the THD above 60 kHz. This is a general shortcoming of the PWM. The solution is to scale the frequency grid (digital clock resolution in other words) to adjust the frequency range of needed sinewaves into the optimum range.
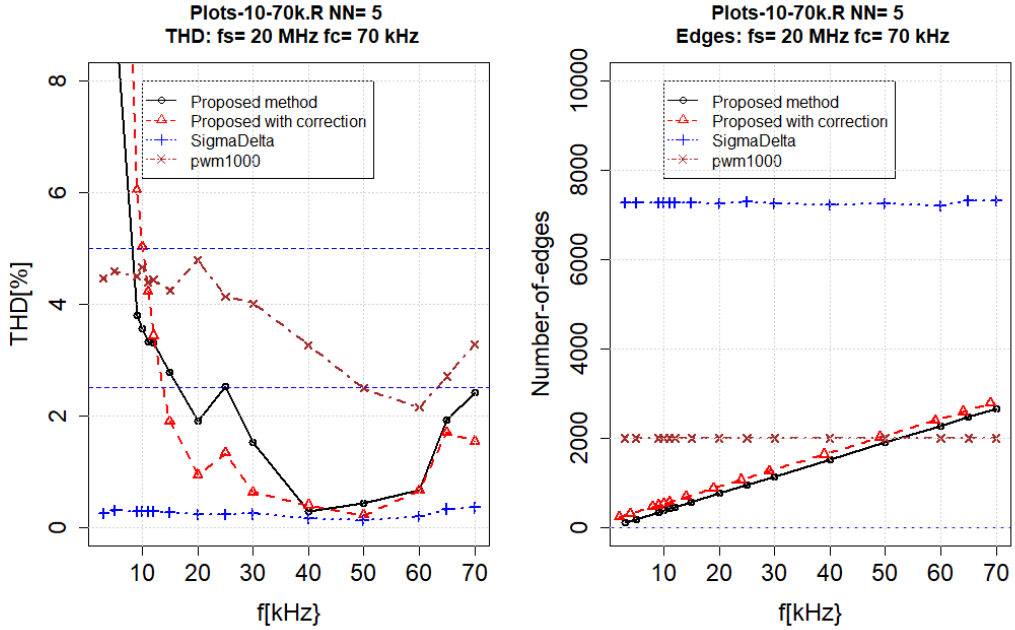
Fig. 7. THD as a function from the frequency of the approximated sinewave for proposed and alternative solutions (left plot); the number of edges in the binary signal for various solutions (right plot)

Also, an additional line is for "corrected" proposed solutions. In this case, the final harmonics are added with a minus sign to the initial sinewave, and the generation of the "quantized segmentation" and conversion to PWM is repeated, in 4 iterations.

Also, as seen from the plots, the delta-sigma approach, compared as well as to conventional PWM, as well as to proposed PWM, has an unreasonably large number of edges (and so binary segments or samples in other words).

Further, for the same conditions, an example of the generation of the 20 kHz sinewave is shown in Fig. 8, for the conventional PWM, proposed PWM, and the delta-sigma methods. Again, the proposed PWM is more efficient than conventional PWM, while simpler and sparser in the time domain, compared and easier to implement than the delta-sigma method.
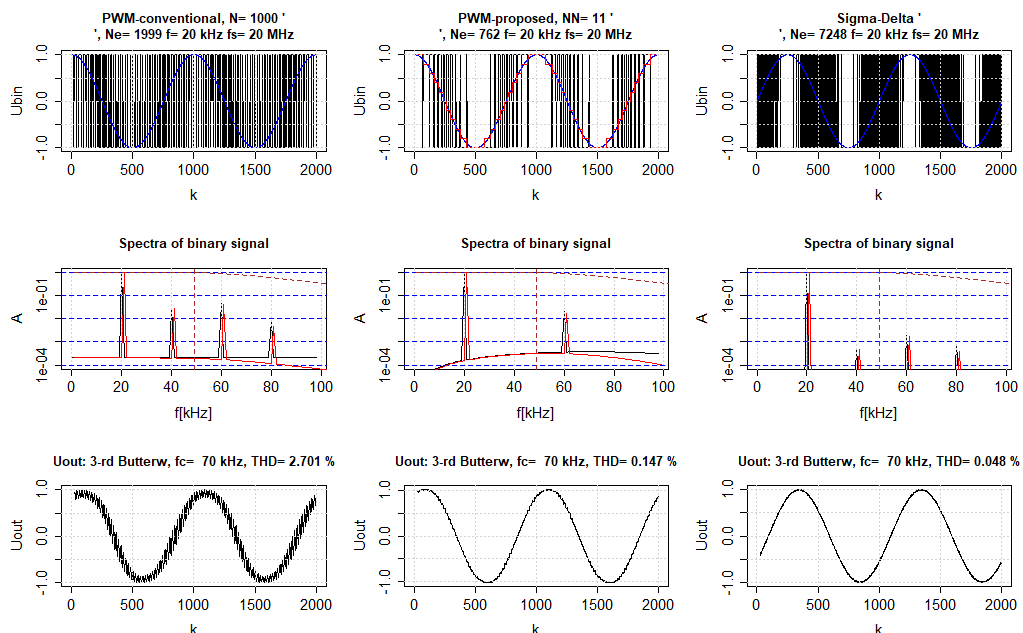
Fig. 8. Example comparison of methods of the generation of the 20 kHz sinewave on the 20 MHz digital clock in the (partly shown) 1 ms time window: comparison of the conventional PWM, proposed PWM, and the delta-sigma method

Also, as seen from the plots, the delta-sigma approach, compared as well as to conventional PWM, as well as to proposed PWM, has an unreasonably large number of edges (and so binary segments or samples in other words).

Example of the circuit simulation

To give some idea of the possible usage of the proposed PWM in the impedance measurement solution, a circuit according to Fig. 9 has been selected. The simulation includes the proposed PWM, corresponding to 10 kHz sinewave (as often used for bio-impedance measurements). For the excitation signal of the device-under-test (DuT) the generated PWM is passing the simple lowpass filter on op-amp U_1 to get the sinusoidal signal. The response signal of the DuT is got from the voltage divider Rref/DuT (DuT is simulated by R_{dut} and C_{dut}). The response signal is synchronously demodulated by FET-switch M1, forming a half-wave synchronous detector with the help of R_1) and a lowpass filter using op-amp U_2. Please note, that both reference signals - directly controlling the FET-switch M1 and the excitation are using the same proposed PWM- approximation of the sinewave. This gives an advantage by more precise impedance measurement, as the excitation signal is real sinewave, as well as reference waveform, is spectrally much improved, compared with typically used rectangular binary switching in the synchronous detectors, making the solution sensitive to much more harmonics.
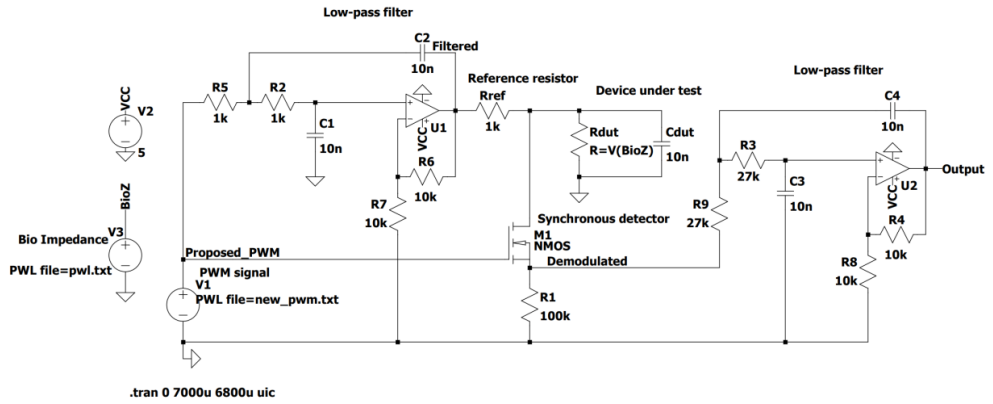
Fig. 9. Schematics of the LT-Spice simulation of the impedance measurement using the proposed PWM

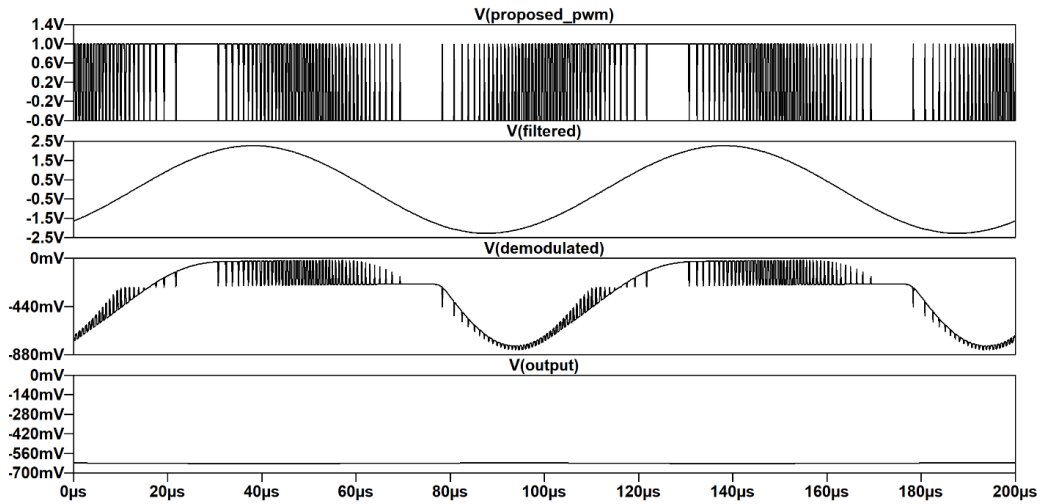The waveforms of the simulation are given in the Fig. 10.

Fig. 10. Waveforms of the LT-Spice, from up to down- a) the proposed PWM; b) low-pass filtered excitation; c) demodulated signal by FET M1; d) output voltage of the solution

In the current solution, only the in-phase ("I") part or detection of the real part of the impedance is shown. To get the imaginary ("Q") part, a similar synchronous detector (SD) can be added in parallel to shown SD. In practice, often the bioimpedance, e.g., in monitoring the hemodynamics of the human person, only the real ("I") part of the impedance can be used.

The remaining ripple of the result can be further suppressed by a more sophisticated analog filter at the output or more reasonably by doing the final filtering in the software of the microcontroller, after digitizing the result.

3. CONCLUSION AND FUTURE WORK

So, the novel PWM generation techniques have been proposed, described, and analyzed, by examples. Also, the benefits of the proposed solutions have been shown, compared to the conventional PWM. It is shown, that for the frequency range of 10 to 70 kHz total harmonic distortion below 2.5% can be achieved by the proposed improved PWM solution, for bio-impedance measurement applications at very reasonable complexity. Also, it has been shown, that the proposed novel-PWM waveforms can be used not only to generate the excitation signal for the impedance measurements but also as reference waveforms to synchronously detect the response signal.

In future work, several aspects could be further investigated:

(1) using the nonuniform quantization levels in the proposed PWM generation; optimizing a number of these levels and their amplitudes;
(2) more investigate the possibilities of using proposed waveforms as the reference binary waveforms, as the reference waveforms for the analog synchronous detectors;
(3) other additional possibilities to compensate for some harmonics;
(4) possibilities to use the method not only for single sinewaves but for multifrequency signals and chirp waveforms;
(5) investigate the practical implementation aspects of the proposed solution;
(6) investigate, could usage of the high-resolutions PWM (HR-PWM), as available in some DSP-s (like TMS320F28379) further improve the quality of the approximation of the sinewaves.

FUNDING

CONFLICT OF INTEREST

The authors declare that they have no conflicts of interest.

REFERENCES

1. M. Min, O. Martens, and T. Parve, "Lock-in measurement of bio-impedance variations," Measurement, vol. 27, no. 1, pp. 21–28, 2000.

2. E. Priidel, P. Annus, M. Metshein, R. Land, O. Martens, and M. Min, "Lock-in integration for detection of tiny bioimpedance variations," in 2018 16th Biennial Baltic Electronics Conference (BEC), 2018, pp. 1–4.

3. D. Fefer, J. Drnovsek, and A. Jeglic, "Comparative analysis of digital sinewave generation methods," in 1993 IEEE Instrumentation and Measurement Technology Conference, 1993, pp. 668–669.

4. K. Wakabayashi, T. Yamada, S. Uemori, O. Kobayashi, K. Kato, H. Kobayashi, K. Niitsu, H. Miyashita, S. Kishigami, K. Rikino, Y. Yano, and T. Gake, "Low-distortion single-tone and two-tone sinewave generation algorithms using an arbitrary waveform generator," in 2011 IEEE 17th International Mixed-Signals, Sensors and Systems Test Workshop, 2011, pp. 33–38.

5. J. Liu, W. Yao, Z. Lu, and X. Xu, "Design and implementation of dsp based high-frequency spwm generator," in 2016 IEEE 8th International Power Electronics and Motion Control Conference (IPEMC-ECCE Asia), 2016, pp. 597–602.

6. T. Adam, I. Ajtonyi, and F. Toth, "High precision ac/ac power supply unit based on dsp controlled pwm inverter," in Proceedings of the Power Conversion Conference-Osaka 2002 (Cat. No.02TH8579), vol. 3, 2002, pp. 1166–1169 vol.3.

7. A. Floros and J. Mourjopoulos, "A novel and efficient pcm to pwm converter for digital audio amplifiers," in ICECS'99. Proceedings of ICECS '99. 6th IEEE International Conference on Electronics, Circuits and Systems (Cat. No.99EX357), vol. 1, 1999, pp. 165–168, vol.1.

8. S. Aase, "Digital removal of pulse-width-modulation-induced distortion in class-d audio amplifiers," IET Signal Processing, vol. 8, pp. 680–692, 08 2014.

9. K. Gao, Z. Cui, Z. Xia, and H. Wang, "Phase sensitive detector for multi-electrode electromagnetic flowmeter," in 2021 IEEE International Instrumentation and Measurement Technology Conference (I2MTC), 2021, pp. 1–5.

10. S. Halonen, J. Kari, P. Ahonen, K. Kronstrom, and J. Hyttinen, "Real-time bioimpedance-based biopsy needle can identify tissue type with high spatial accuracy," Annals of Biomedical Engineering, vol. 47, no. 3, pp. 836–851, Mar 2019. [Online]. Available: https://doi.org/10.1007/s10439-018-02187-9

11. O. G. Martinsen and S. Grimnes, Bioimpedance and Bioelectricity Basics, 3rd ed. Academic Press, Aug 2014.

12. S. Chabchoub and S. Mansouri, "Impedance cardiography: recent applications and developments," Biomedical Research, Nov 2018.

13. J. Garcıa-Martın, J. Gomez-Gil, and E. Vazquez-Sanchez, "Non-destructive techniques based on eddy current testing," Sensors, vol. 11, no. 3, pp. 2525–2565, 2011.

14. M. Min, J. Ojarand, O. Martens, T. Paavle, R. Land, P. Annus, M. Rist, M. Reidla, and T. Parve, "Binary signals in impedance spectroscopy," in 2012 Annual International Conference of the IEEE Engineering in Medicine and Biology Society, 2012, pp. 134–137.

15. M. Rist, M. Reidla, M. Min, T. Parve, O. Martens, and R. Land, "Tms320f28069-based impedance spectroscopy with binary excitation," in 2012 5th European DSP Education and Research Conference (EDERC), 2012, pp. 217–220.

16. O. Martens, R. Land, M. Min, P. Annus, M. Rist, and M. Reidla, "Improved impedance analyzer with binary excitation signals," in 2015 IEEE 9th International Symposium on Intelligent Signal Processing (WISP) Proceedings, 2015, pp. 1–5.

17. O. Martens, "Precise mixed signal synchronous detector with spectrally improved binary switching," in 2009 IEEE International Symposium on Intelligent Signal Processing, 2009, pp. 77–80.

Appendix 5 — A DSP-Based EBI, ECG, and PPG Measurement Platform

V
Anar Abdullayev, Marek Rist, Olev Martens, Margus Metshein, Benoit Larras, Antoine Frappe, Antoine Gautier, Mart Min, Deepu John, Barry Cardiff, Andrei Krivosei, and Paul Annus. A DSP-based EBI, ECG and PPG measurement platform. *IEEE Transactions on Instrumentation and Measurement*, pages 1–8, 2023

A DSP-Based EBI, ECG, and PPG Measurement Platform

Anar Abdullayev, *Student Member, IEEE*, Marek Rist, Olev Martens, *Senior Member, IEEE*,
Margus Metshein, *Member, IEEE*, Benoit Larras, Antoine Frappe, *Senior Member, IEEE*,
Antoine Gautier, *Member, IEEE*, Mart Min, *Life Senior Member, IEEE*, Deepu John, *Senior Member, IEEE*,
Barry Cardiff, *Senior Member, IEEE*, Andrei Krivošei, and Paul Annus, *Senior Member, IEEE*

Abstract—A test and evaluation platform has been developed to research and develop solutions and algorithms for joint acquisition, processing, and reasoning from the electrical bioimpedance (EBI), electro-cardiography (ECG), and photoplethysmography (PPG) signals. The solution is based on the low-cost Launchpad of the Texas Instrument TMS320F28379D dual core 16/32-bit digital signal processor (DSP) with 16-bit multichannel analog-to-digital converter (ADC) and several other peripherals (pulse-width modulation (PWM), ADC, timers, I2C, serial peripheral interface (SPI), a lot of static random-access memory (SRAM) and flash memory). In the simplest mode, the platform is used to simultaneously acquire the EBI, ECG, and PPG signals at 1 kHz and send them to the PC by virtual COMport, for further analysis and presentation. The EBI, ECG, and PPG signals are sampled with a 16-bit ADC and have a resolution of more than four decimal digits, with an EBI error of less than 0.002%. In the next stage, various embedded and "at the edge" measurement algorithms will be developed, tested, demonstrated, and evaluated on this platform.

Index Terms—Digital signal processor (DSP), electrical bioimpedance (EBI), electrocardiography (ECG), impedance cardiography (ICG), photoplethysmography (PPG), test and evaluation platform.

I. INTRODUCTION

CARDIOVASCULAR diseases (CVDs) constitute a primary cause of death, comprising 32% of all deaths globally. Currently, the leading causes of CVDs predominantly stem from physical inactivity, along with alcohol and tobacco misuse, resulting in obesity and overweight conditions, ultimately leading to elevated blood pressure (BP). The history and progress of CVDs tend to manifest slowly, often through unnoticeable signs.

If CVD is discovered in an early phase, suitable treatment can be applied, and normal quality of life can be maintained. To discover CVDs, monitoring is essential, however, requiring convenient devices. Furthermore, in today's COVID-19-affected world, remote ("tele-") monitoring is increasingly embraced. To meet this growing demand, a multimodal smart apparatus is required to convert biological phenomena and markers into electrical signals (electrical bioimpedance (EBI), impedance cardiography (ICG), electro-cardiography (ECG), photoplethysmography (PPG), and so on). These signals are then combined in the most beneficial ways to facilitate on-site preliminary decisions.

A. Role of the EBI Measurements

EBI has many applications, including tissue characterization [1], monitoring fluid overload in dialysis patients [2], drug delivery measurement [3], and so on. A primary application of EBI is to derive ICG by calculating the time derivative. ICG has gained attention in recent years due to its merits in assessing hemodynamic parameters. However, not in the status of gold standard yet, ICG gains great potential in clinical and even more, in personal medicine for early detection of diseases. Being essentially different from ECG, which measures the electrical activity of the heart, ICG describes the actual pumping activity of the heart [4]. If the advances of PPG—the ability to follow the changes in blood circulation and its perfusion into the skin [5]—can also be added, several combined parameters can be followed.

B. Need for Co-Monitoring of EBI, ECG, and PPG

The capability of simultaneous monitoring of EBI, ECG, and PPG presents a significant challenge, especially considering the desire to estimate peripheral BP noninvasively. However, this is not the only challenge. The condition of the cardiovascular system, such as arterial stiffness, and the status of the heart and its moving parts, such as heart valves, are intensive research topics in today's world. Technological advancements have enabled the reduction in the size of measurement devices, ultimately leading to the possibility of providing ubiquitous wearability in patient monitoring.

Anar Abdullayev, Marek Rist, Olev Martens, Margus Metshein, Mart Min, Andrei Krivošei, and Paul Annus are with the Thomas Johann Seebeck Department of Electronics, Tallinn University of Technology, 19086 Tallinn, Estonia (e-mail: anar.abdullayev@taltech.ee).
Benoit Larras, Antoine Frappe, and Antoine Gautier are with CNRS, Centrale Lille, Junia, University of Lille, 59000 Lille, France, and also with UMR 8520–IEMN, University of Polytechnique Hauts-de-France, 59313 Lille, France.
Deepu John and Barry Cardiff are with the School of Electrical and Electronics Engineering, University College Dublin, Dublin 4, D04 V1W8 Ireland.
Digital Object Identifier 10.1109/TIM.2023.3320771

C. Combining ICG and PPG

Here are the parameters, which gain advantage from the combination and co-utilization of all three methods. For example, the preejection period (PEP) denotes the onset of the Q wave, R wave, S wave (QRS) complex (detected from ECG) to the beginning of ventricular ejection (detected from ICG as B-point) [6]. Another example is the pulse transition time (PTT), which measures the time interval from the R-peak (detected from ECG) to the foot or peak of the pulse (detected from the first derivative of PPG) [6]. These two time intervals, PEP and PTT, collectively form the pulse arrival time (PAT), which is widely utilized in current BP estimation applications [7].

D. Relevance and Advances of PPG

The detection of hemodynamic feature points [e.g., left ventricular ejection time (LVET)], classically determined from ICG has also been shown to be present on PPG [8]. However, an exclusive solution based solely on a single approach has not been verified yet. This highlights the necessity for a co-monitoring platform that integrates multiple methods, providing a comprehensive and much-needed solution.

E. Background Art

The aforementioned reasons and the increasing demand from the healthcare sector have propelled the development of medical technologies, including cardiorespiratory activity monitoring. Some more examples of the prior art are given below.

1) *2018: J of Sensors:* Simultaneous recording of ICG and ECG using a z-rpi device with a minimum number of electrodes [9].
2) *2020:* Multisensor fusion approach for cuff-less BP measurement [10].
3) *2021:* Single-channel bioimpedance measurement for wearable continuous BP monitoring [11].
4) *Comparison of Different Methods for Estimating Cardiac Timings:* A comprehensive multimodal echocardiography investigation [12].
5) *2018:* Full ICG measurement device using Raspberry Pi3 and system-on-chip biomedical instrumentation solutions [13].
6) *2019: Nightingale V2:* Low-power compact-sized multisensor platform for wearable health monitoring [14]. It can measure various bio-signals simultaneously at very low power consumption, including ECG, EBI, PPG, motion, and heart sounds. Patient safety aspects related to optical and electrical sensors were investigated in this article.

F. About Digital Signal Processor (DSP)-Based Solutions

The DSP-based approach for impedance measurements in vital sign monitoring has been implemented before. This includes the development of efficient algorithms [15], standalone DSP-based monitors on integrated circuits (ICs) [16] or specific DSP-based on-desk (bio)impedance measurement systems [17]. However, a physical platform that allows seamless switching between data collection using various biomedical
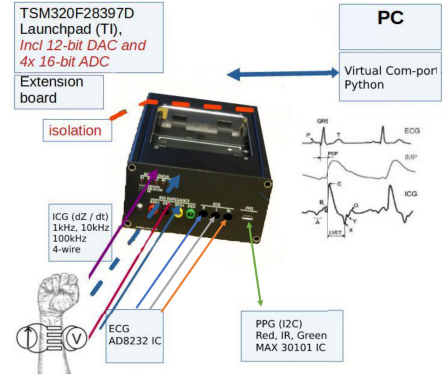

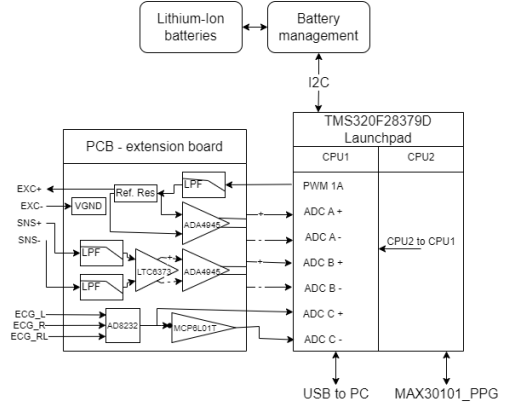Fig. 1. Idea of the proposed test and evaluation platform.

Fig. 2. Block diagram of the proposed solution.

sensors (Bio-Z, ECG, PPG, and so on) and facilitates the development of appropriate algorithms for conditioning and analysis does not currently exist.

II. PROPOSED SOLUTION

The idea of the proposed solutions is shown in Fig. 1.

The device is a DSP-based box, that acquires data from the PPG, ECG, and EBI sensors (electrodes), collecting and aggregating the data. One scenario is that the DSP will process and make reasoning locally. There is also an option that this device can serve as a simple and transparent data acquisition box for the defined modalities, sending data to the PC for presenting and storing it for post-processing.

The block diagram of the proposed solution is given in Fig. 2.

The solution is based on the TMS320F28379D DSP-launchpad of Texas Instruments Company. The DSP has a dual 200 MHz digital signal processing core, four parallel 16-bit fast (successive-approximation type) analog-to-digital converter (ADC)-s, pulse-width modulation (PWM) outputs, three 12-bit DACs, and much more. The launchpad is depicted in Fig. 3(a).

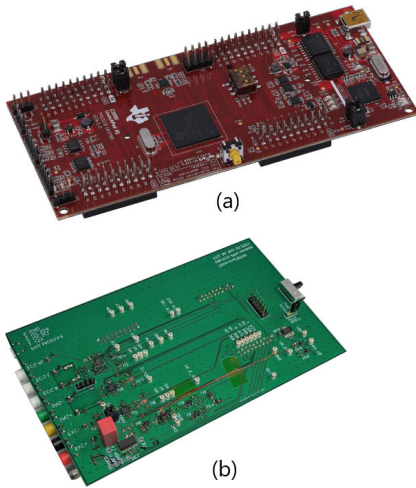The developed extension board to the DSP-Launchpad is shown in Fig. 3(b).

Fig. 3. Photos of the hardware. (a) TMS320F28379D launchpad. (b) PCB of the extension board.

A. Sensor-Front-End Part

The physiological signals are acquired through the following front-end solutions.

1) The process of obtaining the ECG signal involves the use of the AD8232 chip, which serves as a single-lead heart rate monitor. This type of chip is typically employed in portable fitness and activity monitors as well as remote health monitors. Subsequently, the analog signal obtained from the ECG is digitized using the 16-bit ADC of the DSP.

2) For acquiring the optical (PPG) signal the chip MAX30101 is used - this chip can measure the signal in three various color wavelength channels and is communicating with DSP by I2C interface.

3) For acquiring the impedance (EBI) signal, the algorithm is implemented in the DSP while analog ac excitation (1, 10, or 100 kHz) is generated by the on-chip DAC of the DSP, and the response signal is digitized by on-chip 16-bit ADC and discrete Fourier transform (DFT) is made in the software of the DSP to get the real-time impedance values. Also, the excitation current is measured either by $I-> U$ converter at the virtual ground or differentially by the voltage drop on the (connected in series to the measurement object) fixed resistor. The impedance measurement part includes three similar third-order Butterworth type op-amp based analog low-pass filters with a cutoff frequency of about 100 kHz.

For ECG and ICG signal acquisition similar standard solid gel electrodes are used (ECG-electrodes type T709 of Comepa Industries (Albuquerque, NM, USA).

B. Software

To acquire data, we used a DSP device. DSP software is written in the Texas Instrument Code Composer Studio IDE in C/C++ and Assembly languages. We are using both CPUs.
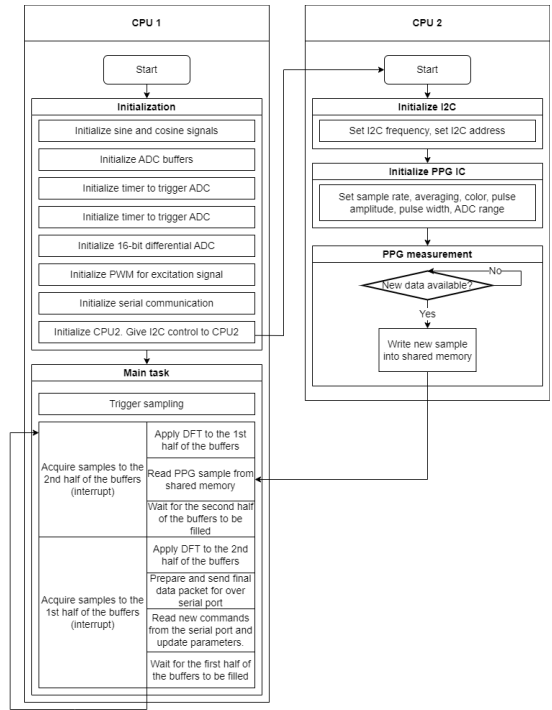

Fig. 4. DSP software flowchart.

The first CPU is in charge of impedance and ECG measurements, as well as serial communication. The second CPU is only responsible for PPG data acquisition. Communication between CPUs is realized over shared memory. The software flowchart can be viewed in Fig. 4.

For data acquisition of the ICG, PPG, and ECG signals double buffers of the size of 500 samples are used. So, while one buffer is filled with data, another buffer with the previous data frame is processed, enabling continuous data acquisition and processing. The complexity of the DFT for ICG signal is 1 multiply-and-accumulate (MAC) per data point in the buffer, of a total of 500 samples for every 1 ms frame. As in DFT, real and imaginary parts have to be calculated and for both excitation and response signals, a total of 2000 MACs are needed to be calculated in every millisecond. As the current DSP can perform in every second dual MAC (DMAC) operation, an amount of 1 MIPS of the total 100 available per DSP core is used.

To calculate the impedance, we generate an excitation signal using PWM and measure both the excitation and response signals. Acquired signals are (MAC instruction of DSP) with the reference sine- and cosine waves of the same expected frequency. The achieved DFT results are then used as complex values, and the complex ratio of the response voltage to the excitation voltage is determined.

ECG data are collected and averaged at the same time as the impedance signal. To suppress the 50/100 Hz power line signal disturbances in the acquired ECG signal, an efficient method is to apply an arithmetic moving average within 20 ms timeframes. For example, at a 200 Hz sampling rate, taking
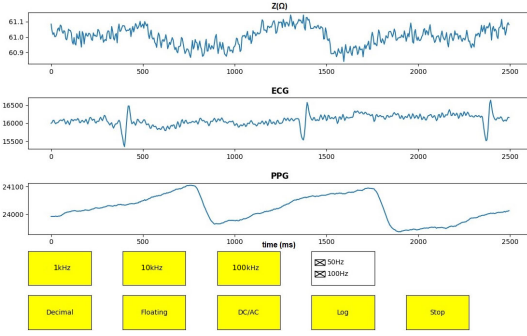
Fig. 5. Graphical user interface.

Fig. 6. Photograph of the developed device with batteries.

the average of four samples allows disturbances of 50 Hz (and multiples) to have one or multiple full periods in the analysis window, resulting in a zero average value over this timeframe as shown in the following equation:

$$\frac{1}{4}\sum_{j=0}^{3} \text{ECG}[i+j] + A \cdot \sin\left[2\pi \cdot 50 \cdot \frac{i+j}{200} + \phi\right]$$
$$= \frac{1}{4}\sum_{j=0}^{3} \text{ECG}[i+j] = \text{ECG}_2[i] \quad (1)$$

where, $\text{ECG}[i]$ represents the original ECG signal, A is the amplitude of the power line disturbance signal, ϕ is the phase angle of the power line disturbance signal and ECG_2 is filtered ECG signal. The moving average filter, discussed alongside other techniques for mitigating power line interference in ECG signals within the reference [18], is essentially an FIR filter. It employs uniform and consistent coefficients and is selected due to its straightforward nature.

The PPG sensor is configured to capture signals with a 16-bit internal ADC, and the output is received by CPU2 and delivered to CPU1.

Obtained data is sent to the PC over the serial interface. We have prepared graphical user interface (GUI) software for PC in Python language and it can be viewed in Fig. 5. GUI is used to demonstrate simultaneously acquired impedance,
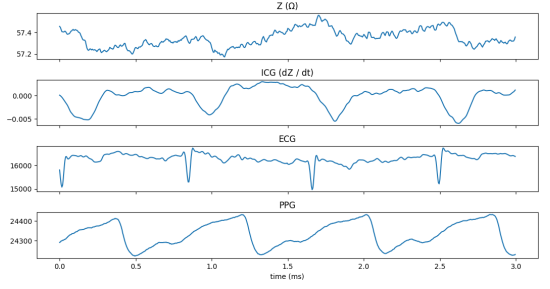

Fig. 7. Plot: impedance (Z), ICG, ECG, and PPG.

TABLE I
REPEATABILITY OF THE MEASUREMENTS

R (kΩ)	f (kHz)	Max (Ω)	Min (Ω)	Average (Ω)	SD (Ω)	CV (%)
0.1	1	100.14	100.12	100.13	0.0032	0.0032
0.1	10	100.54	100.53	100.54	0.0029	0.0029
0.1	100	99.828	99.795	99.813	0.0043	0.0043
1	1	999.96	999.84	999.91	0.0212	0.0021
1	10	1002.1	1002.0	1002.1	0.0197	0.0019
1	100	934.84	934.34	934.58	0.0827	0.0088
10	1	10032	10024	10028	1.1617	0.0116
10	10	9802.7	9794.2	9797.6	1.1648	0.0119
10	100	10106	10069	10088	5.2206	0.0518

Fig. 8. Metrological resistor box.

ECG, and PPG signals in real-time. Besides that, it is possible to change excitation frequency for impedance measurement, control 50 and 100 Hz band-stop filters to eliminate mains-related noise, choose the calculation mode, initiate logging, and so on.

III. EVALUATION

The proposed and developed device is depicted in Fig. 6. The plots in Fig. 7 show an example of the acquired data. Since the software allows us to log the data in addition to real-time visualization, we have visualized previously logged data. Note that we have also included the ICG signal in this graph, which is the derivative of the acquired impedance signal. Since the impedance signal is noisy, it should be filtered to obtain a smooth derivative signal. We applied the Savitzky–Golay filter with the parameters suggested in the article [19].

Since we are using IC-s for ECG and PPG modules and their performances are not dependent on our system, we performed evaluation only for the ICG module, which we implemented
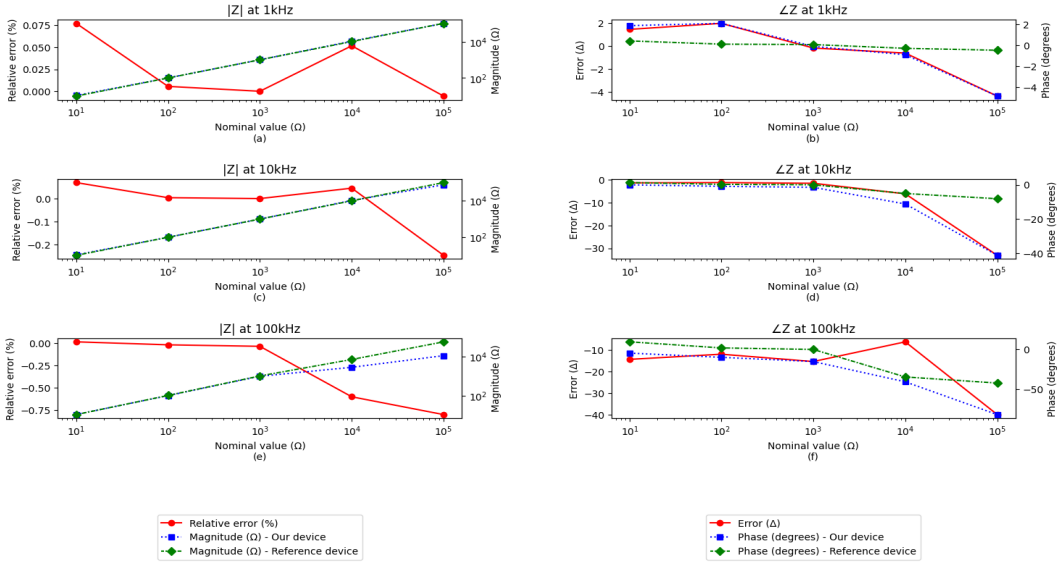
Fig. 9. Resistor box measurements. (a) $|Z|$ at 1 kHz. (b) $\angle Z$ at 1 kHz. (c) $|Z|$ at 10 kHz. (d) $\angle Z$ at 10 kHz. (e) $|Z|$ at 100 kHz. (f) $\angle Z$ at 100 kHz.

from scratch. The device is evaluated in different test scenarios. Measurement data are logged by the already existing GUI software and analyzed.

A. Repeatability Test

To assess the precision of the device, a repeatability test was performed. Three different values (0.1, 1, and 10 kΩ) are measured in three excitation frequency modes of the device (1, 10, and 100 kHz) 1000 ×. From the measurements, maximum, minimum, average, standard deviation, and coefficient of variation are calculated. Results are given in Table I below.

Except for the measurements for 10 kΩ load, the standard deviation is less than 0.01% of the mean value. The worst results are obtained for 100 kHz frequency and 10 kΩ load. This is related to parallel parasitic capacitance, which becomes more effective as frequency and load values increase. Furthermore, when the load value is close to the reference resistor value (1 kΩ), the highest precision is reached. The standard deviation in this situation is about equal to 0.002% of the mean value.

B. Accuracy Test With Resistor Box

We utilized a resistor box that allows one to adjust the resistance by turning different knobs controlling different decades of resistance value connected in series, as shown in Fig. 8. We measured the impedance in the range of 0.1 Ω–100 kΩ with our device and reference device - Agilent Technologies, E4990A impedance analyzer [20]. We made comparisons in all excitation frequencies that our device supports and the result can be seen in Fig. 9.

Measurements of our device and reference device are displayed in subplots Fig. 9(a)–(e) in addition to the error.
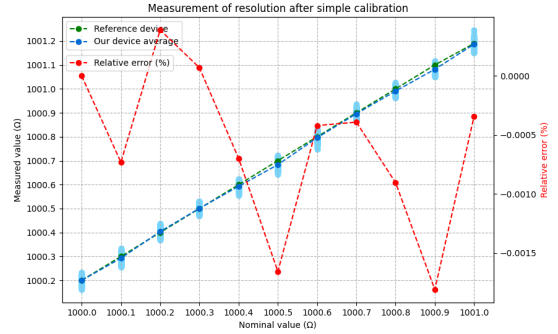
Fig. 10. Accuracy test with resistor box.

We have calculated relative error in percentage for magnitude measurements and absolute error (difference) for phase measurements. Since we use a 1 kΩ reference resistor in our device, measurements in this range are more accurate. On the other hand, as the load values approach the extremes, errors increase. Since the device is designed for bio-impedance measurements, which vary in a relatively narrow range, edge-case errors are not as significant. Also, take note of the systematic error in phase measurements, which increases with frequency. This error is caused by parallel parasitic capacitance, which can be compensated in software.

To test the resolution of the device we performed another test with the resistor box. The resistance of the box was set at 1, 1.0001, 1.0002, and 1.0003 kΩ, . . ., 1.0009 kΩ consecutively and measured by our device at 1 kHz excitation frequency and 34401A digital multimeter (6.5 digit resolution) [21] as a reference device. In this example, we measured the

Fig. 11. Emulator of the cardio-respiratory dynamic impedance [22].

Fig. 12. Test with bio-impedance emulator.

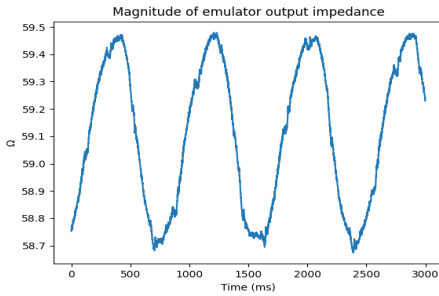real value of the impedance because the resistor box can be modeled as a resistor and small inductor in series, and we are only measuring dc resistance with a multimeter as a reference device, so it is more accurate to compare the reference value with the real value of the impedance. We averaged the result of 1000 consecutive measurements. Since both our device and the resistor box are uncalibrated, a simple calibration was performed at kΩ, to eliminate bias error. In Fig. 10, measured values and measurement error (relative error in percentage) are shown. Because it detects every increment in the fourth decimal place, we can conclude that the device has at least a four-digit resolution. The relative error in this range (around 1 kΩ) is less than 0.002%.

C. Test With Capacitor

100 nF nominal capacitor is used as a load to test the capability of our device to measure capacitive load and calculate the magnitude and phase of the object under test. We set the excitation frequency to 1 kHz and obtained a magnitude of 1876.4 Ω and phase of −1.4751 rad. Using the equation

$$|Z| = \frac{1}{2 \cdot \pi \cdot C \cdot f}. \qquad (2)$$

Capacitance is calculated as 84.819 nF when $|Z|$ is the magnitude of measured impedance and f is the excitation frequency. The same capacitor is also measured by Agilent Technologies, E4990A impedance analyzer [20], and the capacitance is measured as 85.229 nF. This value is comparable with our uncalibrated result.

D. Test With the Emulated Cardio-Respiratory Bio-Impedance Signal

In all previous tests, we used static load. To test the ability of the device to measure dynamic load, we used a bio-impedance emulator box (Fig. 11) previously developed by our research group [22]. This device emulates cardiac bioimpedance with realistic amplitude and time variations.

We used 100 kHz excitation frequency and measured the impedance at the output of the emulator at 1 kHz, later downsampled this data at 200 Hz by using averaging window of length 5. Fig. 12 demonstrates the magnitude of measured impedance over 3 s. The impedance waveform is clearly observable in Fig. 12 and demonstrates the potential of the suggested approach for bioimpedance measurements.

IV. Conclusion

The proposed device was developed and tested. The novelty and contribution of the device are the following. The device, also compared to solutions, described in the background art part, is unique in this combination of three modalities (EBI, ECG, and PPG). Also, the device can acquire impedance signal at more than four digit resolution, with the precision of 0.002%. The device can obtain simultaneous EBI, ECG, and PPG signals at a rate of 1 kHz and can be used for a variety of purposes.

1) To acquire the signals in one of these modalities or any combination or all.
2) As signals can be acquired in real-time, various modalities can be cross-analyzed, and novel information got in this way
3) Various signal processing algorithms can be tried, tested, and evaluated in this real-time platform.

Optimal sampling frequencies for physiological signals (EBI, ECG, and ICG) require further investigation. Downsampling all signals to 200 Hz for user view and analysis is reasonable, preserving the original waveform and facilitating data fusion through convenient signal comparison.

V. Future Work

Future work involves doing more experiments, improving metrological properties, adding auto-ranging features, and implementing more sophisticated calibration techniques. Also, implementing some local "at the edge" artificial intelligence in the DSP via various firmware variations may be very interesting.

Limitation of the current device is working time from the batteries—as DSP in active mode consumes about 390 mA current, the continuous working time is 6–8 h with 3000 mAh accumulators.

Also, the current device has only one channel for the PPG and one for the ICG. Having more channels could add a possibility to investigating the pulse wave propagation, estimating the BP, etc.

Acknowledgment

REFERENCES

[1] C.-J. Peng, K.-S. Cheng, and J.-J. Huang, "Temperature-compensated bioimpedance system for estimating body composition," *IEEE Eng. Med. Biol. Mag.*, vol. 19, no. 6, pp. 66–73, Jun. 2000.

[2] M. Delano and C. Sodini, "Evaluating calf bioimpedance measurements for fluid overload management in a controlled environment," *Physiological Meas.*, vol. 39, no. 12, Dec. 2018, Art. no. 125009.

[3] P. Arpaia, U. Cesaro, and N. Moccaldi, "Noninvasive measurement of transdermal drug delivery by impedance spectroscopy," *Sci. Rep.*, vol. 7, no. 1, p. 44647, Mar. 2017.

[4] O. G. Martinsen and S. Grimnes, *Bioimpedance and Bioelectricity Basics*, 3rd ed. New York, NY, USA: Academic Press, Aug. 2014.

[5] J. Allen, "Photoplethysmography and its application in clinical physiological measurement," *Physiological Meas.*, vol. 28, no. 3, pp. R1–R39, Mar. 2007.

[6] R. Mukkamala et al., "Toward ubiquitous blood pressure monitoring via pulse transit time: Theory and practice," *IEEE Trans. Biomed. Eng.*, vol. 62, no. 8, pp. 1879–1901, Aug. 2015.

[7] J. Lee, S. Yang, S. Lee, and H. C. Kim, "Analysis of pulse arrival time as an indicator of blood pressure in a large surgical biosignal database: Recommendations for developing ubiquitous blood pressure monitoring methods," *J. Clin. Med.*, vol. 8, no. 11, pp. 1–19, 2019.

[8] W. Duan, D. Zheng, C. Eggett, P. Langley, and A. Murray, "Development of techniques for measurement of left ventricular ejection time," in *Proc. Comput. Cardiol.*, 2014, pp. 241–244.

[9] A. Hafid, S. Benouar, M. Kedir-Talha, M. Attari, and F. Seoane, "Simultaneous recording of ICG and ECG using Z-RPI device with minimum number of electrodes," *J. Sensors*, vol. 2018, pp. 1–7, Nov. 2018.

[10] F. Miao, Z.-D. Liu, J.-K. Liu, B. Wen, Q.-Y. He, and Y. Li, "Multi-sensor fusion approach for cuff-less blood pressure measurement," *IEEE J. Biomed. Health Informat.*, vol. 24, no. 1, pp. 79–91, Jan. 2020.

[11] T.-W. Wang, W.-X. Chen, H.-W. Chu, and S.-F. Lin, "Single-channel bioimpedance measurement for wearable continuous blood pressure monitoring," *IEEE Trans. Instrum. Meas.*, vol. 70, pp. 1–9, 2021.

[12] P. Dehkordi et al., "Comparison of different methods for estimating cardiac timings: A comprehensive multimodal echocardiography investigation," *Frontiers Physiol.*, vol. 10, p. 1057, Aug. 2019.

[13] A. Hafid, S. Benouar, M. Kedir-Talha, F. Abtahi, M. Attari, and F. Seoane, "Full impedance cardiography measurement device using raspberry PI3 and system-on-chip biomedical instrumentation solutions," *IEEE J. Biomed. Health Informat.*, vol. 22, no. 6, pp. 1883–1894, Nov. 2018.

[14] S. Lee, B. Grundlehner, R. G. van der Westen, S. Polito, and C. Van Hoof, "Nightingale V2: Low-power compact-sized multi-sensor platform for wearable health monitoring," in *Proc. 41st Annu. Int. Conf. IEEE Eng. Med. Biol. Soc. (EMBC)*, Jul. 2019, pp. 1290–1293.

[15] P. M. Ramos and F. M. Janeiro, "Implementation of DSP based algorithms for impedance measurements," in *Proc. IEEE Int. Conf. Signal Process. Commun.*, Jul. 2007, pp. 816–819.

[16] N. Van Helleputte et al., "A 345 μW multi-sensor biomedical SoC with bio-impedance, 3-channel ECG, motion artifact reduction, and integrated DSP," *IEEE J. Solid-State Circuits*, vol. 50, no. 1, pp. 230–244, Jan. 2015.

[17] M. Min, M. Lehti-Polojärvi, J. Hyttinen, M. Rist, R. Land, and P. Annus, "Bioimpedance spectro-tomography system using binary multifrequency excitation," *Int. J. Bioelectromagnetism*, vol. 20, pp. 76–79, Nov. 2018.

[18] S. Saxena, R. Jais, and M. K. Hota, "Removal of powerline interference from ECG signal using FIR, IIR, DWT and NLMS adaptive filter," in *Proc. Int. Conf. Commun. Signal Process. (ICCSP)*, Apr. 2019, pp. 0012–0016.

[19] O. Martens, M. Metshein, G. Tamberg, and A. Abdullayev, "Impedance cardiography signal processing with Savitzky-Golay and frequency sampling kernels," in *Proc. 18th Biennial Baltic Electron. Conf. (BEC)*, Oct. 2022, pp. 1–5.

[20] Keysight. (2021). *E4990A Impedance Analyzer*. [Online]. Available: https://www.keysight.com/us/en/assets/7018-04256/data-sheets/5991-3890.pdf

[21] Keysight. (2022). *34401A Digital Multimeter, 61/2 Digit*. [Online]. Available: https://www.keysight.com/us/en/product/34401A/digital-multimeter-6-digit.html

[22] M. Rist and M. Min, "Dynamic reference for evaluation of bioimpedance spectroscopy devices," in *Proc. 15th Biennial Baltic Electron. Conf. (BEC)*, Oct. 2016, pp. 107–110.
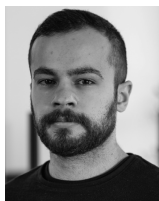
Anar Abdullayev (Student Member, IEEE) was born in Baku, Azerbaijan, in 1995. He received the B.S. degree from Electrical and Electronics Department, Middle East Technical University (METU), Ankara, Turkey, in 2019, the master's degree in communicative electronics program from the Tallinn University of Technology (TUT), Tallinn, Estonia, in 2021, where he is currently pursuing the Ph.D. degree with Thomas Johann Seebeck Department of Electronics, early stage researcher.

His current research interests include related with embedded systems and measurement electronics and especially impedance measurement.

Marek Rist was born in Tallinn, Estonia, in 1980. He received the M.S. degree in electronics and biomedical engineering, and the Ph.D. degree in information and communication technology from the Tallinn University of Technology, Tallinn, in 2007 and 2018, respectively.

The focus of his work has been instrumentation and technology for fast measurement of impedance spectra for monitoring of cardiac and respiratory parameters and impedance spectro-tomography, mainly for biomedical applications.

Dr. Rist was a recipient of the IEEE I2MTC2020 International Instrumentation and Measurement Technology Conference Best Paper Award in 2020.

Olev Martens (Senior Member, IEEE) was born in Tallinn, Estonia, in 1960. He received the Diploma degree in engineer of electronics (cum laude) and the Ph.D. degree from the Tallinn University of Technology (TUT), Tallinn, in 1983 and 2000, respectively.

He has experience from Industrial Research and Development at the Design Office of the Tallinn Radio Factory RET in 1980's, and the SMEs, in 1990's. In academy, since 2000, has been a Senior Researcher of measurement electronics with the Thomas Johann Seebeck Department of Electronics, TUT. He has authored ten technical papers and inventions from the field of instrumentation.

Dr. Martens was a recipient of the IEEE I2MTC2020 International Instrumentation and Measurement Technology Conference Best Paper Award in 2020 and the IEEE IMS Faculty Course Award in 2018. He is also a Outstanding Reviewer of 2022 of IEEE TRANSACTIONS ON INSTRUMENTATION AND MEASUREMENT journal.

Margus Metshein (Member, IEEE) was born in Kuressaare, Estonia, in 1983. He received the B.S. and M.S. degrees in electronics and bionics and the Ph.D. degree in information and communication technology from the Tallinn University of Technology (TUT), Tallinn, Estonia, in 2006, 2010, and 2018, respectively.

From 2016, he worked as a Early-Stage Researcher and a Research Scientist with the Thomas Johann Seebeck Department of Electronics, TUT. He has authored more than 20 scientific papers, one book chapter and two inventions. His current research interests include covering the field of bioimpedance based measurement, biomedical signal acquisition, and interpretation of cardiorespiratory related volume changes in human body through electrical measurements.

Dr. Metshein was a recipient of the IEEE I2MTC2020 International Instrumentation and Measurement Technology Conference Best Paper Award in 2020.

Benoit Larras was born in Nancy, France, in 1988. He received the master's degree in engineering and telecommunications and the Ph.D. degree in electrical engineering from IMT Atlantique, Brest, France, in 2012 and 2015, respectively.

He is currently an Associate Professor with Junia, Lille, France, and leading the Electronic Team. His current research interests include analog/mixed-signal IC design and circuit implementation of neural networks and associative memories, in the context of near-sensor computing and edge computing.

Dr. Larras was a co-recipient of the Best Paper at the IEEE AICAS2020 Conference.

Antoine Frappe (Senior Member, IEEE) received the B.Sc. degree from ISEN, Lille, France, in 2004, and the M.Sc., Ph.D., and HDR degrees in electrical engineering from the University of Lille, Lille, in 2004, 2007, and 2019, respectively.

Since 2004, he has been with IEMN, Villeneuve-d'Ascq, France. He received a Fulbright grant, in 2008 for research at BWRC, University of California at Berkeley, Berkeley, CA, USA. Currently, he is an Associate Professor at Junia ISEN, Lille, leading the Electronics Team. His research interests include digital RF transmitters, converters, mixed-signal design for RF and millimeter-wave communication, energy-efficient systems, and circuits for embedded machine learning.

Dr. Frappe received awards at conferences including VLSI Circuits and IEEE AICAS. He's a Board Member of the IEEE Circuits and Systems Society and a Counselor of the IEEE Lille Student Branch.

Antoine Gautier (Member, IEEE), born in Roubaix, France, in 1998. He received the bachelor's degree in electronics from the Institut Supérieur d'Electronique et du Numérique (ISEN), Lille, France, in 2020. He is currently pursuing the Ph.D. degree with the University of Lille, Lille, and Junia, Hauts-de-France, France.

Topics of the thesis are the implementation of artificial intelligence solution, the acquisition and processing of biological and the use of event-driven and asynchronous techniques. He is also secretary of the IEEE Lille Student Branch.

Mart Min (Life Senior Member, IEEE) received the Diploma Engineer's degree in electronics and underwent engineering studies from Tallinn Polytechnic Institute, Tallinn, Estonia, in 1969, and the Ph.D. degree in measurement science from Kiev Polytechnic Institute, Kyiv, Ukraine, in 1984.

Since 1992, he has been a Full Professor and a Leading Scientist with the Tallinn University of Technology, Tallinn, Estonia. He held positions in Munich, Germany, from 1992 to 1993, and in Heilbad Heiligenstadt, Germany, from 2007 to 2010. He specializes in medical industry applications like pacemaker development. He has authored over 200 papers and 40 patents. He is a part of both the Instrumentation and Measurement Society and Engineering in Medicine and Biology Society.

Dr. Min is a Member of the International Committee for Promotion of Research in Bio-Impedance (ICPRBI) and received the title of Professor Emeritus in 2016.

Deepu John (Senior Member, IEEE) received the B.Tech. degree in electronics and communication engineering from the University of Kerala, Thiruvananthapuram, Kerala, India, in 2002, and the M.Sc. and Ph.D. degrees in electrical engineering from the National University of Singapore, Singapore, in 2008 and 2014, respectively.

Currently, he is an Assistant Professor with the School of Electrical and Electronics Engineering, University College Dublin, Dublin, Ireland. From 2014 to 2017, he served as a Post-Doctoral Researcher at the Bio-Electronics Lab, National University of Singapore, and previously worked as a Senior Engineer at Sanyo Semiconductors, Osaka, Japan. His expertise lies in low-power biomedical circuit design, energy-efficient signal processing, and edge computing.

Dr. John has been recognized with the IEEE Young Professionals, Region Ten Individual Award in 2013 and has actively contributed to Key IEEE Conferences. Additionally, he is served as an Associate Editor for IEEE Transactions on Biomedical Circuits and Systems and IEEE Transactions on Circuits and Systems—II: Express Briefs.

Barry Cardiff (Senior Member, IEEE) received the B.Eng., M.Eng.Sc., and Ph.D. degrees in electronic engineering from University College Dublin, Dublin, Ireland, in 1992, 1995, and 2011, respectively.

He was a Senior Design Engineer or a Systems Architect for Nokia, from 1993 to 2001, moving to Silicon and Software Systems (S3 group), Dublin thereafter as a Systems Architect in their Research and Development division focused on wireless communications and digitally assisted circuit design. Since 2013, he has been an Assistant Professor with University College Dublin. He holds several U.S. patents related to wireless communication. His research interests include digitally assisted circuit design and signal processing for wireless and optical communication systems.

Andrei Krivošei was born in Kohtla-Jérve, Estonia, in 1979. He received the B.Sc. degree from the Department of Electronics, Tallinn University of Technology, Tallinn, Estonia, in 2003, the M.Sc. degree from the Department of Automatics, Tallinn University of Technology, in 2005, and the Ph.D. degree from the Department of Electronics, Tallinn University of Technology, in 2009.

He is currently a Senior Research Scientist with the Thomas Johann Seebeck Department of Electronics, TUT.

Paul Annus (Senior Member, IEEE) was born in Tallinn, Estonia, in 1962. He received the Diploma Engineer's degree in electrical engineering from the BME, Budapest, Hungary, in 1987, and the Ph.D. degree in electronics from the Tallinn University of Technology (TUT), Tallinn, Estonia, in 2010.

He is currently a Senior Research Scientist and a Lecturer with the Thomas Johann Seebeck Department of Electronics, TUT. He has authored or coauthored more than 100 publications and ten inventions. His research interests include related to bioelectromagnetism and embeddable sensorics.

Dr. Annus was a recipient of the IEEE I2MTC2020 International Instrumentation and Measurement Technology Conference Best Paper Award in 2020.

Appendix 6 — A DSP-based Multichannel EBI Measurement Device

A DSP-based Multichannel EBI Measurement Device

Anar Abdullayev
Thomas Johann Seebeck
Department of Electronics,
Tallinn University of Technology,
Tallinn, Estonia
anar.abdullayev@taltech.ee

Marek Rist
Thomas Johann Seebeck
Department of Electronics,
Tallinn University of Technology,
Tallinn, Estonia
marek.rist@taltech.ee

Andrei Krivošei
Thomas Johann Seebeck
Department of Electronics,
Tallinn University of Technology,
Tallinn, Estonia
andrei.krivosei@taltech.ee

Margus Metshein
Thomas Johann Seebeck
Department of Electronics,
Tallinn University of Technology,
Tallinn, Estonia
margus.metshein@taltech.ee

Raul Land
Thomas Johann Seebeck
Department of Electronics,
Tallinn University of Technology,
Tallinn, Estonia
raul.land@taltech.ee

Olev Martens
Thomas Johann Seebeck
Department of Electronics,
Tallinn University of Technology,
Tallinn, Estonia
olev.martens@taltech.ee

Abstract—An advanced DSP-based multichannel electrical bioimpedance (EBI) measurement device has been developed, contributing to the evolution of bioimpedance analysis and hemodynamical monitoring. This device, leveraging the Texas Instrument TMS320F28379D dual-core 16/32-bit DSP, offers enhancements in bioimpedance measurements, including dual-channel simultaneous measurement and a multiplexing system for output electrodes. These features enable extended multi-channel bioimpedance analysis and the potential for more comprehensive physiological monitoring. High-resolution data acquisition is achieved with bioimpedance signals sampled using a 16-bit ADC, aiming for an error margin of less than 0.012%. The combination of simultaneous multi-channel measurements and improved precision positions the device as a promising tool for biomedical research, including applications in cuffless dynamical blood pressure estimation and bioelectrical impedance tomography of various tissues and organs. Additionally, the platform integrates electrocardiography (ECG) and photoplethysmography (PPG) measurements. The device offers multiple data transfer options, such as electrically isolated USB and wireless connectivity (Bluetooth or Wi-Fi), and can also serve as a testbed for evaluating embedded measurement algorithms.

Index Terms—impedance cardiography (ICG), electrical bioimpedance (EBI), electrocardiography (ECG), photoplethysmography (PPG), test and evaluation platform, DSP

I. INTRODUCTION

Electrical impedance is a critical parameter for characterizing the properties of various materials and structures, such as metals, alloys, and electrolytes, as well as physiological entities like soft tissues, as noted in [1]. It also plays a pivotal role in monitoring biological processes, for example, electrical bioimpedance (EBI) measurements are instrumental in assessing cardiac and respiratory activities [2]. A notable application of EBI is in the cuffless estimation of blood pressure, highlighted in [3], [4], which involves the measurement of pulse wave velocity at different anatomical points as illustrated in Fig. 1. This method requires capturing EBI at least from two distinct physical locations, relying on the application of the impedance cardiography (ICG) method on extremities [5].

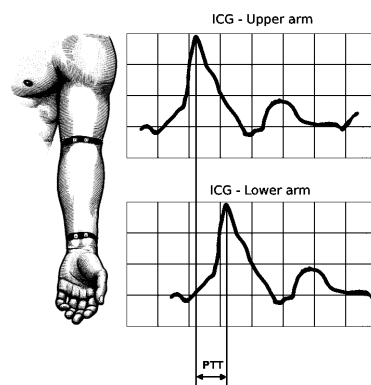Electrical impedance tomography (EIT) takes the potential

Fig. 1. Cuffless blood pressure measurement utilizing pulse transit time obtained through impedance cardiography (ICG) at the arm.
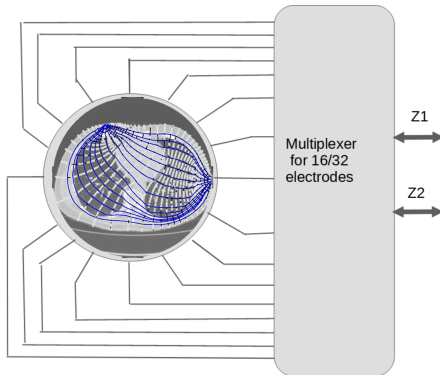
Fig. 2. Electrical Impedance Tomography setup with a multiplexed electrodes.

Fig. 3. Photo of the developed device.

of EBI a step further by acquiring EBI values across various electrode combinations on a two- or three-dimensional object. This technique is used to construct volumetric images [6], such as those used to visualize lung function [7]. The simplest EIT-EBI systems can be implemented by multiplexing the impedance measurement electrodes, as proposed in [6] and demonstrated in Fig. 2.

EBI measurement systems, much like general-purpose impedance measurement setups, require generating an excitation voltage or current and a synchronous measurement of the response signal, known as "Lock-in" detection [8]. Although synchronous detection can be executed in the analog domain, its digital implementation via a microcontroller, or more effectively, through a digital signal processor (DSP), offers greater flexibility. One of the key advantages of employing a DSP is the capability to run multiple synchronous detectors concurrently, allowing simultaneous EBI measurements at various frequencies.

A DSP-based EBI-measurement device, developed at Tallinn University of Technology (*TalTech*), was introduced in 2006 [9]. This initial version was quite large, featuring external analog-to-digital converters (ADCs), excitation signal generators, and other components separate from the then-limited DSP capabilities. A more refined solution, closer to the one proposed here, was again developed by *TalTech* and detailed in 2012 [10]. This design utilized a DSP-chip with internal ADCs and a pulse-width modulator for generating excitation signals. The advantage of this system is its high-speed capability, enabling the measurement of 1000 EBI spectra every second. However, it has certain limitations, such as having only a single EBI measurement channel (albeit with an option for external multiplexing [6]) and being constrained by the internal 12-bit ADC resolution of the DSP chip, which limits the overall accuracy to approximately three decimal digits.

In the field of electrical impedance tomography (EIT), significant contributions include Yerworth et al.'s [11] design of an multifrequency electrical impedance tomography (MFEIT)

system offering a wide range of selectable frequencies and multiple electrodes, particularly for brain imaging. Yang et al. [12] developed an MFEIT system focused on real-time imaging, achieving high frame rates and signal-to-noise ratios. Wi et al. [13] introduced a system notable for its high signal-to-noise ratio and low reciprocity error, ensuring reliable long-term operation.

The solution, proposed in the current paper, is a direct enhancement of the solution described in [14]. This solution was based on the low-cost Launchpad of the Texas Instrument TMS320F28379D dual core 16/32-bit digital signal processor (DSP) with 16-bit multichannel analog-to-digital converter (ADC) and several other peripherals – pulse-width modulation (PWM), ADC, timers, I2C, serial peripheral interface (SPI), a lot of SRAM and flash memory.

The main enhancement of the proposed solution is – the new device can measure in 2 parallel EBI channels and also has a built-in multiplexer for up to 32 measurement electrodes, so allowing, e.g., the blood pressure (Fig. 1) and EIT (Fig. 2) measurements but also tissue characterization. This dual-channel capability reduces the need for high-speed multiplexing. It is designed to exclusively rely on digital signal processing for both signal generation and sensing, in contrast to most EIT designs. Furthermore, our device uniquely offers parallel ECG and PPG measurements, expanding its utility in biomedical monitoring.

II. PROPOSED SOLUTION

A. Overall Device Description

The proposed and developed device is depicted in the Fig. 3 and photos of the hardware inside the device can be seen in Fig. 4

The block diagram of the proposed solution is given in the Fig. 5. The device's hardware core is the Texas Instrument TMS320F28379D Launchpad, a dual-core 16/32-bit DSP that orchestrates the generation of the excitation signal, acquisition

of excitation and response signals via ADC, and performs Discrete Fourier Transform (DFT) operations to establish signal correlations through multiply-accumulate operations. It also manages communication with peripheral components such as the photoplethysmography (PPG) sensor, a connected PC, and the ESP32 module, which extends wireless functionalities by transmitting data via Bluetooth or Wi-Fi.

Adjacent to the DSP core lies the main printed circuit board (PCB), the analog front-end circuitry of the device. This board integrates a series of low-pass and band-pass filters to refine both excitation and response signals. A reference shunt resistor is incorporated to gauge current across the device under test. An alternative excitation signal can be deployed through a current source, with current measurements facilitated by a trans-impedance amplifier on the return path. Programmable gain amplifiers on the board ensure optimal voltage range adaptation for ADC maximization.

The main PCB also features the AD8232, a single-lead heart rate monitor front-end IC, enabling electrocardiography (ECG) functionality. Selection between current measurement methodologies is achieved via a MAX4564 analog switch. Two cascaded 8-bit shift registers on this board enable serial-to-parallel output conversion, minimizing GPIO utilization from the Launchpad for control operations. The main PCB includes J1 connectors for ECG positive (ECG POS), ECG negative (ECG NEG), and ECG right leg drive (ECG RLD), as well
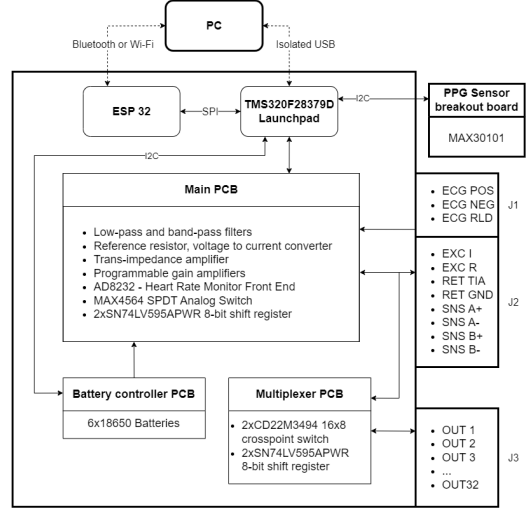

Fig. 5. The block diagram of the proposed solution

Fig. 4. Photos of the hardware. (a) TMS320F28379D launchpad (b) PCB of the multiplexer board to be attached to the main board (c) Main board to be attached to TMS320F28379D launchpad.

as J2 connectors for impedance measurement electrodes such as the excitation current source (EXC I), excitation through reference resistor (EXC R), return path to trans-impedance amplifier (RET TIA), return path to ground (RET GND), and differential sensing electrodes for channel A positive (SNS A+), channel A negative (SNS A-), channel B positive (SNS B+), and channel B negative (SNS B-).

The multiplexer board, connected to the main PCB, receive inputs from the eight electrodes and can route these signals to any of the 32 outputs at J3. The multiplexing actions are governed by two 8-bit shift registers, which in turn receives control signals from the cascaded shift registers of the main PCB. This configuration underpins the device's multi-channel measurement capability, allowing for extensive bioimpedance data collection and analysis.

B. Impedance Measurement Modes

The device is designed to function in two separate impedance measurement modes, *the reference resistor mode* and *the current mode*, as detailed in Fig. 6.

In *the reference resistor mode*, the excitation signal is a voltage applied across a fixed reference resistor. The current passing through the device under test (DUT) is derived from the known value of the reference resistor and the voltage measured across it by the excitation ADC (EXC ADC). Simultaneously, the voltage drop across the DUT is measured by the sensing ADC (SNS ADC).

For *the current mode*, input voltage is transformed into a current by a transconductance amplifier (TCA), which then flows through the DUT. The voltage on DUT is measured by the SNS ADC. The current is then converted back into a proportional voltage signal by a trans-impedance amplifier (TIA) and measured by the EXC ADC.
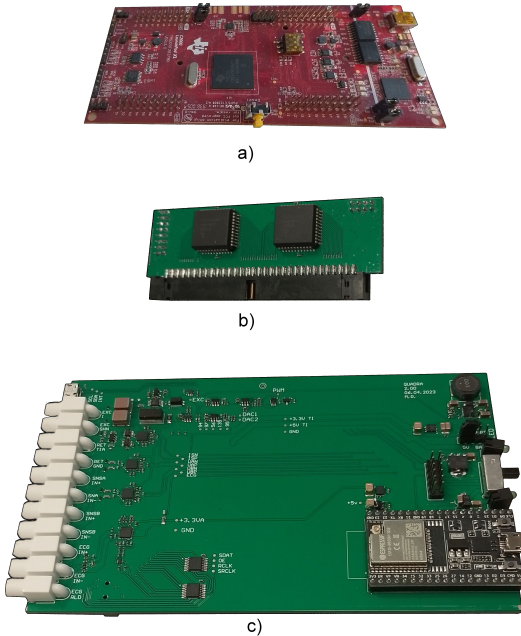
In both modes, the EXC ADC and SNS ADC measure a differential signal provided by the differential programmable gain amplifiers (PGAs), ensuring that the signal is within the optimal range for accurate measurement, thereby improving the accuracy and reliability of the readings.

C. Wireless Interface

In addition to the isolated USB connection, the proposed solution utilizes the ESP32 board to enable wireless communication with external systems. The ESP32 is currently widely employed for embedded signal processing and serves as a communication module for transmitting measurements to external systems [15]–[18], including IoT solutions. Despite the ESP32 board having both Bluetooth and Wi-Fi wireless communication modules, the proposed implementation exclusively employs Wi-Fi communication.

The ESP32 software architecture is illustrated as a block diagram in Fig. 7 and is described below.

1) Wi-Fi Connection: The ESP32 board is set up to function as both a Wi-Fi Access Point (Wi-Fi AP) and a Wi-Fi Station (Wi-Fi STA) simultaneously. Currently, the access point for the Wi-Fi STA mode is hardcoded in the software. The ESP32-based access point can be utilized "out of the box," requiring only the browser and access point IP address for use.

2) Data Manipulation on the ESP32: The data samples received from the DSP module through SPI are transmitted to the WebSocket server using the FreeRTOS queue and subsequently broadcasted to all connected WebSocket clients.

The WebSocket server implemented on the ESP32 board is utilized for delivering data to connected clients. In general, clients can be any third-party applications that support WebSockets. In the proposed solution, we also implemented a web server on the ESP32 board, providing a responsive HTML+CSS+JS page with an embedded WebSocket client. The obtained data is plotted on the web page as waveforms

TABLE I
REPEATABILITY OF THE MEASUREMENTS.

R (kΩ)	Mode	Max (Ω)	Min (Ω)	Average (Ω)	SD (Ω)	CV (%)
0.1	R	100.73	100.70	100.71	0.0038	0.0037
1	R	1001.6	1001.4	1001.5	0.0419	0.0041
10	R	10014	10018	10012	1.1072	0.0110
0.1	I	100.90	100.88	100.89	0.0042	0.0041
1	I	1002.4	1001.4	1001.7	0.1811	0.0180
10	I	10399	10383	10391	2.8315	0.0272

and updated whenever new data is available. The JavaScript version of Plotly [19] is used for interactive waveform plotting.

D. Graphical User Interface

The simple graphical user interface (GUI) for waveform plotting in the described implementation features a responsive HTML+CSS+JS page embedded in a web server on the ESP32 board. The web GUI of the current implementation is displayed in Fig. 8.

The main area of the GUI is dedicated to displaying waveforms. Utilizing Plotly, the GUI can dynamically generate and update interactive plots based on the received data. Users can visualize waveforms in real-time, and the plots are responsive to user interactions. The GUI is designed to update the plotted waveforms every time new data is available from the ESP32 board. This ensures that users see the most recent information. The GUI interacts with the ESP32 board through Websockets. This allows seamless and efficient communication between the server and clients, enabling real-time updates without the need for constant page reloading. Users can zoom in, pan, and explore the plotted data for a more detailed analysis.

III. RESULTS

A. Repeatability Test

To evaluate the precision of the device, a repeatability test was conducted using three resistor values (0.1 kΩ, 1 kΩ, 10 kΩ), each measured 1000 times at 1 kHz under two different excitation modes (I - current source, R - over shunt resistor). The test aimed to determine the device's consistency in measurements by analyzing the maximum, minimum, average, standard deviation (SD), and coefficient of variation (CV - defined as the ratio of the standard deviation to the mean and expressed as percentage) for each setting. The results are summarized in Table I.

An analysis of the table reveals that the device maintains a high level of precision across both excitation modes. For the R mode, the coefficient of variation remains exceptionally low, below 0.01% for all resistor values, indicating minimal variability in the measurements. The maximum and minimum values are also tightly clustered around the average, further confirming the device's consistency.

In the I mode, while the precision is slightly lower than in the R mode, it still demonstrates good repeatability, particularly for lower resistor values. The coefficient of variation for the 0.1 kΩ and 1 kΩ resistors is under 0.02%, increasing
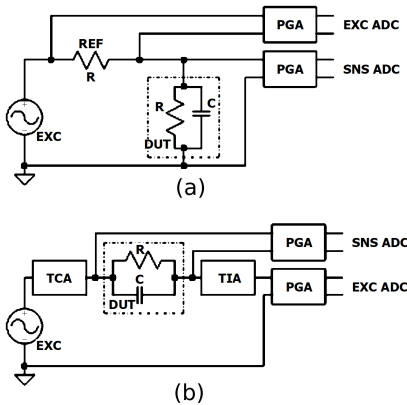

Fig. 6. Description of two impedance measurement modes. (a) Reference resistor mode (R mode) (b) Current mode (I mode).
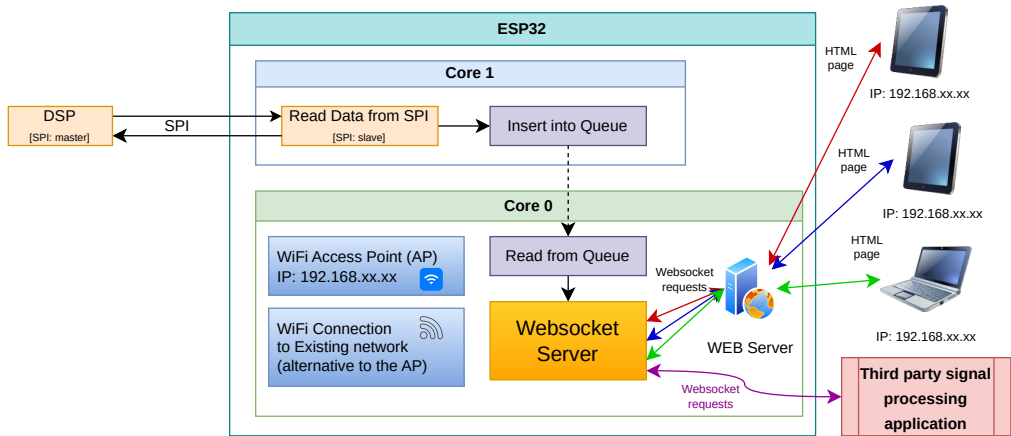
Fig. 7. The block diagram describing the ESP32 software architecture. Both cores of the ESP32 board are used. On the core 1 the measured data reading from the DSP module is running. And the Wi-Fi network handlers, WebSocket server and WEB server, all are running on the Core 0 of the ESP32 board.

slightly for the 10 kΩ resistor. This increment in CV can be attributed to the greater variability in higher resistance measurements, yet it remains within an acceptable range for precise applications.

The higher average values noted in the I mode relative to the R mode are likely a result of the device not being calibrated, along with the utilization of different components and amplifier gains in each mode. Implementing a straightforward calibration procedure can effectively reduce these systematic differences.

B. Measurement Test With Capacitive Load

An RC measurement test was performed to evaluate the linearity and accuracy of the device over a broad range of impedance values. In the test setup, a fixed capacitor with a nominal value of 100 nF was connected in parallel to one of four resistors for each measurement. The nominal values of these resistors were 10, 100, 1000, and 10000 Ohms. This setup aimed to simulate a variety of biological impedances that the device may encounter in practical applications.

Fig. 8. The GUI screenshot displays measured signals on the webpage, running on the ESP32 board using a Wi-Fi Access Point (AP) connection.

The theoretical impedance magnitude and phase angle for each resistor-capacitor pair were calculated using the impedance formula for a parallel RC circuit. The magnitude of impedance, denoted by $|Z|$, was determined using Equation (1), and the phase angle ϕ using the subsequent equation (2):

$$|Z| = \frac{1}{\sqrt{\left(\frac{1}{R}\right)^2 + (2\pi f C)^2}} \tag{1}$$

$$\phi = \arctan\left(-\frac{1}{2\pi f C R}\right) \tag{2}$$

Here, f represents the frequency of the applied signal, set at 10 kHz for our measurements. The nominal values were used to calculate theoretical impedance, while actual component values also measured with high-precision instruments provided a second set of data. Comparisons were drawn between these values and the measurements obtained directly from our device. The detailed results of this comparison, which include various resistor values paired in parallel with a 100 nF capacitor, are showcased in Table II.

TABLE II
COMPARISON OF NOMINAL, ACTUAL, AND MEASURED IMPEDANCE VALUES

Resistor	10 Ω	100 Ω	1000 Ω	10000 Ω
Nominal magnitude (Ω)	9.9803	84.673	157.18	159.13
Actual magnitude (Ω)	10.085	84.636	149.57	151.27
Measured magnitude (Ω)	10.144	84.785	149.81	151.68
Nominal phase (°)	-3.5953	-32.142	-80.957	-89.088
Actual phase (°)	-3.8224	-34.016	-81.374	-89.135
Measured phase (°)	-4.7425	-34.487	-81.612	-89.387

The results showcased in Table II reflect a notable level of linearity in the device's measurements. When comparing the measured values to the actual ones, a consistent trend is evident, suggesting reliable performance across the tested
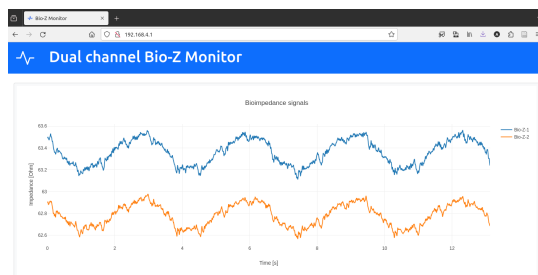
range. Although there are slight deviations, particularly in lower phase values, these differences are within a tolerable margin and could potentially be rectified with simple calibration.

Overall, the device demonstrates a high level of accuracy and consistency. The repeatability test, with low standard deviations and coefficients of variation, confirms the device's precision across various resistance values and modes. Additionally, the RC measurement test shows good linearity, with measured values closely aligning with theoretical expectations. Minor deviations observed are within acceptable limits and can be addressed with calibration. Overall, these results affirm the device's capability for precise bioimpedance measurements, making it a reliable tool for diverse applications.

IV. Conclusion and Future Work

In the simplest mode, the developed device can be used to acquire the EBI signals from 2 parallel channels or 32-multiplexed electrodes (could be accompanied by ECG, and PPG signals) at thousand measurements per second speed and sent to PC by isolated USB-port or by wireless communication for further processing, analysis and presentation, with an EBI error of less than 0.012% at the measurement frequency of 1 kHz in the impedance range from 100 Ω to 10 kΩ.

Also, the device can be used as a testbed to evaluate various signal processing and reasoning algorithms, implemented in the DSP firmware.

While in the current preliminary firmware version, the limited set of measurement frequencies in the range of 1 kHz to 100 kHz is implemented, future work will include enhancing the firmware of the DSP to have more excitation frequencies and waveforms. Also, work on the metrological characterization of the device – e.g., correction of systematic errors and investigation of the calibration issues could further improve the device's performance.

References

[1] E. Barsoukov and J. Macdonald, *Impedance Spectroscopy: Theory, Experiment, and Applications*. Wiley, 2018.

[2] O. G. Martinsen and S. Grimnes, *Bioimpedance and Bioelectricity Basics*, 3rd ed. Academic Press, Aug 2014.

[3] T.-W. Wang, W.-X. Chen, H.-W. Chu, and S.-F. Lin, "Single-channel bioimpedance measurement for wearable continuous blood pressure monitoring," *IEEE Transactions on Instrumentation and Measurement*, vol. 70, pp. 1–9, 2021.

[4] T. H. Huynh, R. Jafari, and W.-Y. Chung, "Noninvasive cuffless blood pressure estimation using pulse transit time and impedance plethysmography," *IEEE Transactions on Biomedical Engineering*, vol. 66, no. 4, pp. 967–976, 2019.

[5] M. Metshein, A. Gautier, B. Larras, A. Frappe, D. John, B. Cardiff, P. Annus, R. Land, and O. Martens, "Study of electrode locations for joint acquisition of impedance- and electro-cardiography signals," in *2021 43rd Annual International Conference of the IEEE Engineering in Medicine & Biology Society (EMBC)*, 2021, pp. 7264–7264.

[6] M. Min, M. Lehti-Polojärvi, J. Hyttinen, M. Rist, R. Land, and P. Annus, "Bioimpedance spectro-tomography system using binary multifrequency excitation," *International Journal of Bioelectromagnetism*, vol. 20, pp. 76–79, 2018.

[7] D. Maciejewski, Z. Putowski, M. Czok, and Łukasz J. Krzych, "Electrical impedance tomography as a tool for monitoring mechanical ventilation. an introduction to the technique," *Advances in Medical Sciences*, vol. 66, no. 2, pp. 388–395, 2021. [Online]. Available: https://www.sciencedirect.com/science/article/pii/S1896112621000420

[8] M. Min, O. Märtens, and T. Parve, "Lock-in measurement of bio-impedance variations," *Measurement*, vol. 27, no. 1, pp. 21–28, 2000. [Online]. Available: https://www.sciencedirect.com/science/article/pii/S0263224199000482

[9] O. Martens, M. Min, R. Land, and P. Annus, "Multi-frequency and multi-channel bio-impedance measurement solution," in *Proceedings of the 7th Nordic Signal Processing Symposium - NORSIG 2006*, 2006, pp. 178–181.

[10] M. Rist, M. Reidla, M. Min, T. Parve, O. Martens, and R. Land, "Tms320f28069-based impedance spectroscopy with binary excitation," in *2012 5th European DSP Education and Research Conference (ED-ERC)*, 2012, pp. 217–220.

[11] R. J. Yerworth, R. H. Bayford, B. Brown, P. Milnes, M. Conway, and D. S. Holder, "Electrical impedance tomography spectroscopy (eits) for human head imaging," *Physiol. Meas.*, vol. 24, no. 2, pp. 477–489, May 2003.

[12] Y. Y and J. J, "A multi-frequency electrical impedance tomography system for real-time 2d and 3d imaging," *Rev. Sci. Instrum.*, vol. 88, no. 8, p. 085110, Aug 2017.

[13] H. Wi, H. Sohal, A. Mcewan, E. J. Woo, and T. Oh, "Multi-frequency electrical impedance tomography system with automatic self-calibration for long-term monitoring," *IEEE Transactions on Biomedical Circuits and Systems*, vol. 8, pp. 119–128, 06 2013.

[14] A. Abdullayev, M. Rist, O. Martens, M. Metshein, B. Larras, A. Frappe, A. Gautier, M. Min, D. John, B. Cardiff, A. Krivošei, and P. Annus, "A DSP-Based EBI, ECG, and PPG Measurement Platform," *IEEE Transactions on Instrumentation and Measurement*, vol. 72, pp. 1–8, 2023.

[15] F. Tueche, Y. Mohamadou, A. Djeukam, L. C. N. Kouekeu, R. Seujip, and M. Tonka, "Embedded Algorithm for QRS Detection Based on Signal Shape," *IEEE Transactions on Instrumentation and Measurement*, vol. 70, pp. 1–12, 2021.

[16] J. López, J. Lozada, M. Terán, A. Cediel, and M. C. Tole, "An IoT System for Telemedicine Utilizing Electrocardiogram Technology," in *2023 IEEE Colombian Conference on Communications and Computing (COLCOM)*, Jul. 2023, pp. 1–6.

[17] R. Ahmad, H. M. Kaidi, M. N. Nordin, A. F. Ramli, M. A. Abu, and Y. Kadase, "Development of Blood Oxygen Level, Heart Rate And Temperature Monitoring System by Using ESP32," in *2022 4th International Conference on Smart Sensors and Application (ICSSA)*, Jul. 2022, pp. 167–172.

[18] V. Di Pinto, F. Tramarin, and L. Rovati, "Health Status Remote Monitoring System: ECG Peaks Detection by Successive Thresholding Algorithm Employing Envelope Function," in *2023 IEEE International Instrumentation and Measurement Technology Conference (I2MTC)*, May 2023, pp. 01–06.

[19] Plot.ly, "Collaborative data science," https://plot.ly, Plotly Technologies Inc., Montreal, QC, 2015.

Appendix 7 — DSP-based Electrical Impedance Tomography Device: Implementation and Experiments

VII

Anar Abdullayev, Marek Rist, Margus Metshein, and Olev Martens. DSP-based electrical impedance tomography device: Implementation and experiments. *2025 IEEE International Instrumentation and Measurement Technology Conference (I2MTC)*, pages 1–6, 2025

DSP-based Electrical Impedance Tomography Device: Implementation and Experiments

Anar Abdullayev
Thomas Johann Seebeck Department of Electronics
Tallinn University of Technology
Tallinn, Estonia
anar.abdullayev@taltech.ee

Marek Rist
Thomas Johann Seebeck Department of Electronics
Tallinn University of Technology
Tallinn, Estonia
marek.rist@taltech.ee

Margus Metshein
Thomas Johann Seebeck Department of Electronics
Tallinn University of Technology
Tallinn, Estonia
margus.metshein@taltech.ee

Olev Martens
Thomas Johann Seebeck Department of Electronics
Tallinn University of Technology
Tallinn, Estonia
olev.martens@taltech.ee

Abstract—**Electrical Impedance Tomography (EIT) is a non-invasive imaging technique for volumetric visualization of objects in an electrically conductive environment. This paper presents a multifunctional, DSP-based impedance measurement device designed primarily for physiological applications, including electrical bioimpedance (EBI), with additional support for electrocardiography (ECG) and photoplethysmography (PPG) inputs. The device features one excitation channel and two parallel differential sensing channels, supporting up to 32 multiplexed electrodes. Operating across a frequency range of 1 kHz to 200 kHz, it provides both magnitude and phase impedance measurements with a refresh rate of 2 frames per second. The DSP-based implementation allows for high-resolution measurements using a built-in 16-bit ADC and supports implementing of multifrequency measurement modes. This capability is particularly advantageous for addressing challenges in EIT imaging, such as frequency difference imaging. The device was tested using Python-based PyEIT software and effective imaging was demonstrated in various experimental setups. Results show the potential of the proposed device to produce high-contrast EIT images while minimizing background interference. Overall, the developed system offers a portable, versatile, and efficient solution for EIT applications in biomedical and industrial domains.**

Index Terms—**digital signal processor (DSP), electrical bioimpedance (EBI), electrical impedance tomography (EIT)**

I. INTRODUCTION

Electrical Impedance Tomography is a non-invasive imaging technique capable of producing low-resolution 2D and 3D images of objects composed of soft tissues, metals, plastics, and other materials, including biological phantoms like vegetables and fruits, within an electrically conductive environment. A simple and commonly used conductive medium is a saline solution, which closely mimics physiological conditions.

An EIT system typically comprises specialized electronic hardware and firmware, which facilitate the multiplexing of excitation and impedance response signals. The setup includes a measurement tank with electrodes positioned along its border (e.g., filled with saline water) connected to a multichannel impedance measurement device. Additionally, dedicated software is required to reconstruct conductivity images, such as MATLAB-based EIDORS [1] or Python-based PyEIT [2].

A. Applications of EIT

EIT devices can be applied to the human body using either wet electrodes [3], metal dry electrodes [4], or fabric dry electrodes [5], in various configurations such as adhesive patches or wearable electrode belts. EIT has been widely applied in thoracic monitoring by analyzing impedance variations over time and across different frequencies, particularly for lung function assessment and cardiac monitoring. Key applications, as described in several studies [6]–[9], include:

- **Thoracic Monitoring:** EIT is widely used to monitor lung and cardiac functions due to the significant conductivity differences between air-filled, fluid-filled, and blood-perfused tissues. Applications include assessing mechanical ventilation [8], [9], pulmonary function testing [8], and monitoring heart activity and fluid volume changes in heart failure patients [6], [7].
- **Neurological and Brain Activity:** EIT detects changes in conductivity during ion channel openings, offering potential for studying neural activity and brain disorders [6].
- **Cancer Detection:** EIT supports the identification of cancerous tissues, which exhibit distinct electrical properties compared to healthy tissues. Specific applications include detecting breast cancer-related lymphedema [7], pulmonary nodules [7], and prostate cancer [10].
- **Other Biomedical Applications:** Emerging applications include non-invasive glucose monitoring by analyzing changes in tissue impedance [11] and monitoring the fluid volume and size of the urinary bladder [12].

TABLE I
COMPARISON OF EIT DEVICES

Feature	Analog Modulator System [13]	Wearable EIT System [14]	AFE4300 EIT System [15]	FPGA EIT System [16]	DSP EIT System (This Work)
Controller	AD630ADZ	Teensy	ESP32	Altera Cyclone V SoC	TMS320F28379D
Cost	N/A	$260	$49.17	N/A	$200
Excitation Frequency	50 kHz (fixed)	Configurable	1kHz-50 kHz	2 kHz–500 kHz	1 kHz–200 kHz
Frame Rate	0.5 fps	up to 25 fps	50 fps	0.5 fps	2 fps
SNR	60.6 dB	36 dB to 63 dB	N/A	89 dB	78.4 dB
Connection	Wired	Wired	Bluetooth, Wired	Wired	Bluetooth, Wired
Impedance Measurement	Magnitude only	Magnitude and phase	Magnitude only	Real part only	Magnitude and phase
Application Focus	Biological phantom	Lung monitoring	Body composition	Skin sodium	Biomedical
Demodulation	Analog demodulation	Digital (Microcontroller-based)	AFE4300 IC	Digital (FPGA-based)	Digital (DSP-based)
Electrodes	16	16	32	16	32

B. Similar EIT Devices

Various EIT devices have been developed for a range of medical applications, with recent advancements focusing on affordability, portability, and open-source accessibility.

The analog modulator-based EIT system [13] employs an AD630ADZ analog modulator with a fixed 50 kHz excitation frequency, and operates as an open-source device. With a frame rate of around 0.5 Hz, it incorporates a low-pass filter with an extended integration period, which may introduce latency. A limitation of this configuration is that it only uses a single reference signal, enabling the measurement of modulus values but lacking a quadrature component, and thus does not capture complex impedance. This system was evaluated using a beef tongue as a biological phantom to introduce and assess conductivity variations.

The Teensy microcontroller-based open-source EIT system [14] is designed for lung monitoring applications. Priced at approximately $260, this wearable system adheres to accepted industry safety standards for continuous monitoring. The device achieves a signal-to-noise ratio (SNR) ranging from 36 dB to 63 dB, with a minimum measurement accuracy of 91%. Tested on a physiologically representative phantom, it demonstrated performance comparable to other state-of-the-art systems.

The AFE4300-Based EIT System [15] is a highly affordable EIT system (USD 49.17) controlled by an ESP32 microcontroller. This device features a pseudo-3D imaging with four rings of eight electrodes each, which allows multi-sectional conductivity imaging. Equipped with Bluetooth and USB connectivity, it operates at a frame rate of 50 fps, making it suitable for dynamic monitoring. However, it only captures modulus impedance values via full-wave rectification, limiting its capability to provide complex impedance measurements in real time, and it requires manual data processing in MATLAB.

Another portable EIT device is based on an FPGA platform and described in [16]. This device addresses two critical challenges: maintaining current stability and extending the voltage measurement range. It utilizes a double feedback Howland constant-current pump to ensure stable current injection across a frequency range of 2 kHz to 500 kHz, and a programmable gain amplifier to accommodate a wider voltage range. The system is designed primarily for imaging skin sodium content and provides only the real part of the impedance using a 14-bit ADC. The device leverages the Altera Cyclone V SoC FPGA as its core and features signal-to-noise ratio (SNR) of 89 dB and a frame acquisition time of 2 seconds.

In addition to these systems, our DSP-based EIT device (this work) offers a practical solution for impedance measurements across a frequency range of 1 kHz to 200 kHz. Built around the Texas Instruments TMS320F28379D digital signal processor, it provides both magnitude and phase impedance measurements with a frame rate of 2 fps and an SNR of 78.4 dB. The system features two parallel impedance measurement channels, supporting up to 32 electrodes for enhanced spatial resolution. One key advantage of the device is its ability to perform multifrequency measurements, enabled by its DSP-based digital implementation. This capability not only supports time-variation image reconstruction but also allows the use of frequency difference methods for EIT imaging. The device achieves high-resolution measurements through its integrated 16-bit multichannel ADC. Unlike other designs that achieve constant current through methods such as double feedback [16] or two-step resistor calibration [14], our device streamlines the process by simultaneously measuring the voltage and current. It calculates the current in real time by measuring the voltage across a known resistor for each sample. This method reduces the dependency on the linearity of the current pump and provides accurate current measurement for each impedance reading. The DSP-based EIT system utilizes the built-in 16-bit ADC and DAC for signal acquisition and

generation, ensuring a compact and efficient hardware design. Additionally, demodulation is performed entirely in the digital domain, simplifying the implementation of multifrequency measurements. This approach eliminates the need for separate analog modulator circuits for each frequency, instead leveraging digital signal processing operations like multiply-accumulate (MAC) for simultaneous multifrequency analysis. The device is powered by a battery, making it portable and well-suited for various applications outside controlled laboratory environments. It supports multiple communication options, including USB, Bluetooth (via a virtual serial port), and WiFi. Furthermore, the device is equipped with PPG and ECG functionality. ECG provides electrical activity data of the heart, while ICG reflects the mechanical response of blood flow. Combining ECG with ICG allows synchronized EIT image acquisition with the cardiac cycle, improving cardiovascular assessment by extracting hemodynamic parameters such as stroke volume and cardiac output [17]. Additionally, ECG can serve as a timing reference to segment ICG data per heartbeat, enabling ensemble averaging for enhanced signal clarity. PPG, being an optical measurement, does not interfere with the injected current and can be used to track vascular activity, for example, by measuring pulse transit time from the finger. Table I compares the key features of our device with other recent EIT systems.

II. Experimental Setup and Results

A. System Overview

The custom-designed DSP-based EIT system is demonstrated in Fig. 1. The setup consists of the impedance tomography device, an electrode array, and a computer interface for data visualization. In this experiment, a tomato is used as a test object to evaluate the system's imaging capability.

Fig. 1. Experimental setup of the DSP-based EIT system

The block diagram of DSP-based EIT system's is given in Fig. 2 and more technical description was presented in a previous paper [18]. The DSP software first initializes system components, including ADC, DAC, UART, and direct memory
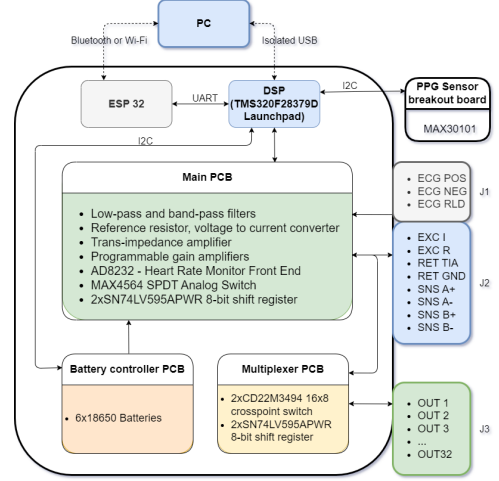

Fig. 2. Block diagram of the DSP-based EIT system

access (DMA). The DAC is linked to DMA to offload processing and maximize computation time. In main loop, ping-pong buffer approach is used, where sampled data is processed via MAC operations while new data is acquired. The DSP concurrently samples ECG along with impedance data and transmits results to the PC. The second core interfaces with the PPG sensor over I²C, storing data in shared memory for synchronized transmission with impedance and ECG measurements. The ESP32 module enables wireless communication between the DSP and PC via Bluetooth or Wi-Fi.

Its performance as an impedance measurement device was assessed by calculating the voltage measurement error, defined as the ratio of the standard deviation to the mean value of the measured voltage, and found to be 0.012%. SNR was then computed using the formula (1):

$$\text{SNR (dB)} = 20 \log_{10} \left(\frac{P_{\text{signal}}}{P_{\text{noise}}} \right). \tag{1}$$

Substituting the mean voltage as the signal and the standard deviation as the noise into (1), the SNR was calculated to be approximately 78.4 dB.

B. Measurement and Visualization

One significant advantage of our DSP-based EIT device is its ability to measure both the real and imaginary parts of the impedance, unlike many competitors that focus solely on the real part or magnitude. Furthermore, the device supports configurable excitation frequencies, enabling the implementation of frequency difference EIT mode. This capability allows the use of complex impedance information, which is particularly valuable for generating EIT images.

EIT imaging is an inherently ill-posed problem that requires both actual data and reference data to stabilize the solution. Typically, reference data is obtained from a homogeneous

solution, such as a saline water tank without any object. While effective in controlled test setups, this approach is often impractical in real-life scenarios, such as imaging the human thorax, where homogeneous reference data cannot be reliably obtained.

To address this limitation, frequency difference EIT mode offers a viable alternative. In this method, reference data is acquired at one frequency, and actual data is measured at another. The resulting visualization highlights impedance changes in the object. However, a challenge arises: when using two frequencies, both the object impedance and the background impedance (e.g., saline water) may change. This variation in background impedance can degrade image quality, as the objective is to visualize only the object's impedance change while keeping the background stable. The ability of our device to operate at multiple excitation frequencies provides the flexibility needed to mitigate this issue, improving the contrast and quality of the resulting EIT images.

Biological tissues exhibit significant frequency-dependent dielectric properties, as described in [19], making the selection of appropriate frequencies critical for effective imaging. Vegetables such as potato and tomato, which are frequency-dependent biological objects, can serve as convenient phantoms to mimic the impedance characteristics of human tissues. To further investigate the frequency dependency of biological objects and validate the potential of vegetables as tissue phantoms, we conducted direct 4-wire impedance measurements on a potato and a tomato.

The setup employed our device's 4-wire direct measurement mode to measure impedance across a frequency range of 1 kHz to 200 kHz, as shown in Fig. 3. The actual resistivity of the potato was derived from the measured impedance using the formula provided in [20]. The results, depicted in Fig. 4, illustrate the magnitude of the measured impedance, with notable variations observed across the tested frequencies.
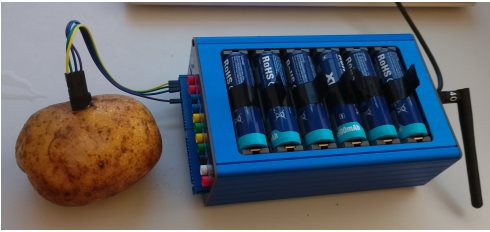

Fig. 3. 4-wire direct measurement of potato

To further explore the applicability of frequency difference EIT mode, we conducted additional measurements in various setups:

- Salty water with no anomaly (homogeneous solution).
- Biological phantoms such as potato and tomato placed in the center and at the edge (between electrodes 1 and 2) of the water tank.
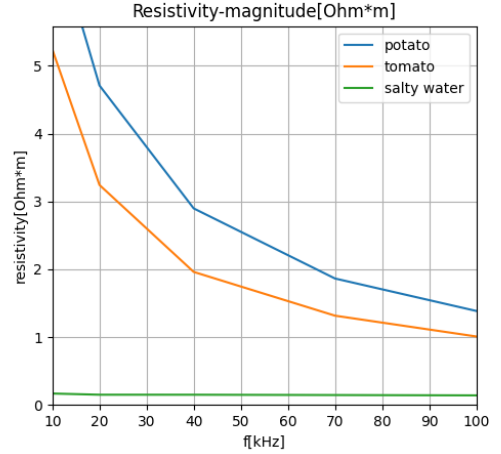- A frequency-independent object (glass) placed in the water tank.

Fig. 4. Directly measured complex resistivity of the object under test - magnitude

For each scenario, EIT measurements were taken across a frequency range of 1 kHz to 200 kHz, and the data was saved for further analysis.

Fig. 5 illustrates different EIT image reconstruction methods in an experiment where a potato was placed between electrodes 1 and 2 at the periphery of the tank, simulating a scenario where a localized conductivity change occurs near the boundary of a biological tissue, such as a lung or fluid accumulation near the chest wall.

Fig. 5(a) shows the reconstructed image using the imaginary part of the impedance, resulting in enhanced object contrast and reduced background artifacts. In contrast, Fig. 5(b) demonstrates that using the real part of the impedance results in stronger background variations, reducing the object's visibility and overall image clarity. Furthermore, Fig. 5(c) illustrates the EIT image generated using the conventional time-difference method, where saline water without any object serves as the reference, and the potato is used as the test object. This method provides the clearest representation by subtracting a reference frame measured in homogeneous saline, but it requires a stable reference measurement, which is not always practical in real-world applications.

This comparison highlights the significance of capturing both the real and imaginary components of impedance as a practical alternative for frequency-difference EIT, particularly when reliable reference data is unavailable.

C. Image quality assessment

Yasin et al. [21] provide a systematic approach for evaluating EIT systems using several performance metrics, including amplitude response, detectability, and resolution. These metrics characterize the quality of reconstructed EIT images and have been used in similar studies, including by Creegan

Reconstituted EIT Image (Imaginary)

Reference		Data	
● potato_edge	● 4kHz	● potato_edge	● 70kHz

(a) Frequency difference EIT image using the imaginary part of impedance data.

Reconstituted EIT Image (Real)

Reference		Data	
● potato_edge	● 4kHz	● potato_edge	● 70kHz

(b) Frequency difference EIT image using the real part of impedance data.

Reconstituted EIT

Reference		Data	
● water	● 70kHz	● potato_edge	● 70kHz

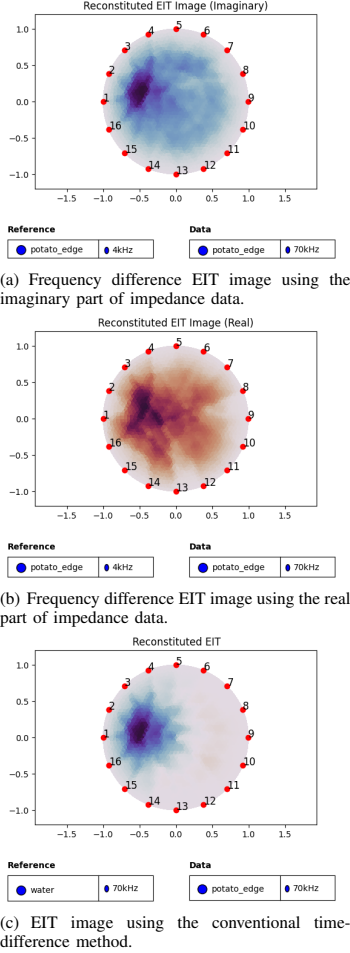(c) EIT image using the conventional time-difference method.

Fig. 5. Comparison of EIT images generated using different data inputs and methods.

et al. [14]. Amplitude response measures the average pixel intensity within the entire reconstructed image, normalized to the target volume. This metric provides an indication of the image amplitude's consistency across regions of interest. Detectability quantifies the ability to reliably detect a target within the image. It is calculated as the ratio of the mean pixel intensity in the region of interest (ROI) to the standard deviation of the same region, expressed in decibels (dB). This metric highlights the contrast-to-noise ratio in the reconstructed image. Resolution evaluates the size of the reconstructed target relative to the total area of the medium. It is calculated as the square root of the ratio of the target's reconstructed area to the total area.

To measure these performance parameters of our EIT system, we conducted experiments using a saline water bath

as the conductive medium and a glass object as the non-conductive target. This setup was chosen to achieve a high conductivity contrast, as recommended by Yasin et al. [21]. The glass object was positioned at nine distinct locations along the x-axis, passing through the center of the medium. Figure 6 illustrates the results of these performance metrics for our EIT system. Detectability values are shown in Figure 6(a), resolution in Figure 6(b), and amplitude response in Figure 6(c). For all three performance metrics, the x-axis in the subfigures represents the radius proportion, defined as the ratio of the distance from the object's center to the center of the medium, normalized by the medium's radius.

In addition to providing performance metrics, Yasin et al. [21] also report the evaluation of three EIT devices using these metrics. Here, we compare our results to those reported EIT devices. For detectability, the reported devices achieve values ranging from 15 dB to 29 dB when the object is close to the center, with detectability tending to increase as the object moves toward the edges (closer to the electrodes). In contrast, our device demonstrates a more stable detectability, varying only slightly between 22 dB and 23 dB as the object moves, which indicates average but more consistent performance across all positions.

As for resolution, Yasin et al. report values ranging from approximately 0.5 to 0.3, reflecting a 40% change as the object moves from the center to the edge. For our device, the resolution varies between approximately 0.23 and 0.14, corresponding to a 39% change, indicating similar performance in terms of relative resolution change.

Regarding amplitude response, our device shows very consistent pixel values (representing conductivity changes), except for the center position, where the value rises slightly. In contrast, the average-performing device reported by Yasin et al. exhibits greater variability in amplitude response, with notable fluctuations across different target positions. Our system maintains a more consistent amplitude response regardless of the target's position, which aligns with the expected behavior for imaging systems where amplitude response should ideally remain stable.

Overall, our device demonstrates consistent detectability and amplitude response, with resolution performance closely matching the relative changes reported in the literature.

III. CONCLUSION AND FUTURE WORK

This paper presents a competitive DSP-based EIT prototype, demonstrating advanced features and capabilities that address the challenges associated with traditional EIT systems. Table I provides a detailed comparison of our device with other state-of-the-art systems.

The proposed EIT device is well-suited for physiological measurements, including cardio-respiratory monitoring and impedance-based imaging, and is characterized by the following key features:

- The digital (DSP-based) implementation enables easy integration of multi-frequency measurement modes, facilitating not only time-variation image reconstruction but
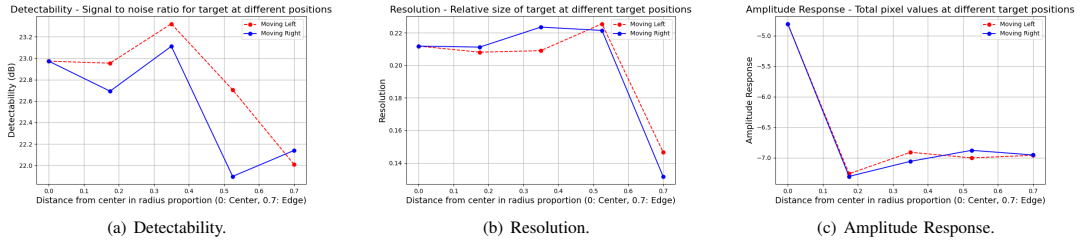
Fig. 6. Comparison of EIT performance metrics: (a) Detectability, (b) Resolution, and (c) Amplitude Response for objects moving left and right within the saline water bath.

also frequency difference methods for enhanced imaging versatility.

- The device achieves high resolution through its integrated 16-bit multichannel ADC and fast multiplexing capabilities (below 1 ms), supporting configurations with 16 or 32 electrodes in the EIT measurement setup.
- Portability is ensured through battery operation, making the device suitable for both controlled laboratory experiments and field applications.
- Multiple communication options, including USB, Bluetooth (via a virtual serial port), and WiFi.
- Additional inputs for PPG and ECG signals.
- Measuring voltage and current simultaneously in real time, reducing dependence on current pump linearity for impedance calculation.

The experimental results demonstrate the device's ability to measure both real and imaginary parts of impedance, enabling frequency difference EIT mode to enhance image quality by improving object contrast and minimizing background changes. Future work will focus on optimizing imaging algorithms, integrating machine learning for image reconstruction, and developing advanced phantoms to expand the clinical and industrial applications of the proposed EIT solution.

REFERENCES

[1] N. Polydorides, "Image reconstruction algorithms for soft-field tomography," Ph.D. Thesis, University of Manchester Institute of Science and Technology, 2002.

[2] B. Liu, B. Yang, C. Xu, J. Xia, M. Dai, Z. Ji, F. You, X. Dong, X. Shi, and F. Fu, "pyeit: A python based framework for electrical impedance tomography," *SoftwareX*, vol. 7, pp. 304–308, 2018.

[3] M. H. Lee, G. Y. Jang, Y. E. Kim, P. J. Yoo, H. Wi, T. I. Oh, and E. J. Woo, "Portable multi-parameter electrical impedance tomography for sleep apnea and hypoventilation monitoring: Feasibility study," *Physiological Measurement*, vol. 39, no. 12, p. 124004, 2018.

[4] B.-S. Lin, H.-R. Yu, Y.-T. Kuo, Y.-W. Liu, H.-Y. Chen, and B.-S. Lin, "Wearable electrical impedance tomography belt with dry electrodes," *IEEE Transactions on Biomedical Engineering*, vol. 69, no. 2, pp. 955–962, 2022.

[5] L. Sophocleous, I. Frerichs, M. Miedema, M. Kallio, T. Papadouri, C. Karaoli *et al.*, "Clinical performance of a novel textile interface for neonatal chest electrical impedance tomography," *Physiological Measurement*, vol. 39, no. 4, p. 044004, 2018.

[6] A. Adler and A. Boyle, "Electrical impedance tomography: Tissue properties to image measures," *IEEE Transactions on Biomedical Engineering*, vol. 64, no. 11, pp. 2494–2504, 2017.

[7] M. Kluza and I. Karpiel, *Bioimpedance Spectroscopy – Modern Applications*, 02 2024, pp. 241–248.

[8] I. Frerichs, M. Amato, A. Kaam, D. Tingay, Z. Zhao, B. Grychtol *et al.*, "Chest electrical impedance tomography examination, data analysis, terminology, clinical use and recommendations: consensus statement of the translational eit development study group," *Thorax*, vol. 72, pp. 83–93, 09 2016.

[9] V. Tomicic and R. Cornejo, "Lung monitoring with electrical impedance tomography: technical considerations and clinical applications," *Journal of Thoracic Disease*, vol. 11, no. 7, pp. 3122–3135, 2019.

[10] A. Borsic *et al.*, "Sensitivity study and optimization of a 3d electric impedance tomography prostate probe," *Physiological Measurement*, vol. 30, pp. S1–S19, 2009.

[11] B. G. Pedro, D. W. C. Marcôndes, and P. Bertemes-Filho, "Analytical model for blood glucose detection using electrical impedance spectroscopy," *Sensors*, vol. 20, no. 23, 2020.

[12] S. Leonhardt *et al.*, "Electric impedance tomography for monitoring volume and size of the urinary bladder," *Biomedizinische Technik*, vol. 56, pp. 301–307, 2011.

[13] B. Brazey, Y. Haddab, N. Zemiti, F. Mailly, and P. Nouet, "An open-source and easily replicable hardware for electrical impedance tomography," *HardwareX*, vol. 11, p. e00278, 2022.

[14] A. Creegan, J. Bradfield, S. Richardson, L. Sims Johns, K. Burrowes, H. Kumar, P. M. Nielsen, and M. H. Tawhai, "A wearable open-source electrical impedance tomography device," *HardwareX*, vol. 18, p. e00521, 2024.

[15] J. E. Fernández, C. M. López, and V. M. Leyton, "A low-cost, portable 32-channel eit system with four rings based on afe4300 for body composition analysis," *HardwareX*, vol. 16, p. e00494, 2023.

[16] I. Nur Rifai, P. A. Sejati, S. Akita, and M. Takei, "Fpga-based planar sensor electrical impedance tomography (fpga-pseit) system characterized by double feedback howland constant- current pump and programmable front-end measurement," *IEEE Transactions on Instrumentation and Measurement*, vol. 73, pp. 1–10, 2024.

[17] M. Metshein, A. Gautier, B. Larras, A. Frappe, D. John, B. Cardiff, P. Annus, R. Land, and O. Martens, "Study of electrode locations for joint acquisition of impedance- and electro-cardiography signals," in *2021 43rd Annual International Conference of the IEEE Engineering in Medicine & Biology Society (EMBC)*, 2021, pp. 7264–7264.

[18] A. Abdullayev, M. Rist, A. Krivošei, M. Metshein, R. Land, and O. Martens, "A dsp-based multichannel ebi measurement device," in *2024 IEEE International Instrumentation and Measurement Technology Conference (I2MTC)*, 2024, pp. 1–6.

[19] S. Gabriel, R. W. Lau, and C. Gabriel, "The dielectric properties of biological tissues: Ii. measurements in the frequency range 10 hz to 20 ghz," *Physics in Medicine and Biology*, vol. 41, no. 11, pp. 2251–2269, 1996.

[20] Dieter K. Schroder, *Semiconductor Material and Device Characterization, Chapter 1: Resistivity*. John Wiley & Sons, Ltd, 2005, pp. 1–59.

[21] M. Yasin, S. Böhm, P. O. Gaggero, and A. Adler, "Evaluation of eit system performance," *Physiological Measurement*, vol. 32, no. 7, pp. 851–865, 2011.

Appendix 8 — The Impedance Cardiography Device

VIII

O. Märtens, A. Abdullayev, M. Metshein, A. Gautier, A. Frappe, A. Krivošei, M. Rist; P. Annus, B. Larras, D. John; B. Cardiff. The impedance cardiography device, October 23, 2023. Estonian patent application P202200004, US patent application US2023/0320606 A1

US 20230320606A1

(54) **IMPEDANCE CARDIOGRAPHY DEVICE**

(71) Applicant: **Tallinn University of Technology,**
Tallinn (EE)

(72) Inventors: **Olev Märtens**, Tallinn (EE); **Anar
Abdullayev**, Tallinn (EE); **Margus
Metshein**, Tallinn (EE); **Antoine
Gautier**, Lille Cedex (FR); **Antoine
Frappe**, Lille Cedex (FR); **Andrei
Krivošei**, Tallinn (EE); **Marek Rist**,
Tallinn (EE); **Paul Annus**, Tallinn (EE);
Benoit Larras, Lille Cedex (FR); **Deepu
John**, Belfield (IE); **Barry Cardiff**,
Dublin (IE)

Publication Classification
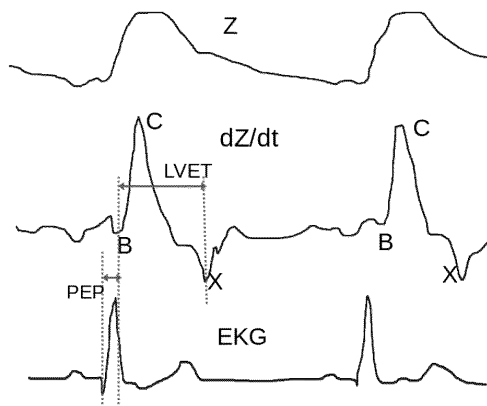
(57) **ABSTRACT**

The impedance cardiography device comprises an impedance measuring unit, connected to the human body to be measured, a differentiator, a comparator and a microcontroller integrated with an analog-to-digital converter, characterized by that the device further comprises two peak voltage detection units with different polarities (positive and negative), the strobing outputs of them being connected to the digital (binary) inputs of the microcontroller and the analog hold outputs to the inputs of the analog-to-digital converter.
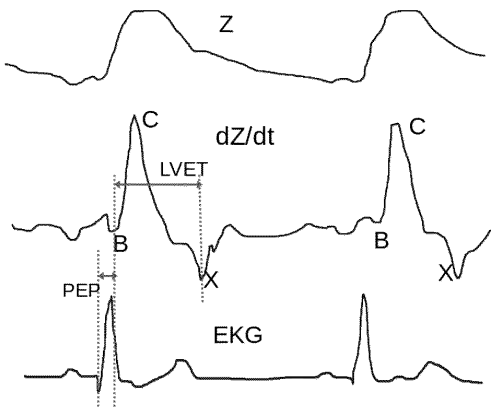
FIG. 1

BACKGROUND ART

FIG. 2

ICG para-meters

61

ADC
A0
A1

Micro-controller

6

Digital clock

8

strob1

strob2

strob3

+Peak detection unit

4

- Peak detection unit

7

Compa-rator

5

Differen-tiator

3

Ecxitation signal generator

21

Detector

22

Filter

23

Unit of the impedance measurement

2

Measured Human Body

1

FIG. 3

FIG. 4

FIG. 5

ICG para-meters

ADC
A0
A1
A2

Micro-controller

DAC

6

8 Digital clock

41 +Peak detection and hold unit

strob1

-Peak detection and hold unit

strob2

Compa-rator

strob3

62

5

71

3 Differen-tiator

21 Excitation signal generator

22 Detector

23 Filter

Unit of the impedance measurement

2

Measured Human Body

1

FIG. 6

FIG. 7

V-

Analog output

D1 1N4148

C11 1,5uF

R10 820kOhm

Uin

V+

V+   V-

Strobe Pulse

FIG. 8

12a
AEPC-1

Z->

12b
AEPC-3 ->dZ/dt->

-> B,C,X
determination
of fiducial points

ICG:
estimation
of
parameters

TEPC-1   13   14

11

FIG. 9

FIG. 10

FIG. 11

IMPEDANCE CARDIOGRAPHY DEVICE

PRIORITY

[0001] This application claims priority to Estonian patent application number P202200004 filed on Mar. 29, 2022.

TECHNICAL FIELD

[0002] The invention belongs to the field of the measurement technology in healthcare, more precisely to the field of assessment and diagnostics of the work of the heart. The important uses of the invention are medical and daily health monitoring and diagnostics, to receive warnings of cardiac disorders as early as possible.

BACKGROUND OF THE INVENTION

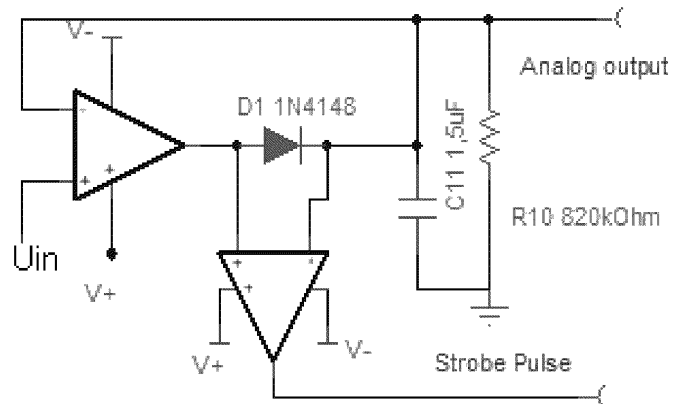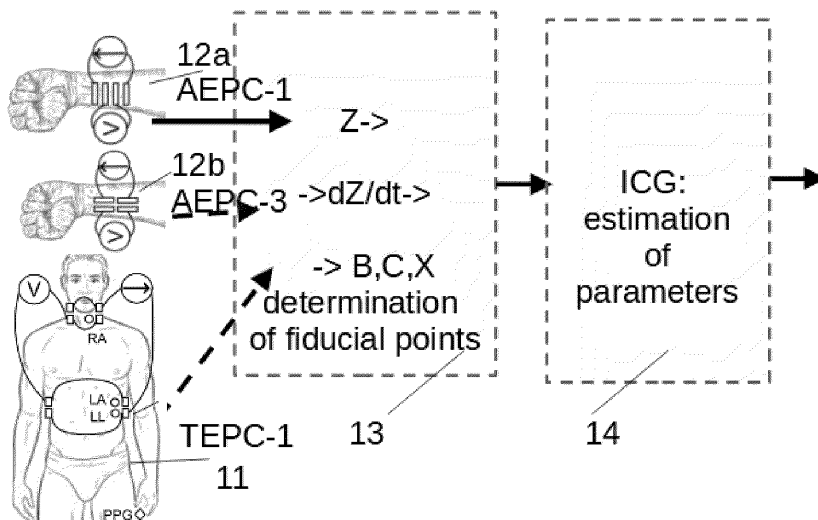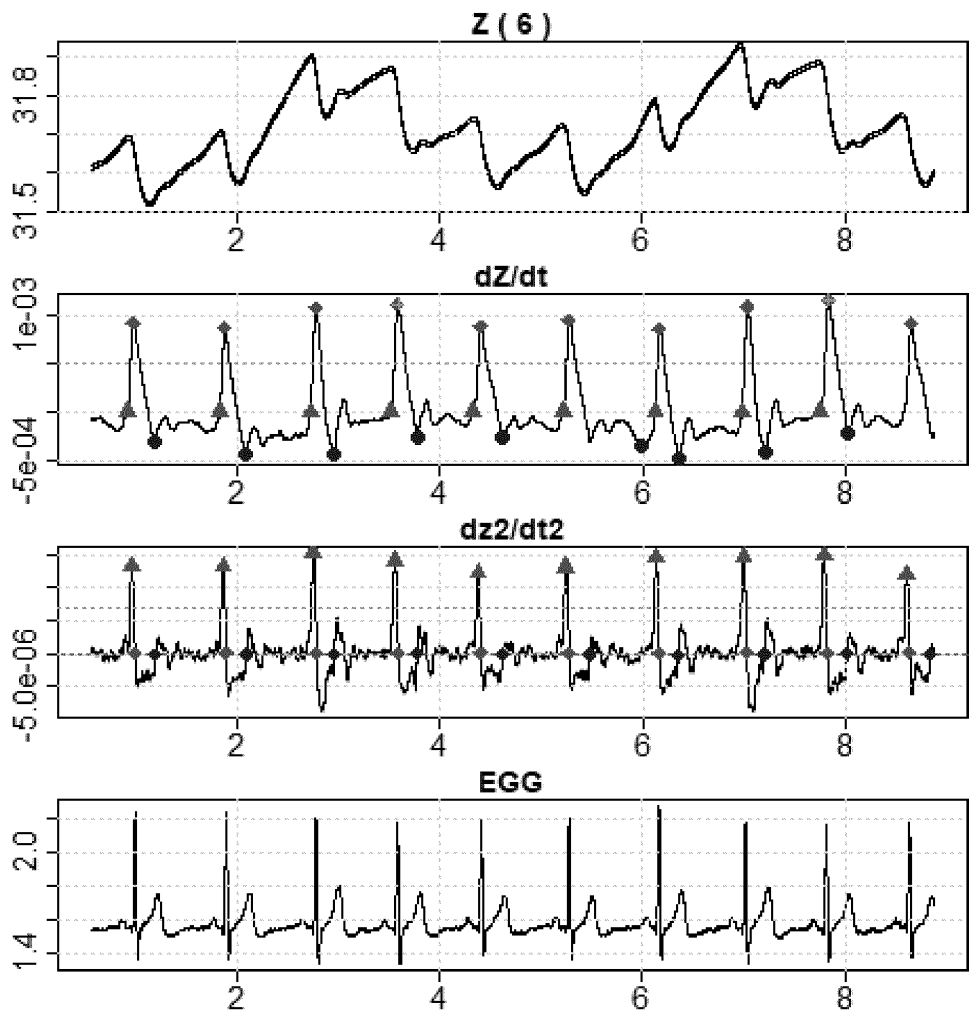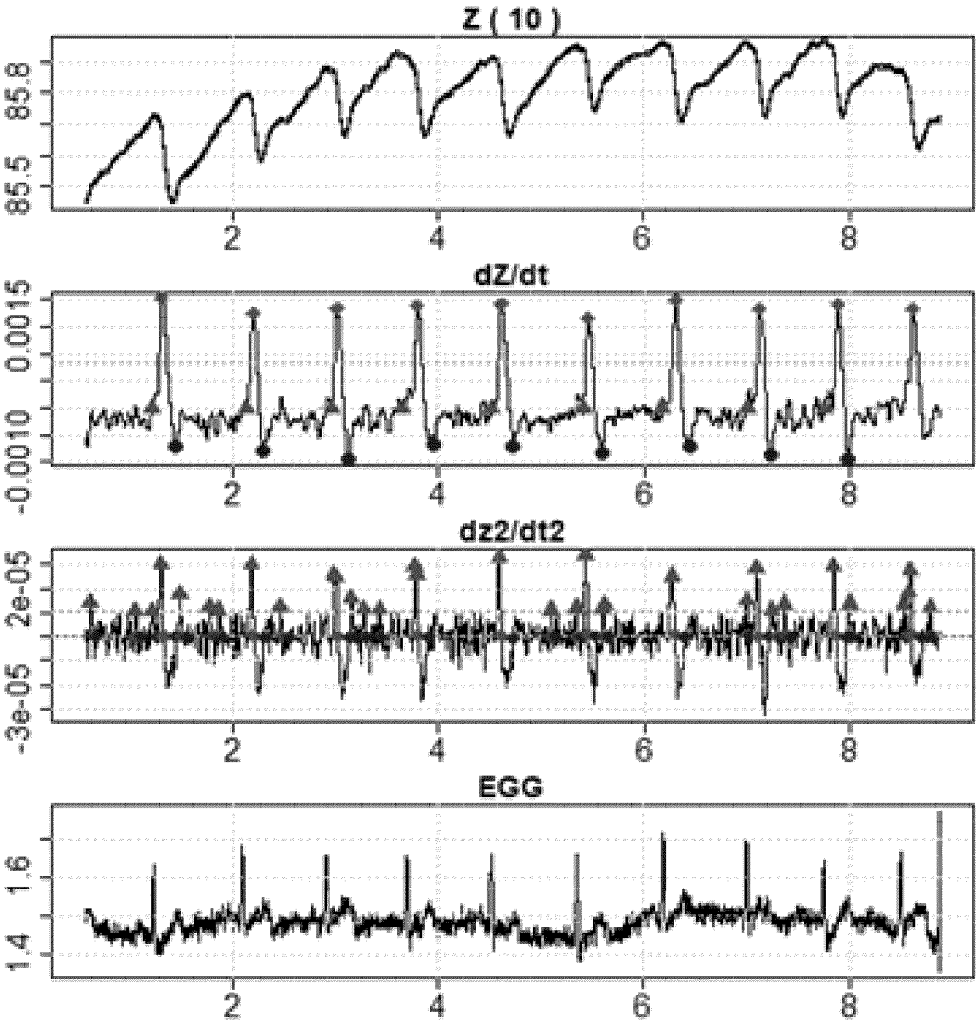[0003] There are known impedance cardiography (ICG) solutions, where the electrical bioimpedance signal (acquired, for example, from the patient's chest or wrist) is digitized with a relatively high resolution and sampling frequency (e.g. with a 16-bit analog-to-digital converter with a frequency of 200 samples per second) and the resulting digitized waveform is further analyzed with special software in a local microprocessor (US4450527) or in an embedded system (A. Gautier et al., "Embedded ICG-based Stroke Volume Measurement System: Comparison of Discrete-Time and Continuous-Time Architectures", hal.archives-ouvertes.fr/hal-03482323) or sent (e.g. via wireless connection) to a computer or similar device for analysis (e.g. H. Yazdanian et al., 2016, "Design and Implementation of a Portable Impedance Cardiography System for Noninvasive Stroke Volume Monitoring", Journ. of Medical Signals and Sensors. 6, pp. 47-56).

[0004] Such solutions have several disadvantages:

[0005] 1) the external computer as part of the system cannot be the basis of autonomous (with event detection with local intelligence) or small-sized and low-energy devices;

[0006] 2) to determine the characteristic points (B, C, X) of the heart cycle (see the mentioned H. Yazdanian et al.), the local digital processor includes sophisticated analysis and calculations over a relatively large number of samples of the signal, which makes it impossible to implement the device as a very small-size low-power and low-cost chips and wearables;

[0007] 3) known solutions have also an important drawback - the high-resolution and high-sampling frequency analog-to-digital converters have sophisticated schematics and high energy consumption;

[0008] 4) while reducing the sampling frequency or the resolution of the analog-to-digital converter (ADC) in order to achieve lower power consumption, the accuracy of the measurement of ICG values, both in time and amplitude domains, while determining the characteristic points of ICG cycles and, consequently, also in the further estimation of ICG parameters, is significantly reduced.

[0009] Known impedance cardiography device solution is described in US4450527 (B. Sramek, "Noninvasive continuous cardio monitor"), where the first differentiator finds the derivative (dZ/dt) of the bioimpedance (Z) result measured from a person (eg from the chest) as the impedance cardiography (ICG) signal. And to find the ICG characteristic points (B, C, X) (where C and X are the maximum and minimum of dZ/dt during one period of cardiac cycle), this solution contains a second differentiator for taking the derivative and a comparator at its output to fix the zero crossings of the second derivative. From the B, C, X value of each heart cycle, hemodynamic parameters such as LVET (left ventricular ejection time), CO (cardiac output), SV (heart stroke volume) and others can be calculated.

[0010] The disadvantage of this solution is the use of two cascaded differentiators in the solution, increasing significantly the noise and disturbances of the signal. Differentiation (taking the derivative) as a function is known to be sensitive to small rapid changes, and the double derivative even more.

SUMMARY OF THE INVENTION

[0011] The aim of the invention is an improved ICG device for more accurate assessment of ICG parameters by more accurate determination of ICG characteristic points from the ICG waveform, using relatively simple and energy-efficient hardware.

[0012] This goal is achieved by a technical solution (FIG. 3), where compared to the known solution, which includes an impedance measurement unit 2, a differentiator 3, a comparator 5 and an analog-to-digital converter 61 integrated with the microcontroller 6, human body 1 to be measured, by the impedance measurement unit 2, output of which is connected to the input of the differentiator 3, the output of which is in turn connected to the input of the analog-to-digital converter 61 integrated with the microcontroller 6 and through the first input of the comparator 5 to the first binary input of the microcontroller 6, wherein the device includes a positive peak value detection unit 4 and a negative peak value detection unit 7, whose inputs are connected to the output of the differentiator 3 and whose binary outputs are connected to the respectively to the second and third binary inputs of the microcontroller 6.

[0013] As a rule, the microcontroller 6 needs a clock generator 8.

[0014] It can be reasonable (FIG. 4) that the mentioned positive peak value detection unit 4 is, in addition to detecting the peak value event with corresponding strobing pulses, has also means of holding the corresponding analog peak values (until the next ICG signal peak), wherein the analog output of the corresponding positive peak value detection and hold unit 41 is connected to the corresponding input of the analog-to-digital converter 61, integrated with the microcontroller 6.

[0015] It may be reasonable (FIG. 5) that the comparator 5 has a second input to which the analog voltage from the hold output of the positive peak value detection and hold unit 41 for detecting and holding the positive peak value mentioned - is given through the voltage divider 9. In that case, it can be reasonable that the transfer coefficient of the mentioned voltage divider 9 is from about 0.1 to 0.20, preferably around 0.15.

[0016] Alternatively, it may be reasonable (FIG. 6) that the comparator 5 has a second input to which voltage is supplied from the digital-to-analog converter 62, integrated with the microcontroller 6.

[0017] It can also be reasonable (FIG. 7), that in addition to the mentioned positive peak value detection unit 4, the mentioned negative peak value detection unit 71 has also

means to hold the corresponding negative analog peak value (until the next ICG signal peak), while the output of this negative analog peak value unit is connected to a separate input of the analog-to-digital converter **61** integrated with the microcontroller **6**.

[0018] It can be reasonable (FIG. **8**) that the mentioned positive peak value detection unit **4**, positive peak value detection and hold unit **41**, negative peak value detection unit **7** and negative peak value detection and hold unit **71** consist of an operational amplifier, a comparator, of a diode, a capacitor and a resistor, while the non-inverting input of the operational amplifier is connected to the input of the given unit, the output through the semiconductor diode to the inverting input of the same operational amplifier, which in turn is connected to ground through the parallel connection of the resistor and capacitor, and the first input of the comparator is connected to one terminal of the diode, and the second input to the second terminal of the diode, and the output of the comparator is the output of the peak value detection unit. The peak value hold output of the peak value detection unit is connected to the inverting input of the operational amplifier.

BRIEF DESCRIPTION OF THE DRAWINGS

[0019] The patent or application file contains at least one drawing executed in color. Copies of this patent or patent application publication with color drawing(s) will be provided by the Office upon request and payment of the necessary fee.

[0020] The invention is illustrated by the following figures.

[0021] FIG. **1** shows the ICG waveform of one cardiac cycle (see e.g. H. Yazdanian et al.) — the upper curve shows the electrical bioimpedance waveform (Z) signal, the middle — ICG signal (the first derivative of the impedance signal dZ/dt) and the lower curve the ECG (electrocardiography) waveform as for background information.

[0022] FIG. **2** shows the circuit diagram of the known solution (US4450527).

[0023] FIG. **3** shows the circuit diagram of the device according to the invention, where the positive peak value detection unit **4** and the negative peak value detection unit **7** have only a binary (strobing) outputs connected to the microcontroller.

[0024] FIG. **4** shows the circuit diagram of the device according to the invention, where the positive peak value detection and hold unit **41** has, in addition to the binary (strobing) output, also an analog peak value hold output, which is connected to the corresponding input of the analog-to-digital converter integrated with the microcontroller.

[0025] FIG. **5** shows the basic diagram of the device according to the invention, where the signal from the output of the unit **41** for detecting and holding the positive peak value is taken through the voltage divider **9** (with a transmission factor of 0.15) to the second input of the comparator.

[0026] FIG. **6** shows the basic diagram of the device according to the invention, where the second input of the comparator **5** receives a signal from the output **61** of the digital-analog converter integrated with the microcontroller **6**.

[0027] FIG. **7** shows the circuit diagram of the device according to the invention, where both positive and negative peak value detection units have, in addition to the strobing

output, analog peak value hold outputs **41**, **71**, which are connected to the inputs of the analog-to-digital converter **61** integrated with the microcontroller **6**.

[0028] FIG. **8** shows the circuit diagram of a possible implementation example of the positive peak value detection unit **4** and the positive peak value detection and hold unit **41**, together with the analog peak value hold output. For the negative peak value detection unit **7** and the negative peak value detection and hold unit **71**, the polarity of the diode must be changed.

[0029] FIG. **9** shows the measurement configurations for ICG signal acquisition. TEPC **11** represents examples of signal measurement from chest and AEPC **12a**, **12b** from the wrist, and units **13** and **14** are for determining ICG fiducial points and calculating the estimated ICG parameters.

[0030] FIGS. **10** and **11** show examples of the impedance signals (from top to bottom, impedance Z, then the first derivative dZ/dt as the ICG signal, then the second derivative, which is used by a known solution, and then the ECG signal for the background), while in the case of FIG. **10**, the signal comes from the chest (measurement configuration TEPC, FIG. **10**) and in the case of FIG. **11** from the wrist (FIG. **11**, AEPC).

EXAMPLES OF IMPLEMENTATION OF THE INVENTION

[0031] The device is connected to a human body **1**, for example by electrodes on the chest **11** or on the wrist **12a**, **12b** (see FIG. **9**). The device (FIG. **3**) comprises an impedance measurement unit **2** which typically comprises, for example, a sinusoidal excitation signal generator **21** that generates an excitation signal for measurement, and a detector **22** that demodulates the response signal from the body **1**. Preferably, a synchronous detector is used to demodulate the response signal. It is also reasonable to use a low-pass or band-pass filter **23** in the impedance measurement unit at the output of the signal detector, both for suppressing the ripple that occurs during demodulation and interference and artifacts.

[0032] The detected and filtered impedance (Z) signal passes through the differentiator **3**, where the derivative of the impedance signal, ie the ICG signal (dZ/dt), is found. Important points B, C, X (FIG. **1**) in each heart cycle are determined in the dZ/dt signal in the simplest case as follows:

   [0033] C is the maximum (peak value) of the dZ/dt signal in the period;

   [0034] B is the last zero crossing of the dZ/dt signal before point C;

   [0035] X is the minimum value (peak value) between two C points.

[0036] To calculate the important parameters of the heart's work, such as CO and SV, it is necessary to know the time values and amplitudes of these three points, first of all the interval between the B and X points (LVET) and the amplitude of the C point.

[0037] In the proposed solution (according to FIG. **3**), the corresponding time instances are found as follows:

   [0038] In order to find the C-point, there is a positive polarity peak value detection unit **4** which fixes the corresponding time moment (eg as the corresponding reading of the internal counter of the microcontroller) by using the strobing pulse, by means of which the micro-

controller **6** (eg by using the interrupt function) and the ADC **61** integrated with the microcontroller **6** fixes and converts the current dZ/dt value to the corresponding numerical value of the signal;

[0039] in order to find point B in the diagram, there is a comparator **5**, which, when dZ/dt passes zero, generates a strobing pulse of the corresponding moment of time, by means of which the microcontroller **6** (eg using the interrupt function) fixes the corresponding moment of time (eg as a corresponding reading of the internal counter of the microcontroller); if several time values of a possible B point are fixed in the microcontroller between two C points, the last fixed value before the next C point is selected (that is, before the next C point, each possible time value of the B point overwrites the previous value);

[0040] In order to find the X-point, there is a negative polarity peak value detection unit **7**, which fixes the corresponding time instant (e.g. as the corresponding reading of the internal counter of the microcontroller **6**) by using the strobing pulse, by means of which the microcontroller **6** (eg using the interrupt function) fixes and converts the current dZ/dt to the numerical value corresponding to the X-point of the signal.

[0041] The proposed solution according to FIG. **4** differs from the previously described solution in that the positive polarity peak value detection unit **4** (for determining the timing and value of point C) includes also the functionality of fixing the corresponding analog peak value itself and transmits the fixed (hold) value to a separate input of the analog-to-digital converter. Such a solution allows to use significantly slower ADC **61**, since the positive peak value detection and hold unit **41** operates in this case as a voltage hold unit. The schematic solution of the possible peak value detection and hold unit **41** is shown in FIG. **8**.

[0042] The solutions according to FIG. **5** and FIG. **6** differ in that the threshold for fixing point B (dZ/dt crossing from zero) is raised above the zero voltage (for example, to 15% of the amplitude value of point C), which is obtained in the case of FIG. **5** with a peak value with positive polarity from the hold output of the detection and hold unit **41** or, in the case of FIG. **6**, generated by the digital-to-analog converter (DAC) **62** (performed, for example, by pulse-width modulation through a simple RC low-pass filter), integrated with the microcontroller **6**.

[0043] The proposed solution according to FIG. **7** differs from the previously described solution in that both the positive and negative peak value detection units **4** and **7** contain also the functionality of fixing the corresponding analog peak values, and the positive peak value detection and hold unit **41** and the negative peak value detection and hold unit **71** send a fixed (hold) value to a separate input of the analog-to-digital converter. Such a solution allows the use of a significantly slower (eg integrative type) ADC **61**, since the peak value detection unit works in this case as a fixed voltage holder, where the analog value is kept relatively constant for a longer time.

[0044] FIG. **8** shows an example of a possible implementation of the peak value detection unit. The circuit diagram includes an operational amplifier A1, non-inverting input of which is the input of the given unit, and negative feedback loop of it has a peak detector (D1, R1, C1). The voltage peak (maximum voltage value) is fixed on the capacitor C1. If the unit input voltage is less than the fixed peak value, the diode

closes. Capacitor C1 holds a voltage that slowly decreases through resistor R1 (discharge rate depends on the time constant R1, C1).

[0045] FIG. **9** shows the measurement configurations for ICG signal acquisition. TEPC is from the chest **11** and AEPC is from the wrist **12**a, **12**b are examples of signals measured.

[0046] FIGS. **10** and **11** show examples of impedance signals (from top to bottom impedance Z, then the first derivative dZ/dt or ICG signal and the points B, X, C found by the proposed invention, then the second derivative used by the known solution, and then the ECG signal for background. In the case of FIG. **6**, the signal originates from the chest (FIG. **5** - measurement configuration TEPC) and in FIG. **7** from the wrist (FIG. **5** - AEPC). The given results have been obtained by simulating the well-known solution proposed in this invention (US patent 4450527) as electronic circuits, using real-life captured bioimpedance signals. A particularly large difference in the improvement of the accuracy of the detection of ICG points (compared to the known solution) is in the case of the (relatively small amplitude) signal received from the wrist.

1. Impedance cardiography device, which includes an impedance measurement unit (**2**) connected to the human body (**1**) to be measured, a differentiator (**3**), a comparator (**5**) and a microcontroller (**6**) integrated with an analog-to-digital converter (**61**), wherein the impedance measurement unit (**2**) the output is connected to the input of the differentiator (**3**), the output of which is connected to the input of the analog-to-digital converter (**61**) integrated with the microcontroller (**6**) and through the comparator (**5**) to the first binary input of the microcontroller, wherein the device comprises a positive polarity peak value signal detection unit (**4**) and a negative polarity peak value detection unit (**7**), whose binary outputs are connected to the second and third binary inputs of the microcontroller (**6**), respectively.

2. The impedance cardiography device according to claim **1**, wherein the unit for detecting the positive polarity peak value (**4**) comprises the unit (**41**) for holding the analog value of the positive peak value, whereby the analog output for holding the peak value of this unit is connected to the microcontroller (**6**) integrated analog- to the second input of the digital converter (**61**).

3. The impedance cardiography device according to claim **2**, wherein the second input of the comparator (**5**) is connected through the voltage divider (**9**) to the analog hold output of unit (**41**) for detecting and holding the positive peak value.

4. The impedance cardiography device according to claim **3**, wherein the transfer coefficient of said voltage divider (**9**) is 0.15.

5. The impedance cardiography device according to claim **2**, wherein the second input of the comparator (**5**) is connected to the output of the digital-to-analog converter (**62**) integrated with the microcontroller (**6**).

6. The impedance cardiography device according to claim **1**, wherein the units for detecting the peak value of positive and negative polarity signals are also units (**41**, **71**) for holding the analog value of the peak value, wherein the analog outputs of the hold values of the peak value of positive and negative polarity are connected to the second and third inputs respectively of the analog-to-digital converter (**61**) integrated with the microcontroller (**6**).

7. The impedance cardiography device according to claim **2**, wherein said positive peak value detection unit (**4**), negative peak value detection unit (**7**), positive peak value detection and hold unit (**41**) and negative peak value detection and hold unit (**71**) consist of an operational amplifier, a comparator, a diode, a capacitor and a resistor, with the non-inverting input of the operational amplifier connected to the input of the given unit, the output through a (semiconductor) diode to the inverting input of the same operational amplifier, which in turn is connected to ground through the parallel connection of the resistor and capacitor, and the first input of the comparator is connected with one terminal of the diode and the other input with the other terminal of the diode and the output of the comparator is the binary output of the unit.

8. The impedance cardiography device according to claim **7**, wherein said positive peak value detection unit (**4**) and negative peak value detection unit (**7**) contain an analog peak value hold output connected to the inverting input of the operational amplifier.

* * * * *

Appendix 9 — A Method and Device For Synthesizing Binary Waveforms

IX

O. Märtens, A. Abdullayev, M. Metshein, M. Rist, P. Annus, A. Krivošei. A method and device for synthesizing binary waveforms, December 19, 2024. Estonian patent application P202300017, US Patent application US2024/0421805 A1

(19) **United States**

(12) **Patent Application Publication** (10) Pub. No.: **US 2024/0421805 A1**

Märtens et al. (43) **Pub. Date:** **Dec. 19, 2024**

(72) Inventors: **Olev Märtens**, Tallinn (EE); **Anar Abdullayev**, Tallinn (EE); **Margus Metshein**, Tallinn (EE); **Marek Rist**, Tallinn (EE); **Paul Annus**, Tallinn (EE); **Andrei Krivošei**, Tallinn (EE)

(57) **ABSTRACT**

A method and device for synthesizing binary waveforms, wherein the initial analogue waveform is first converted into the segments with discrete levels, then each said discrete level section is in turn converted into a binary pulse of the same time duration as the given segment, and the average value of the generated pulse is proportional to the average value of the given initial waveform over the time duration of the given segment.
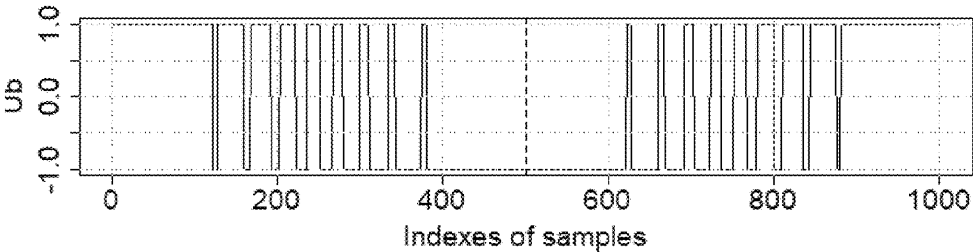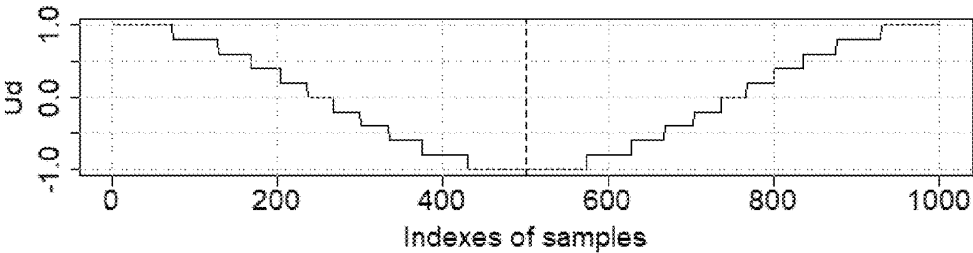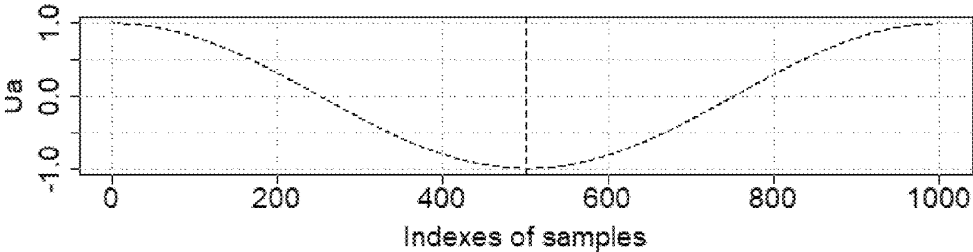
Fig. 1

Fig. 2

Fig. 3

METHOD AND APPARATUS FOR SYNTHESIZING BINARY WAVEFORMS

RELATED APPLICATIONS

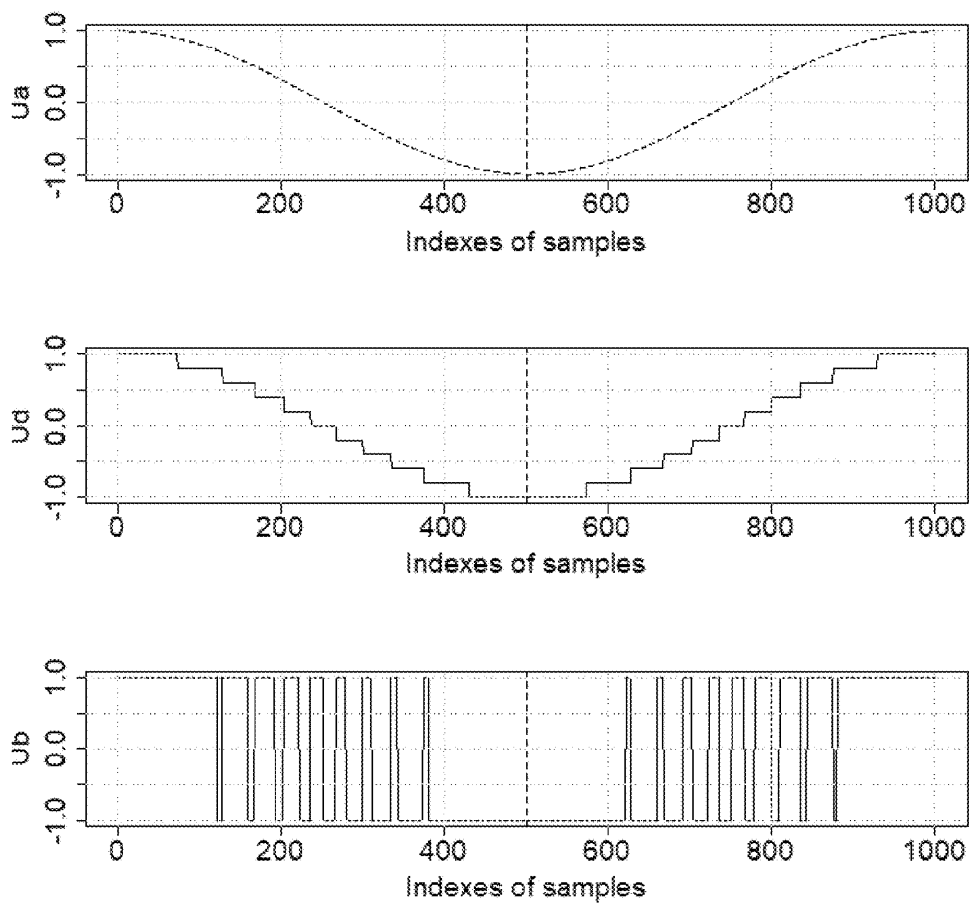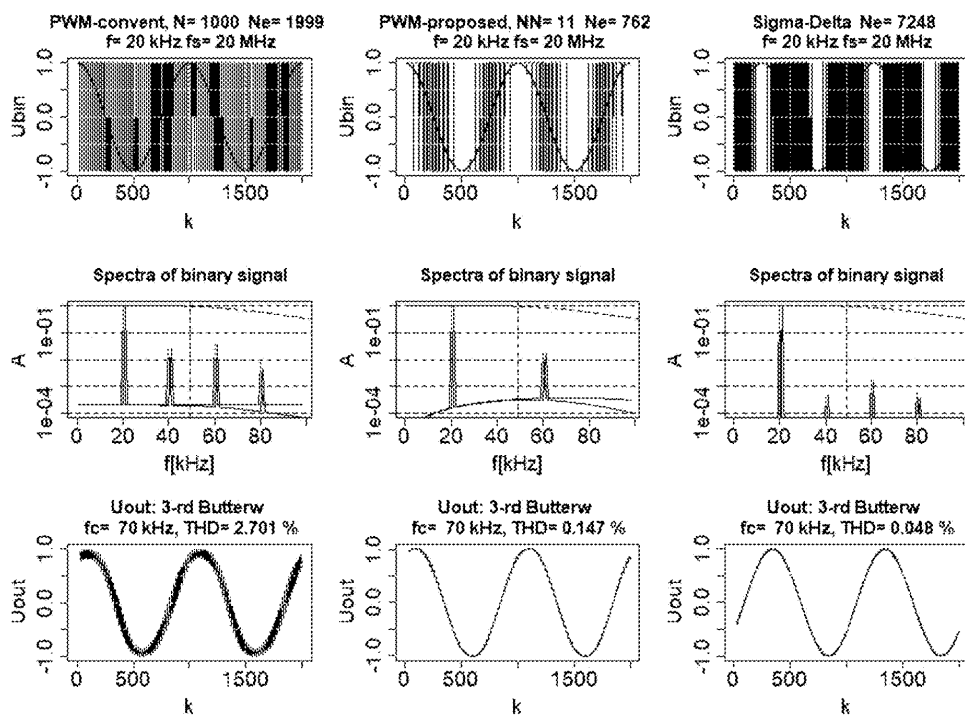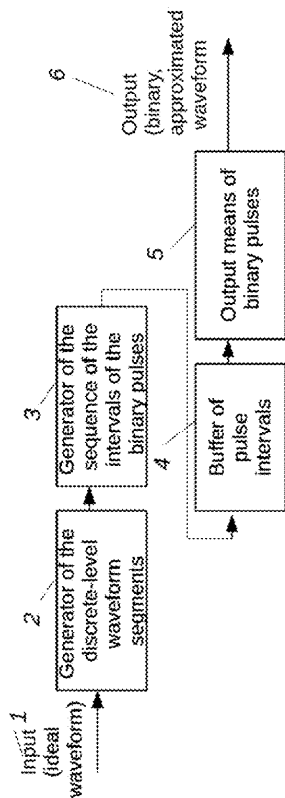[0001]   This application claims priority to EE Patent Application P202300017 filed Jun. 19, 2023. This application is herein incorporated by reference in its entirety for all purposes.

TECHNICAL FIELD

[0002]   The invention belongs to the field of measurement techniques. The invention can be applied for generation of measurement signals, among other things—for synchronous measurements, including the electrical complex impedance measurements. Also, the invention can be used to generate AC voltage in power supply converters.

BACKGROUND OF THE INVENTION

[0003]   There are known solutions that use delta-sigma modulation to approximate analog waveforms by binary signals (corresponding implementation in digital electronics-see e.g. N. D. Patel and U. K. Madawala, "*Sinewave generation using bit-streams,*" 2008 34*th Annual Conference of IEEE Industrial Electronics*, Orlando, FL, USA, 2008, pp. 1391-1396). The disadvantage of such solution is the frequent alternation of the resulting binary signal levels 1 and 0. In other words, the approximated binary signal consist a very large number of segments, which are often of very short time duration, which complicates the implementation of such a solution and also adds many higher harmonic components to the resulting binary waveform.

[0004]   There are well-known solutions for generating binary signals to approximate analog waveforms, using pulse-width modulation (PWM), implemented in the analog technique with "natural sweep" (e.g. M. H. Rashid, *Electrónica de Potencia. Circuitos, Dispositivos y Aplicaciones, Third Edition*. Prentice Hall, 2003), where the approximating original signal (such as a sine wave or audio signal) is compared by a comparator with a sawtooth waveform of a higher frequency than the original signal, and the result is a sequence of binary pulses with variable widths-so a PWM signal. The disadvantage of this solution is—that there are relatively many harmonic components in the resulting binary signal, which requires a complex additional analog filter to obtain a pure analog waveform, or when using such a binary signal as a reference signal in synchronous measurements, the mentioned harmonics significantly decrease the quality of synchronous detection.

[0005]   The closest solution to the proposed invention is the use of the so-called "uniform sampling" PWM to generate binary signals from an analog waveform, where after every fixed time period a pulse with a width corresponding to the approximated value of that time is generated (e.g. J. Richardson and O. T. Kukrer, "*Implementation of a PWM Regular Sampling Strategy for AC Drives,*" *IEEE Trans.*, vol. 645-655). The features and the disadvantages of the mentioned solution are similar to the "naturally generated" solutions described above.

SUMMARY OF THE INVENTION

[0006]   The goal of the invention is to significantly improve the method and device for the synthesis of binary waveforms with an improved spectrum when approximating analog waveforms.

[0007]   The stated goal is achieved by a technical solution, where compared to the known solution for generating binary waveforms to approximate the desired waveform—the waveform to be approximated is first converted into segments of discrete levels, then each discrete level segment is further converted into a binary pulse with the same time duration as the given segment, the average value of which is proportional to the average value of the waveform to be approximated over the time duration of the given segment.

[0008]   It can be reasonable that the values of the mentioned discrete levels are optimized for the best approximation of the desired waveform of the resulting binary waveform according to some criteria.

[0009]   It can be reasonable that the generation of the mentioned waveform takes place at discrete time values with a uniform time step.

[0010]   It can also be reasonable that the generation of the mentioned waveform takes place at discrete time values with a non-uniform time step.

[0011]   It is reasonable that each mentioned binary pulse starts with a positive value, if the mentioned segments of discrete levels have decreasing values in the time; and with a negative value if the mentioned segments with discrete levels have increasing values in time.

[0012]   It can be reasonable that the initial desired waveform is symmetrical in the time-domain window, and the second half of the binary waveform in the time domain is realized as a mirror image of the first half of the binary waveform.

[0013]   The waveform to be approximated can be a single frequency sinewave. Alternatively, the waveform to be approximated may contain multiple frequency components (for example, a multi-frequency signal or a time-varying-frequency signal).

[0014]   It can be reasonable that a correction waveform is added to the waveform to be approximated, which is optimized to get the best approximation of the desired waveform of the resulting binary waveform according to some criteria.

[0015]   A device for generating binary waveforms may include generator of the discrete-level waveform segments (2), connected in series to an input (ideal waveform) (1), generator of the sequence of the intervals of the binary pulses (3), a buffer of pulse intervals (4) and output means of binary pulses (5), which is connected to the device output (6) (FIG. 3).

BRIEF DESCRIPTION OF THE DRAWINGS

[0016]   The invention is illustrated by the following figures.

[0017]   In FIG. 1 (from top to bottom):

[0018]   the initial ideal (desired) waveform (for example, a sine or cosine waveform, given by one or more periods;

[0019]   the same converted to discrete level segments; and

[0020]   the given segments converted into binary pulses of the corresponding width.

[0021]   In FIG. 2 shows examples from left to right:

[0022]   from top to bottom, the conventional uniformly sampled PWM waveform and its spectrum and the analog waveform of the given binary signal after the 3-rd order Butterworth analog filter;

[0023] the waveform and its spectrum of the proposed solution and the analog waveform of the given binary signal after the 3-rd order Butterworth analog filter; and

[0024] the waveform and its spectrum of the solution with delta-sigma modulation and the analog waveform of the given binary signal after the 3rd order Butterworth analog filter.

[0025] In FIG. 3 a block diagram of the proposed device is shown.

EXAMPLES OF IMPLEMENTATION OF THE INVENTION

[0026] The starting point of binary waveform synthesis is the initial ideal (desired) waveform, which is approximated during synthesis—for example, a sine or cosine waveform, given with one or more periods (FIG. 1, upper waveform—as an example, one period of a cosine function). As a second step, the original waveform is converted into discrete-level segments (FIG. 1, middle waveform). In essence, it is a quantization of the original waveform. In the example in addition to the zero level, 5 positive and 5 negative values are used for the discrete levels mentioned, a total of 11 levels. As a third step, each segment with the mentioned discrete level is further converted into a binary pulse with the same time duration as the given segment, the average value of which segment is proportional to the average value of the approximated waveform and the time duration of the given section (FIG. 1, lower waveform).

[0027] FIG. 2 shows examples from left to right of the PWM-waveform with uniform sampling, then the plots of the proposed solution and the solution with delta-sigma modulation in comparison (from top to bottom—the original to be approximated waveform, the resulting binary signal spectrum and the signal shape after the 3-rd order Butterworth analog filter (cutoff frequency fc=70 kHz). It can be seen from the figure that compared to the regular PWM, the proposed solution has a cleaner spectrum and after the mentioned low-pass filter, also a more accurate waveform in the time domain (compared to the original signal). Also the number of needed pulses (and correspondingly the required number of edges of the binary signal) is smaller for proposed solution, compared to delta-sigma modulation solution.

[0028] The mentioned discrete levels can be generated by using of a uniform amplitude step. At the same time, it could be beneficial to choose these levels unevenly, optimizing the resulting binary signal by reducing the amplitude of the additional harmonics, either before or after an additional analog low-pass filter. A suitable criteria can be, for example, the minimization of the cumulative linear distortion obtained by the binary approximation of a sine wave, before or after an additional analog low-pass filter.

[0029] Binary waveform synthesis can be performed using uniform or alternatively non-uniform sampling in the tome domain.

[0030] It is reasonable, that each binary pulse starts with a positive value if the mentioned discrete level sections are of decreasing values in time; and with a negative value if the mentioned segments with discrete levels have increasing values in time.

[0031] The original waveform to be approximated may be a single-frequency sine (or cosine) waveform, but may alternatively be a waveform containing multiple frequency components. The latter can be, for example, multi-frequency

with the sum of two or more sinuses or a time-varying frequency waveform, e.g. a chirp waveform.

[0032] For further (e.g. spectral) improvement of the resulting binary signal, a corrective waveform can be added to the initial approximating waveform, which is optimized to best approximate the desired waveform of the resulting binary waveform according to some criteria. The criteria can be the minimization of the harmonics with the highest amplitude in the generated binary signal, not present in the original waveform. The criteria can also be the minimization of the total sum of harmonics not contained in the original waveform (the total distortion factor of the harmonic components). The mentioned spectral criteria can be used by evaluating the harmonic composition of the resulting binary waveform either before or after an appropriate additional analog low-pass filter. However, the resulting binary signal waveform after an appropriate analog low-pass filter can also be used as an optimization criteria, minimizing the time-domain difference between the original waveform and the resulting waveform, eg by minimizing the root-mean-square error between the approximation and the original waveform.

[0033] FIG. 3 shows an example of the implementation of the device as a block diagram. Here, the desired (ideal) analog waveform (1) is the input for the generator of the discrete-level waveform segments (2), the output of which is the input to the generator of the sequence of the intervals of the binary pulses (3), which output is the input for the Buffer of pulse intervals (4), which output is connected to output means of binary pulses (5), which is connected to device output (6).

[0034] Since such a solution is reasonable to implement in a microcontroller or other digital electronics, it could be reasonable to use the on-chip direct memory access (DMA) unit to generate pulses by using the on-chip PWM hardware units, serving as output means of binary pulses (5), with PWM-values based on the array of values of the buffer of pulse intervals (4), functioning as look-up-table based in the memory buffer of the microcontroller.

1. A method of generating binary waveform(s) to approximate a desired waveform as a sequence of binary pulses, wherein the waveform to be approximated is first converted into segments with discrete levels, then each said segment with discrete levels is further converted into a binary pulse of the same time duration as the given segment so, that the mean value of this pulse is proportional to the mean value of the approximated waveform over the time duration of the given segment.

2. The method of generating waveforms according to claim 1, characterized in that the values of said discrete levels are optimized for the best approximation of the desired waveform of the resulting binary waveform according to some criteria.

3. The method of generating waveforms according to claim 1, wherein the generation of said waveform takes place at discrete time values by a uniform time step.

4. The method of generating waveforms according to claim 1, wherein the generation of said waveform takes place at discrete time values with a non-uniform time step.

5. The method of generating waveforms according to claim 1, wherein each binary pulse starts with a positive value, in the case if said segments with discrete levels are of

decreasing values in time, and with a negative value if the mentioned segments with discrete levels have increasing values in time.

6. The method of generating waveforms according to claim **1**, wherein the initial desired waveform is a symmetrical in a time window, and the second half of the binary waveform is realized as a mirror waveform of the first half of the binary waveform.

7. The method of generating waveforms according to claim **1**, wherein the waveform to be approximated is a single-frequency sinewave.

8. The method of generating waveforms according to claim **1**, wherein the waveform to be approximated contains several frequency components.

9. The method of generating waveforms according to claim **1**, wherein a corrective waveform is added to the waveform to be approximated, which is optimized as the best approximation of the desired waveform of the resulting binary waveform according to some criteria.

10. A device for generating binary waveforms, the device comprising:

a generator of the discrete-level waveform segments, connected in series to an input, a generator of the sequence of the intervals of the binary pulses, a buffer of pulse intervals, and output means of binary pulses, which is connected to an output of the device.

* * * * *

Curriculum Vitae

1. Personal data

Name	Anar Abdullayev
Date and place of birth	26 March 1995 Baku, Azerbaijan
Nationality	Azerbaijani

2. Contact information

Address	Tallinn University of Technology,
	Thomas Johann Seebeck Department of Electronics,
	Ehitajate tee 5, 19086 Tallinn, Estonia
Phone	+37253673029
E-mail	anar.abdullayev@taltech.ee

3. Education

2021–…	Tallinn University of Technology, School of Information Technologies, Thomas Johann Seebeck Department of Electronics, PhD studies
2019–2021	Tallinn University of Technology, School of Information Technologies, Thomas Johann Seebeck Department of Electronics, MSc
2012–2019	Middle East Technical University, Faculty of Engineering, Department of Electrical and Electronics Engineering, BSc

4. Language competence

Azerbaijani	native
Turkish	fluent
English	fluent
Estonian	intermediate

5. Professional employment

2021 …	Tallinn University of Technology, Early stage researcher
2020	Ericsson, Electronics engineer intern
2016	LNL Technology, Electronics engineer intern
2015	BestComp Group, Electronics engineer intern

6. Computer and electronics skills

- Programming languages: Assembly, C, C++, Python

- Electronics design: LTSpice, Altium, Quartus

- Microprocessor programming: ARM, PIC, Arduino, ESP32

7. Defended theses

- 2021, DSP Based Impedance Spectroscopy Device, MSc, supervisor Olev Märtens, Tallinn University of Technology School of Information Technologies, Thomas Johann Seebeck Department of Electronics

8. Field of research

- Embedded systems

- Impedance measurement

9. Scientific work
Papers

1. Margus Metshein, Andrei Krivošei, Anar Abdullayev, Paul Annus, and Olev Märtens. Non-standard electrode placement strategies for ECG signal acquisition. *Sensors*, 22(23), 2022

2. Anar Abdullayev, Marek Rist, Olev Martens, Margus Metshein, Benoit Larras, Antoine Frappe, Antoine Gautier, Mart Min, Deepu John, Barry Cardiff, Andrei Krivošei, and Paul Annus. A DSP-based EBI, ECG and PPG measurement platform. *IEEE Transactions on Instrumentation and Measurement*, pages 1–8, 2023

3. Anar Abdullayev, Paul Annus, Andrei Krivošei, Margus Metshein, Olev Märtens, and Marek Rist. Improved PWM-based sinewave generation: Example of the impedance measurement. *Automatic Control and Computer Sciences*, pages 1–13, 2023

Conference presentations

1. Olev Martens, Margus Metshein, Anar Abdullayev, Benoit Larras, Antoine Frappe, Antoine Gautier, Maryam Saeed, Deepu John, Barry Cardiff, Andrei Krivošei, Paul Annus, and Marek Rist. Fiducial point estimation solution for impedance cardiography measurements. *2022 IEEE International Instrumentation and Measurement Technology Conference (I2MTC)*, pages 1–6, 2022

2. Anar Abdullayev, Olev Martens, Marek Rist, Margus Metshein, Mart Min, and Paul Annus. A DSP-based impedance measurement device. *2022 18th Biennial Baltic Electronics Conference (BEC)*, pages 1–5, 2022

3. Olev Martens, Margus Metshein, Gert Tamberg, and Anar Abdullayev. Impedance cardiography signal processing with Savitzky-Golay and frequency sampling kernels. *2022 18th Biennial Baltic Electronics Conference (BEC)*, pages 1–5, 2022

4. Anar Abdullayev, Olev Martens, Margus Metshein, Marek Rist, Raul Land, and Andrei Krivosei. A DSP-based multichannel EBI measurement device. *2024 IEEE International Instrumentation and Measurement Technology Conference (I2MTC)*, pages 1–6, 2024

5. Anar Abdullayev, Marek Rist, Margus Metshein, and Olev Martens. DSP-based electrical impedance tomography device: Implementation and experiments. *2025 IEEE International Instrumentation and Measurement Technology Conference (I2MTC)*, pages 1–6, 2025

Patent applications

1. O. Märtens, A. Abdullayev, M. Metshein, A. Gautier, A. Frappe, A. Krivošei, M. Rist; P. Annus, B. Larras, D. John; B. Cardiff. The impedance cardiography device, October 23, 2023. Estonian patent application P202200004, US patent application US2023/0320606 A1

2. O. Märtens, A. Abdullayev, M. Metshein, M. Rist, P. Annus, A. Krivošei. A method and device for synthesizing binary waveforms, December 19, 2024. Estonian patent application P202300017, US Patent application US2024/0421805 A1

Elulookirjeldus

1. Isikuandmed

Nimi	Anar Abdullayev
Sünniaeg ja -koht	26. märts 1995, Baku, Aserbaidžaan
Kodakondsus	Aserbaidžaani

2. Kontaktandmed

Aadress	Tallinna Tehnikaülikool,
	Thomas Johann Seebecki elektroonikainstituut,
	Ehitajate tee 5, 19086 Tallinn, Estonia
Telefon	+37253673029
E-post	anar.abdullayev@taltech.ee

3. Haridus

2021–...	Tallinna Tehnikaülikool, Infotehnoloogia teaduskond, Thomas Johann Seebecki elektroonikainstituut, doktoriõpe
2019–2021	Tallinna Tehnikaülikool, Infotehnoloogia teaduskond, Thomas Johann Seebecki elektroonikainstituut, MSc
2012–2019	Middle East Technical University, Faculty of Engineering, Department of Electrical and Electronics Engineering, BSc

4. Keelteoskus

aserbaidžaani keel	emakeel
türgi keel	heal tasemel
inglise keel	heal tasemel
eesti keel	kesktase

5. Teenistuskäik

2021–...	Tallinna Tehnikaülikool, nooremteadur
2020	Ericsson, Elektroonika inseneri praktikant
2016	LNL Technology, Elektroonika inseneri praktikant
2015	BestComp Group, Elektroonika inseneri praktikant

6. Arvuti- ja elektroonikaoskus

- Programmeerimiskeeled: assembler, C, C++, Python

- Elektroonika kujundus: LTSpice, Altium, Quartus

- Mikroprotsessorite programmeerimine: ARM, PIC, Arduino, ESP32

7. Kaitstud lõputööd

- 2021, DSP-põhine impedantsspektroskoopia seade, MSc, juhendaja Olev Märtens, Tallinna Tehnikaülikool, Infotehnoloogia teaduskond, Thomas Johann Seebecki elektroonikainstituut

8. Teadustöö põhisuunad

- Sisseehitatud süsteemid

- Takistusmõõtmine

9. Teadustegevus
Artiklid

1. Margus Metshein, Andrei Krivošei, Anar Abdullayev, Paul Annus, and Olev Märtens. Non-standard electrode placement strategies for ECG signal acquisition. *Sensors*, 22(23), 2022

2. Anar Abdullayev, Marek Rist, Olev Martens, Margus Metshein, Benoit Larras, Antoine Frappe, Antoine Gautier, Mart Min, Deepu John, Barry Cardiff, Andrei Krivosei, and Paul Annus. A DSP-based EBI, ECG and PPG measurement platform. *IEEE Transactions on Instrumentation and Measurement*, pages 1–8, 2023

3. Anar Abdullayev, Paul Annus, Andrei Krivošei, Margus Metshein, Olev Märtens, and Marek Rist. Improved PWM-based sinewave generation: Example of the impedance measurement. *Automatic Control and Computer Sciences*, pages 1–13, 2023

Konverentsiettekanded

1. Olev Martens, Margus Metshein, Anar Abdullayev, Benoit Larras, Antoine Frappe, Antoine Gautier, Maryam Saeed, Deepu John, Barry Cardiff, Andrei Krivošei, Paul Annus, and Marek Rist. Fiducial point estimation solution for impedance cardiography measurements. *2022 IEEE International Instrumentation and Measurement Technology Conference (I2MTC)*, pages 1–6, 2022

2. Anar Abdullayev, Olev Martens, Marek Rist, Margus Metshein, Mart Min, and Paul Annus. A DSP-based impedance measurement device. *2022 18th Biennial Baltic Electronics Conference (BEC)*, pages 1–5, 2022

3. Olev Martens, Margus Metshein, Gert Tamberg, and Anar Abdullayev. Impedance cardiography signal processing with Savitzky-Golay and frequency sampling kernels. *2022 18th Biennial Baltic Electronics Conference (BEC)*, pages 1–5, 2022

4. Anar Abdullayev, Olev Martens, Margus Metshein, Marek Rist, Raul Land, and Andrei Krivosei. A DSP-based multichannel EBI measurement device. *2024 IEEE International Instrumentation and Measurement Technology Conference (I2MTC)*, pages 1–6, 2024

5. Anar Abdullayev, Marek Rist, Margus Metshein, and Olev Martens. DSP-based electrical impedance tomography device: Implementation and experiments. *2025 IEEE International Instrumentation and Measurement Technology Conference (I2MTC)*, pages 1–6, 2025

Patenditaotlused

1. O. Märtens, A. Abdullayev, M. Metshein, A. Gautier, A. Frappe, A. Krivošei, M. Rist; P. Annus, B. Larras, D. John; B. Cardiff. The impedance cardiography device, October 23, 2023. Estonian patent application P202200004, US patent application US2023/0320606 A1

2. O. Märtens, A. Abdullayev, M. Metshein, M. Rist, P. Annus, A. Krivošei. A method and device for synthesizing binary waveforms, December 19, 2024. Estonian patent application P202300017, US Patent application US2024/0421805 A1